FEDERAL UNIVERSITY OF SÃO CARLOS
CENTER OF EXACT SCIENCE AND TECHNOLOGY
GRADUATE PROGRAM ON MATERIALS SCIENCE
AND ENGINEERING

HIGHLY POROUS GEOPOLYMERS: EFFECT OF THE PROCESSING ROUTE ON THE REACHED PROPERTIES

Marcelo Strozi Cilla

SÃO CARLOS – SP - BR
2015

FEDERAL UNIVERSITY OF SÃO CARLOS
CENTER OF EXACT SCIENCE AND TECHNOLOGY
GRADUATE PROGRAM ON MATERIALS SCIENCE
AND ENGINEERING

HIGHLY POROUS GEOPOLYMERS: EFFECT OF THE PROCESSING ROUTE ON THE REACHED PROPERTIES

Marcelo Strozi Cilla

Thesis presented to the Graduate Program on Materials Science and Engineering as a partial requirement to obtaining the title of DOCTOR IN MATERIALS SCIENCE AND ENGINEERING

Tutor: Prof. Dr. Márcio Raymundo Morelli
Cotutor: Prof. Dr. Paolo Colombo

Founding Agency: FAPESP

SÃO CARLOS – SP - BR
2015

DEDICATORY

To all those who were involved, participated and supported me during this work, especially my parents, my wife and my son.

CURRICULUM OF THE CANDIDATE

Master in Materials Science and Engineering (UFSCar – 2011), Materials Engineer (UFSCar – 1999)

Marcelo Strozi Cilla
PPG – CEM / UFSCar

Prof. Dr. Márcio Raymundo Morelli
Tutor
PPG – CEM / UFSCar

Prof. Dr. Paolo Colombo
Cotutor
UNIPD (ITALY)

ACKNOWLEDGEMENTS

To God, for making me strong and believe in completing this challenge, especially in the difficult times.

“Aos meus pais, Francisco e Maria, aos quais serei eternamente grato pelas lições de amor, honestidade e perseverança.”

To my wife Isabel, for accompanying me and support me throughout this work.

To my son and source of inspiration, Vinícius.

To my tutor and friend, prof. Dr. Márcio Raymundo Morelli, for believing in this project from the beginning, by the encouragement and confidence deposited in this period.

To my tutor, prof. Dr. Paolo Colombo, by the empathy shown from the beginning, even before the period in Italy, for all the support during the period in Italy, and after by the recognition and maintenance in the academic collaboration.

To the teachers and staff of PPGCEM and UNIPD by the support in professional and scientific development.

To the lab partners, and other people in Brazil and in Italy, who directly or indirectly, contributed to this work.

To FAPESP for the financial support that enabled the development of this project.

ABSTRACT

The geopolymers (inorganic polymers formed basically of silicates) have attracted increasing attention from academia for several reasons, particularly because it is considered a sustainable material where industrial by-products (fly ash and blast furnace slag) can be used as raw material, and is based on a low energy cost process. Such materials find applications in virtually all industrial sectors, depending on the molar ratio Si:Al, responsible for its properties. Currently the application of large volumes of geopolymers is focused on replacement of Portland cement, a material with an extremely aggressive process of obtaining to the environment. However, due to their similar properties to the ceramic material and increase search for new applications, studies of porous geopolymers are also of great interest. Processing routes currently used to obtain porous geopolymers are based on the civil construction for the production of aerated concrete with closed porosity, limiting their application. Thus, the development of a new processing route to produce porous geopolymers, which permits the formation of a structure with open porosity, enabling the expansion in the applications of such material is essential. Two different routes are proposed based on porous ceramic processing routes with highly porous geopolymers results, with a homogeneous microstructure, and open cell porosity of up to about 85vol%, with physical properties that suggest they may be used as a substitute for low-cost highly porous ceramics for applications such as catalyst supports, filtration of hot gases, adsorption and insulating refractory furnaces.

GEOPOLÍMEROS ALTAMENTE POROSOS: EFEITO DA ROTA DE PROCESSAMENTO SOBRE AS PROPRIEDADES ALCANÇADAS

ABSTRACT (PORTUGUESE)

Os geopolímeros (polímeros inorgânicos formados basicamente por silicatos) têm atraído cada vez mais a atenção do meio acadêmico por várias razões, em particular pelo fato de ser considerado um material sustentável onde subprodutos industriais (cinzas volantes e escórias de alto forno) podem ser utilizados como matéria prima, além de se basear em um processo de baixo custo energético. Tais materiais encontram aplicações em praticamente todos os setores industriais, dependendo da razão molar Si:Al, responsável por suas propriedades. Atualmente o grande volume de aplicação dos geopolímeros está concentrado na substituição do cimento Portland, um material com um processo de obtenção extremamente agressivo ao meio ambiente. Porém, devido às suas propriedades similares aos materiais cerâmicos e a busca cada vez maior por novas aplicações, estudos sobre geopolímeros porosos também tem despertado grande interesse. Rotas de processamento usadas atualmente na obtenção de geopolímeros porosos são baseadas nas da construção civil para a produção do concreto aerado, com porosidade fechada, limitando sua aplicação. Dessa maneira, o desenvolvimento de uma nova rota de processamento para os geopolímeros porosos, que proporcione o desenvolvimento de uma estrutura com porosidade aberta, possibilitando a ampliação nas aplicações de tal material é fundamental. Duas diferentes rotas são propostas, baseadas em rotas de processamento de cerâmicas porosas com resultados de geopolímeros altamente porosos, com microestrutura homogênea, células abertas e porosidade da ordem de até 85vol%, com propriedades físicas que sugerem que eles podem ser utilizados como substituto de baixo custo para produtos cerâmicos altamente porosos em aplicações, tais como suportes de catalisadores, filtração de gases quentes, adsorção e isolamento refratário de fornos.

GEOPOLIMERI ALTAMENTE POROSI: EFFETTO DELLA VIA DI TRASFORMAZIONE SULLE PROPRIETÀ RAGGIUNTI

ABSTRACT (ITALIAN)

I geopolimeri (polimeri inorganici formate principalmente da silicati) hanno attirato sempre più attenzione da parte del mondo accademico per diversi motivi, soprattutto perché è considerato un materiale sostenibile dove industriale (ceneri volanti e scorie di altoforno) può essere utilizzato come materia prima, e si basa su un processo a basso costo energetico. Tali materiali trovano applicazione in tutti i settori industriali, in funzione del rapporto molare Si:Al, responsabile delle sue proprietà. Attualmente l'applicazione di grandi volumi di geopolimeri è focalizzata sulla sostituzione del cemento Portland, un materiale con un processo estremamente aggressiva ottenere dell'ambiente. Tuttavia, a causa delle loro proprietà simili al materiale ceramico e aumentando la ricerca di nuove applicazioni, studi di geopolimeri porosi è anche di grande interesse. Percorsi di lavorazione attualmente utilizzate per ottenere geopolimeri porosi sono basate sulla produzione di calcestruzzo aerato con porosità chiusa, limitando la loro applicazione. Pertanto, lo sviluppo di una nuova via di elaborazione per geopolimeri porosi, che consente lo sviluppo di una struttura con porosità aperta, consentendo l'espansione nelle applicazioni di tale materiale è essenziale. Due percorsi differenti sono proposti basato su percorsi utilizzato con ceramici porosi, con risultati di geopolimeri altamente porosi, con una microstruttura omogenea, cellula aperta e porosità fino a circa 85vol%, con proprietà fisiche che suggeriscono che possono essere utilizzati come un sostituto basso costo per ceramica altamente porosi in applicazioni come supporti di catalizzatore, filtrazione di gas caldi, adsorbimento e isolamento refrattario per forni.

x

PUBLICATIONS

CILLA, M. S.; MORELLI, M. R.; COLOMBO, P. Effect of process parameters on the physical properties of porous geopolymers obtained by gelcasting. **Ceramics International**, v. 40, n. 8, p. 13585–13590, doi:10.1016/j.ceramint.2014.05.074, 2014.

CILLA, M. S.; MORELLI, M. R.; COLOMBO, P. Open cell geopolymer foams by a novel saponification/peroxide/gelcasting combined route. **Journal of the European Ceramic Society**, v. 34, p. 3133–3137, doi:10.1016/j.jeurceramsoc.2014.04.001, 2014.

CILLA, M. S.; MORELLI, M. R.; COLOMBO, P. Geopolymer foams by gelcasting. **Ceramics International**, v. 40, n. 4, p. 5723–5730, doi:10.1016/j.ceramint.2013.11.011, 2014.

CILLA, M. S. ; MORELLI, M. R. . Influência do ativador alcalino sobre a refratariedade de um geopolímero contendo metacaulim e cinzas volantes. In: 20º CBECIMAT - Congresso Brasileiro de Engenharia e Ciência dos Materiais, 2012, Joinville. Anais 20º CBECIMAT - Congresso Brasileiro de Engenharia e Ciência dos Materiais, 2012.

CILLA, M. S. ; MORELLI, M. R. . How the Alkaline Activator and Percentage of Fly Ash Influence the Microstructure of a Geopolymer Obtained from Metakaolin. In: The 5th Latin American Conference on Metastable and Nanostructured Materials NANOMAT 2012, 2012, São Carlos. Program and Book of Abstracts, 2012. p. 80-80.

SUMARY

		Page
EXAMINING BOARD		i
ACKNOWLEDGMENTS		iii
ABSTRACT		v
ABSTRACT (PORTUGUESE)		vii
ABSTRACT (ITALIAN)		ix
PUBLICATIONS		xi
SUMARY		xiii
INDEX OF TABLES		xvii
INDEX OF FIGURES		xix
SYMBOLS AND ABREVIATIONS		xxv
1	INTRODUCTION	1
1.1	Generality on porous geopolymers	3
2	LITERATURE REVIEW	5
2.1	Geopolymers	5
2.1.1	Precursors	8
2.1.2	Activators	9
2.1.3	Geopolymers to medium-high temperature applications	9
2.2	Ceramic foams (filters)	9
2.3	Industrial applications of ceramic filters	11
2.4	Processing routes to macroporous ceramics	13
2.4.1	Replica technique	13
2.4.2	Sacrificial template method	14
2.4.3	Direct foaming method	14
2.5	Saponification	15
2.6	Triglycerides sources	16
3	MATERIALS AND METHODS	19
3.1	Materials	19
3.1.1	Gelcasting route (GCR)	19
3.1.2	Gelcasting / Saponification / Peroxide Combined Route (GCSPCR)	19

3.2	Methods	20
3.2.1	Gelcasting route (GCR)	21
3.2.1.1	Total and open porosity	22
3.2.1.2	Mechanical strength	23
3.2.1.3	Permeability	23
3.2.1.4	Morphological analysis	24
3.2.1.5	Specific surface area	24
3.2.1.6	Linear thermal shrinkage	25
3.2.1.7	TG/DTA analysis	25
3.2.2	Gelcasting/saponification/peroxide combined route (GCSPCR)	25
3.2.2.1	Total an open porosity	27
3.2.2.2	Mechanical strength	27
3.2.2.3	Permeability	27
3.2.2.4	Morphological analysis	27
3.2.2.5	Specific surface area	28
3.2.2.6	Linear thermal shrinkage and TG/DTA analysis	28
4	RESULTS AND DISCUSSION	29
4.1	Gelcasting route (GCR)	29
4.1.1	Total and open porosity	29
4.1.2	Mechanical strength	34
4.1.3	Permeability	35
4.1.4	Morphological analysis	39
4.1.5	Specific surface area	44
4.1.6	Linear thermal shrinkage	45
4.1.7	TG/DTA analysis	47
4.2	Gelcasting/saponification/peroxide combine route (GCSPCR)	48
4.2.1	Total and open porosity	50
4.2.2	Mechanical strength	53
4.2.3	Permeability	53
4.2.4	Morphological analysis	55
4.2.5	Specific surface area	60
4.2.6	Linear thermal shrinkage and TG/DTA analysis	62

5	CONCLUSIONS	63
6	SUGGESTIONS FOR FUTURE WORKS	65
7	REFERENCES	67
	APENDIX A	75

INDEX OF TABLES

		Page
Table A.1	Chemical analysis of precursors -* supplier - ** XRF….....	75
Table A.2	Real density of precursors……..…	77
Table A.3	Specific surface area of precursors……..…	78
Table A.4	Amount of the oxide presented in the geopolymer composition…….....	79
Table A.5	Amount of majoritarian oxides in the geopolymer composition……...	80
Table A.6	Different geopolymer compositions with variations in the precursors (metakaolin: type and amount) and activators (type of based alkaline solution)……	83

INDEX OF FIGURES

		Page
Figure 1.1	Overall framework of the applications according to the molar ratio Si:Al [3]……..……..…..	2
Figure 2.1	Schematic diagram for geopolymer production [6]…..…..….	5
Figure 2.2	Conceptual schematic model for geopolimerization reaction [6]…….	7
Figure 2.3	Classification of porous materials by pore size and corresponding typical applications and fabrication processes [25]……..……	11
Figure 2.4	Scheme of possible processing routes used for the production of macroporous ceramics [33]…….……..…	13
Figure 2.5	Saponification reaction of a triglyceride with KOH to form a mixture of potassium carboxylates (soap) and glycerol.....…	16
Figure 3.1	Schematic diagram for the production of geopolymer foams by gelcasting route [42]……...	22
Figure 3.2	Schematic diagram for the production of geopolymer foams by gelcasting/saponification/peroxide combined route [46]…….....	26
Figure 4.1	Effect of solid content in the slurry on total porosity. All samples were produced using 2 wt% of surfactant and mixing at 1500 rpm mixing speed……..……..	30
Figure 4.2	Effect of rotation speed and surfactant content in the slurry (solid content set at 68 wt%); a) 2 wt% surfactant; b) 4 wt% surfactant……...	31
Figure 4.3	Relation between total porosity and open porosity estimated by the Archimedes Principle; surfactant content set at 2 wt% (a) and 4 wt.....……	32
Figure 4.4	Total porosity as a function of the heat treatment of geopolymer foams: (a) 2 wt% of surfactant; (b) 4 wt% of surfactant……..…….	33

Figure 4.5 Correlation among compressive strength, relative density and total porosity of geopolymer foams.(a) 2 wt% of surfactant; (b) 4 wt% of surfactant……. 35

Figure 4.6 Permeability constants (k_1, k_2) of geopolymer foams produced with different surfactants (type and content) and different mixing speeds, as a function of open porosity estimated by the Archimedes Principle. (a) 2 wt% of surfactant; (b) 4 wt% of surfactant……. 38

Figure 4.7 Location of k_1 and k_2 data for geopolymer foams obtained by gelcasting in a comprehensive permeability map [44]….. 39

Figure 4.8 Effect of mixing speed on the average cell size and cell size distribution of samples produced using 2 wt% of surfactant (solid content set at 68 wt%). a) Tween 80, 1500 rpm; b) Tween 80, 2000 rpm; c) Triton X-100, 1500 rpm; d) Triton X-100, 2000 rpm. In the insets are shown the pore size distribution for each sample……... 40

Figure 4.9 Effect of mixing speed on the average cell size and cell size distribution of samples produced using 4 wt% of surfactant (solid content set at 68 wt%). a) Tween 80, 1500 rpm; b) Tween 80, 2000 rpm; c) Triton X-100, 1500 rpm; d) Triton X-100, 2000 rpm. In the insets are shown the pore size distribution for each sample……... 41

Figure 4.10 Effect of surfactant content on the average cell size and its relation with the relative density of samples (solid content set at 68 wt% and mixing speed at 1500 rpm)…… 43

Figure 4.11 Morphology of geopolymer foam obtained from slurry with 68 wt% solids, 2 wt% surfactant Tween and stirred at 2000 rpm. (a) lowest magnification; (b) and (c) intermediate magnification in different regions; and (d) highest magnification……. 44

Figure 4.12 Linear shrinkage of geopolymer foam as a function of temperature……... 45

Figure 4.13 Open porosity as a function of the heat treatment of geopolymer foams with (a) 2 wt% of surfactant; (b) 4 wt% of surfactant…….. 46
Figure 4.14 TG/DTA curve for a sample produced using surfactant Tween 80 (2 wt % – 1500 rpm)…….. 47
Figure 4.15 Effect of heat treatment on the surface morphology for a sample produced using Tween 80 as surfactant (2 wt% – 1500 rpm): (a) room temperature; (b) 700°C; (c) 1200°C…. 48
Figure 4.16 SEM image highlighting the struts of samples produced with different surfactants: (a) Tween 80; (b) Triton X-100, as prepared and dried……. 48
Figure 4.17 SEM micrographs of geopolymer foams, as-prepared and dried, produced using different processing approaches: (a) saponification/peroxide/gelcasting combined route; (b) saponification route; (c) peroxide route…… 49
Figure 4.18 Effect of the type of triglyceride and temperature on the total porosity of the geopolymer foams. a) real values of the total porosity according the heat treatment of 300, 600, 900 and 1200°C and b) decrement values of the open porosity of each triglyceride source due the heat treatment in the same temperatures……... 51
Figure 4.19 Effect of the type of triglyceride and temperature on the open porosity of the geopolymer foams. a) real values of the open porosity according the heat treatment of 300, 600, 900 and 1200°C and b) decrement values of the open porosity of each triglyceride source due the heat treatment in the same temperatures……... 52
Figure 4.20 Effect of the type of triglyceride and heat treatment on the mechanical strength of the geopolymer foams…… 53
Figure 4.21 Location of k_1 and k_2 data for geopolymer foams obtained by gelcasting in a comprehensive permeability map [44]……... 54

Figure 4.22 Effect of the type of triglyceride on the morphology (macro-pore architecture) of the geopolymer foams heat treated at 300°C……. 56
Figure 4.23 Average cell size of geopolymer foams according triglyceride source after heat treatment at 300°C…….. 56
Figure 4.24 Effect of the type of triglyceride on the morphology (macro-pore architecture) of the geopolymer foams heat treated at 600°C……. 57
Figure 4.25 Average cell size of geopolymer foams according triglyceride source after heat treatment at 600°C 57
Figure 4.26 Effect of the type of triglyceride on the morphology (macro-pore architecture) of the geopolymer foams heat treated at 900°C……. 58
Figure 4.27 Average cell size of geopolymer foams according triglyceride source after heat treatment at 900°C……... 58
Figure 4.28 Effect of the type of triglyceride on the morphology (macro-pore architecture) of the geopolymer foams heat treated at 1200°C……... 59
Figure 4.29 Average cell size of geopolymer foams according triglyceride source after heat treatment at 1200°C……. 59
Figure 4.30 Effect of the type of triglyceride and temperature on the specific surface area of the geopolymer foams. a) real values of the specific surface area according the heat treatment of 300, 600, 900 and 1200°C and b) decrement values of the specific surface area of each triglyceride source due the heat treatment in the same temperatures 60
Figure A.1 XRD pattern of HP metakaolin (HPMK)……. 76
Figure A.2 XRD pattern of Minasolo metakaolin (MSMK)……. 76
Figure A.3 XRD pattern of fly-ash (FA)……. 77

Figure A.4 Phase equilibrium diagram of the three majority oxide in the geopolymer composition where the green line represents the SiO_2, red line represents the Al_2O_3 and blue line represents the K_2O and their intersection sets the composition according Table A.5…….. 81

Figure A.5 XRD pattern of the geopolymer composition……... 82

Figure A.6 Effect of the type and amount of metakaolin (MSMK and HPMK) and type of alkali based solution……. 84

Figure A.7 Effect of temperature in different geopolymer composition activated with Na based solution……... 85

Figure A.8 Effect of temperature in different geopolymer composition activated with K based solution……. 86

SYMBOLS AND ABREVIATIONS

°C	Celsius degree
Al	aluminum
Al_2O_3	aluminum oxide
ASTM	American Society for Testing and Materials
Ca	calcium
FA	fly ash
FDA	US Food and Drug Administration
GCR	gelcasting route
GCSPCR	gelcasting/saponification/peroxide combined route
H_2O	water
H_2O_2	hydrogen peroxide
HPMK	HP metakaolin
K	potassium
K_2O	potassium oxide
K_2SiO_3 (PS)	potassium silicate
KOH	potassium hydroxide
Li	lithium
M	Molar concentration (Molarity)
MPa	Megapascal
MSMK	Minasolo metakaolin
Na	sodium
Na_2O	sodium oxide
Na_2SiO_3 (ASA)	alkaline sodium silicate
NaOH	sodium hydroxide
OH^-	hydroxyl
pH	hydrogen potential
Si	silicon
SV	saponification value
SiO_2	silicon oxide
SSA	specific surface area

Ti	titanium
US	United States
Zr	zircon

1 INTRODUCTION

The term geopolymer was created by Davidovits [1] in 1978 to define a class of materials of mineral nature with chemical composition similar to that of zeolite, but with a mixed microstructure (from amorphous to semi-crystalline).

The silica (SiO_2) and alumina (Al_2O_3) species present in the raw materials react in a highly alkaline medium, organizing themselves in a continuous three dimensional structure by sharing oxygen atoms, forming bonds such as Si-O-Al-O (sialate), Si-O-Al-O-Si-O (sialate-siloxo) or Si-O-Al-O-Si-O-Si-O (sialate-disiloxo), also called polysialates, where the term sialate is an abbreviation for silicon-aluminate.

Among the different types of geopolymers, those based on potassium activators show improved mechanical and thermal properties due to the larger size of the potassium ion compared to sodium [2].

These materials have found application in virtually all fields of industry, depending in particular on the SiO_2/Al_2O_3 molar ratio, which provides, among its properties, high mechanical strength, resistance to freeze-thaw, high chemical inertness and excellent fire resistance, being considered as replacement for conventional cement-based applications as well as for ceramic components that can be used up to medium-high temperature (typically below 1200°C) [1].

Explored applications include bricks, thermal insulation, and encapsulation of radioactive and toxic waste, foundry equipment and composites, as presented in Figure 1.1 [3].

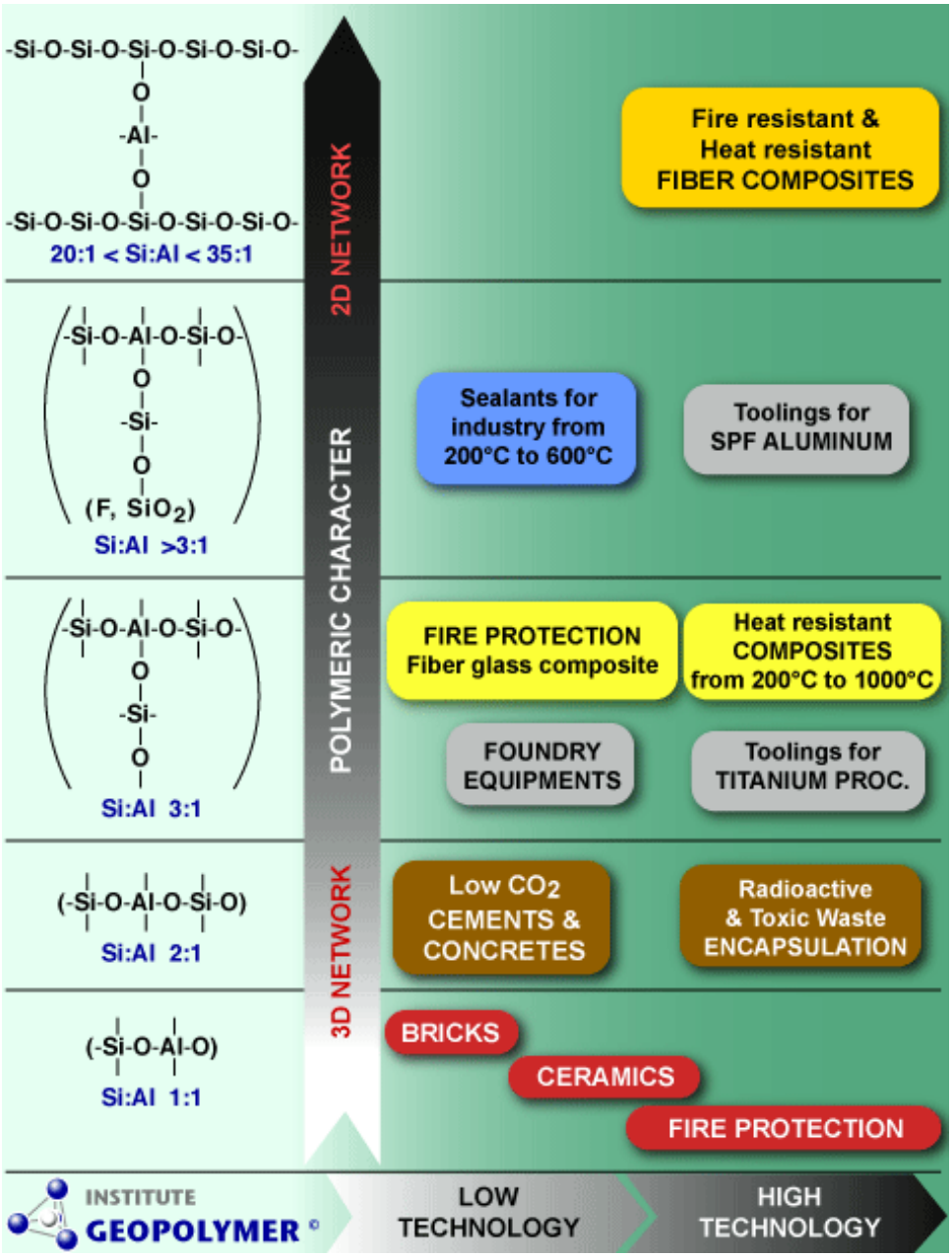

Figure 1.1 Overall framework of the applications according to the molar ratio Si:Al [3].

In addition, these materials can be considered sustainable, because they reach their final properties, which could be improved to some specific applications by heat treatment, at temperatures not exceeding 100°C during the geopolymerization reaction, even considering the thermal energy employed for obtaining metakaolin and silicates, thereby limiting the energy required to produce a component.

Moreover, geopolymers could be produced using as raw materials, industrial waste as fly ash and furnace slag or building wastes as bricks and tiles, all of them rich in Al_2O_3 and SiO_2 in a non-crystalline form.

1.1 Generality on porous geopolymers

Several papers describe the production of porous components based on geopolymers borrowing the typical approach used in the cement industry to procedure aerated concrete, that is the addition to an aqueous geopolymer slurry of components (such as silica fume or Al powder) capable of generating *in situ* gaseous H_2 because of the oxidation reaction occurring with metallic Si or Al in a highly alkaline environment [2, 4]. Another approach that has been proposed is the addition of peroxides, which decompose generating gas [5].

These approaches provide a suitable way of fabricating highly porous components, but when these processing routes are used the cells are typically closed, i.e., no interconnecting pores are present on the cell walls, thereby greatly limiting properties such as the permeability to liquids or gases of the component. Despite all these studies, little work has been devoted to the production of geopolymer foams in alternative ways.

Within this context, was studied and applied for the first time a gelcasting approach based on the presence of appropriate surfactants and also a combined (gelcasting/saponification/peroxide) route for the production of highly porous components from geopolymer precursors with predominantly open cells, which can extend the range of applications, including for example, processes where permeability and adsorption are required.

2 LITERATURE REVIEW

2.1 Geopolymers

Indeed, a geopolymer is an inorganic binder, which is synthesized by mixing at ambient or slightly above temperatures (e.g. 90°C) a reactive aluminosilicate powder (e.g. metakaolin, calcined clay, fly ash) with an alkaline activator that contains alkali hydroxide, silicates, aluminates, carbonates or sulphates, or a combination thereof (Figure 2.1). The reaction product consists mainly by an amorphous aluminosilicate phase due by interlinked SiO_4^{4-} and AlO_4^{5-} tetrahedral forming a 3D-structure [6].

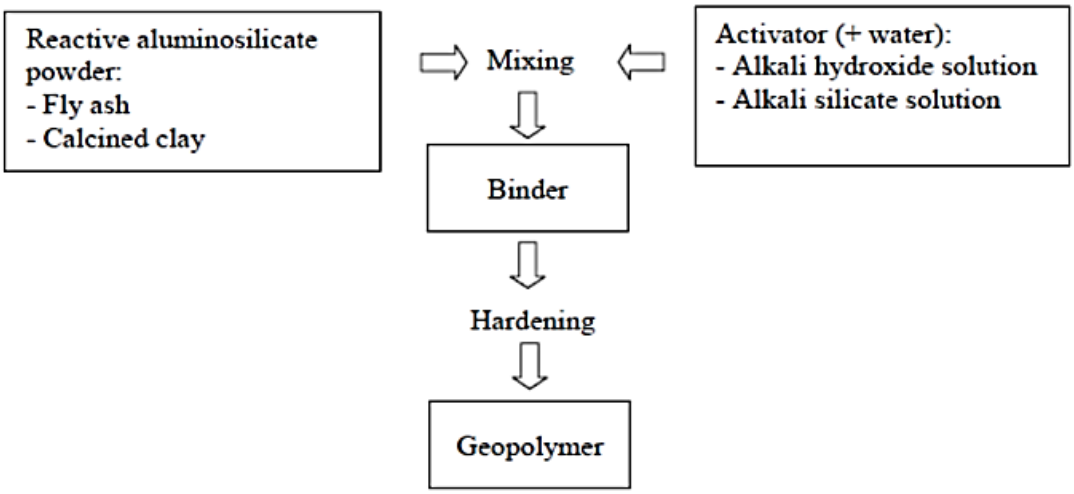

Figure 2.1 Schematic diagram for geopolymer production [6].

Even the term geopolymer is commonly used to describe the amorphous to crystalline reaction products from synthesis of alkali aluminosilicates due the reaction with alkali hydroxide/alkali silicate solution [7], geopolymeric gels and composites are also usually applied to designate materials which are synthetized utilizing the same chemistry as: low-temperature aluminosilicate glass [8], alkali-activated cement [9], geocement [10], alkali-bonded ceramic [11], inorganic polymer concrete [12], and hydroceramic [13].

Generally, the alkali activation is a hydration reaction that comprises dissolution and precipitation of aluminosilicates (precursors) in an aqueous solution of alkaline or alkaline earth metal, such as:

- ✓ hydroxide (ROH, $R(OH)_2$),
- ✓ salts of weak acids (R_2CO_3, R_2S, RF),
- ✓ salts of strong acids salts (Na_2SO_4, $CaSO_4.2H_2O$),
- ✓ or silicate salts of type $R_2(n)SiO_2$,

  where R is an alkaline ion such as Na, K or Li, or an alkaline earth such as Ca [3].

Considering the zeolite chemistry, Davidovits [1, 3] suggests several molar ratios and parameters that should be controlled, because they affect substantially the geopolymer properties like durability and mechanical strength:

- ✓ Geopolymer mixture: $0.20 < Na_2O/SiO_2 < 0.48$
  $3.30 < SiO_2/Al_2O_3 < 4.50$
  $0.80 < Na_2O/Al_2O_3 < 1.60$,

  being possible the replacement of Na by K or Li.
- ✓ Water content in the mixture: $10.00 < H_2O/Na_2O < 25.00$,

  also respecting the workability.
- ✓ Curing temperature in the range 30-90°C;
- ✓ Curing time in the range 6-96 hours.

Regardless several macroscopic characteristics of geopolymers obtained from different aluminosilicate sources may appear similar, their microstructure and physical, mechanical, chemical and thermal properties are distinct and depending essentially on the raw material from which they are produced [7]. The microstructure of metakaolin derived geopolymers, for example, has been investigated by systematic variation of activator composition and its effect on the mechanical strength [14–16]. Also, it was observed that the microstructure changed from containing large pores to being more homogenous with small pores as the Si/Al ratio was increased, which could be explained by

the strong correlation with the Young's modulus and large increases in mechanical strength [14], however, any effect on the microstructure of changing the alkali cations from Na to K was not observed [15].

In this way, different microstructures and properties observed and cited in the literature may be explained by the conceptual geopolymer reaction proposed model presented in Figure 2.2, which shows a highly simplified reaction mechanism for the geopolymerization [6].

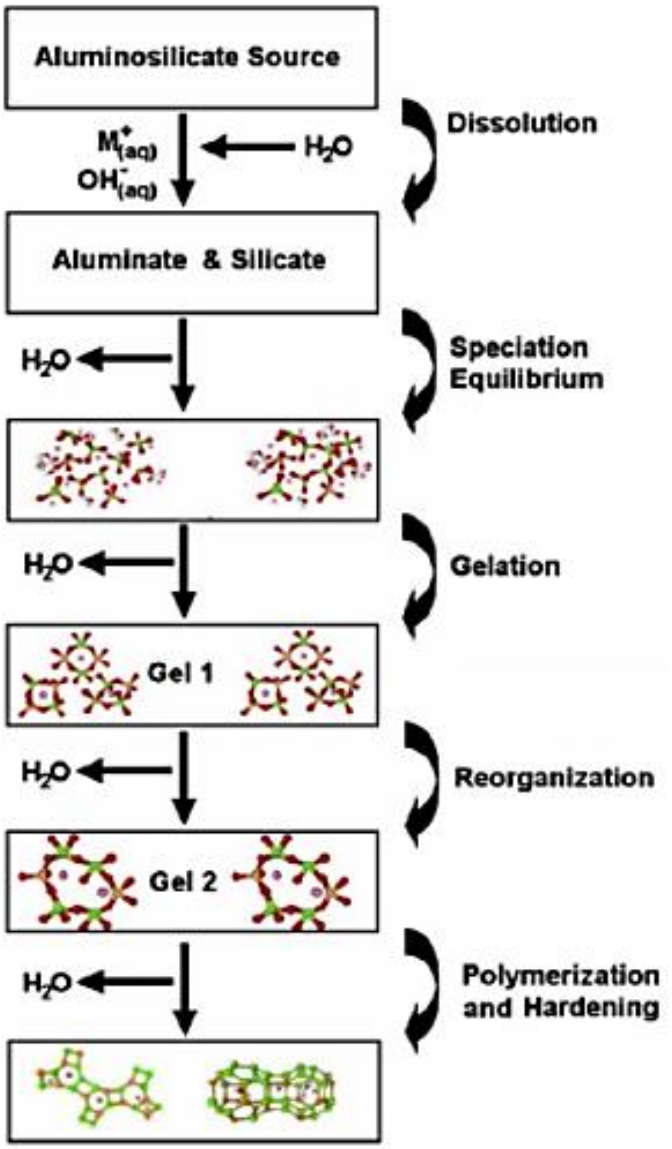

Figure 2.2 Conceptual schematic model for geopolimerization reaction [6].

Figure 2.2 outlines the reaction mechanism that occurs during the transformation of a solid aluminosilicate source into a synthetic alkali aluminosilicate. Once in solution, the species released by dissolution are incorporated into the aqueous phase, which may already contain silicate present in the activating solution [6]. Hence, a complex mixture of silicate, aluminate and aluminosilicate species is thereby formed, and the equilibrium within these solutions have been intensively studied [17-19].

Even though presented linearly, these processes are largely coupled and occur concurrently, where dissolution of the solid aluminosilicate source by alkaline hydrolysis (consuming water) produces aluminate and silicate species. It is important to note that the dissolution of solid particles at the surface resulting in the liberation of aluminate and silicate into solution has always been assumed to be the mechanism responsible for conversion of the solid particles during geopolymerization [20].

Despite this, the actual process of particle-to-gel conversion has never been confirmed in the highly alkaline and poorly solvated conditions as occurs during geopolymer synthesis. Thus, without of conclusive mechanistic understanding of solid particle conversion will be assumed the surface dissolution, as described in the model presented in Figure 2.2 [6].

2.1.1 Precursors

Aluminosilicates such as slag (obtained in blast furnaces), fly ash (obtained from the burning of coal in thermoelectric plants), volcanic ash (with natural thermal treatment) and powder tile or stone (passing through industrial furnaces) are potential starting materials for alkaline activation, because they have a prior heat treatment [1].

Thus, kaolin, a natural aluminosilicate, since undergone a suitable heat treatment to dehydroxylation and change of the coordination of aluminum, leads to metakaolin, which may also undergo alkaline activation. As a result of these changes, the material loses much of its crystalline structure, getting a

substantially amorphous state of high entropy, increasing their tendency to combine chemically [1, 3].

One important aspect to be observed in these materials is the very low or almost zero amount of calcium, not entering the traditional line of binders where calcium, as in Portland cement, has a prominent role [1, 3].

2.1.2 Activators

The most common alkaline activators used to obtain geopolymeric materials are sodium or potassium hydroxide, potassium carbonate, sodium or potassium silicates, and especially mixtures thereof [1].

2.1.3 Geopolymers to medium-high temperature applications

In several studies, it has been observed a high degree of thermal stability of geopolymers, especially in K-polisialates with melting temperature in the range of 1400°C [21]. However, geopolymers for application at temperatures between 1000 and 1200°C were also obtained with sodium activators for applications such as thermal insulators [22].

2.2 Ceramic foams (filters)

Ceramic filters have been used in many industrial applications, not only where polymeric membranes could not perform acceptably, but also where superior system integrity is required [23].

The most commonly encountered advantages of ceramic filters, when compared to other membrane types used in pressure driven membrane processes, include the following [24, 26]:

- ✓ long and reliable working lifetime
- ✓ resistance to high temperatures across the entire pH range
- ✓ excellent chemical stability
- ✓ corrosion and abrasion resistant
- ✓ bacteria resistant and, frequently, bio inert
- ✓ compatibility with highly viscous fluids
- ✓ enhanced ease of cleaning and sterilization

Ceramic filters are used, among the most mature filtration technologies, in the pressure-driven membrane processes for liquid separations, and are generally classified into four categories, according the size of the materials which should be retained:

- ✓ Reverse osmosis (<0.5 μm, no ‘‘real’’ pores)
- ✓ Nanofiltration (0.005–0.0005 μm)
- ✓ Ultrafiltration (0.1–0.001 μm)
- ✓ Microfiltration (0.05–10 μm)

Regarding the materials which are made, the most common ceramic membranes are produced of Al, Si, Ti, or Zr oxides, but also with other materials including non-oxides (carbides, borides, nitrides, silicides) and with combinations thereof.

Specifically for food and pharmaceutical applications, membranes made of Al, Zr, and Ti oxides are suitable, since they meet the US Food and Drug Administration (FDA) requirements detailed in 21 Code of Federal Regulations (Good manufacturing practices) [24].

Despite the advantages presented, the higher cost of raw materials and elevate temperature sintering to produce these ceramic membranes (oxide / non-oxide based) limits their use for some industrial application. Thus, various researchers have reported the study of clay-based low cost ceramic membranes, using kaolin as starting material with other additives, as quartz and calcium carbonate, for industrial applications. [27-29].

2.3 Industrial applications of ceramic filters

Initially, ceramic filters were developed for uranium enrichment and were also used in wastewater treatment. Over the past years, successful solutions and possible applications covered all industries and ceramic filters are increasingly being used in industries such as biotechnology and pharmaceutical, dairy, food and beverage, as well as chemical and petrochemical, microelectronics, metal finishing, and power generation [24].

Figure 2.3 shows the classification of porous materials by pore size and corresponding typical applications and fabrication processes.

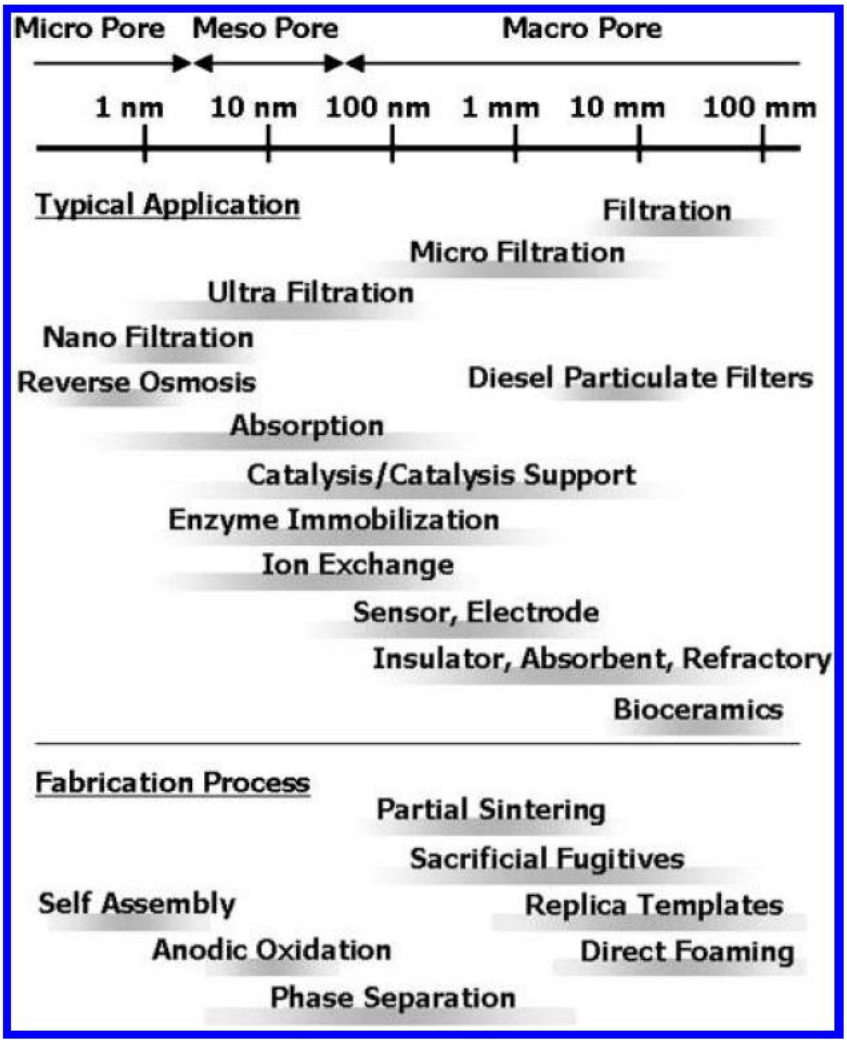

Figure 2.3 Classification of porous materials by pore size and corresponding typical applications and fabrication processes [25].

Besides the applications that are industry-specific, a number of common approaches are being used in different industries. Two examples are oil/water separation and the recovery of cleaning chemicals [30-32]. Many examples can be found in food industry, metal fabrication and allied industries, automotive industry, chemical manufacturing industry, and oil refinery, including petroleum oils from tanker washers, spills, drilling, various processing steps, etc. The benefits of ceramic membranes are also employed in recycling technology, for example, for degreasing cleaning baths, paint, coating and enamel, or petrochemicals recycling. The wastewater typically contains emulsified oils that are difficult to separate with conventional treatment technologies such as coalescers and oil skimmers. Furthermore, many polymeric membranes are unsuitable due to their limited stability in aggressive chemical environments such as highly contaminated oily wastewater (e.g., lube oils, petroleum fractions) as previously mentioned [24].

Once geopolymers can be used to replace ceramic components in several applications, it is possible to extend and apply this concept to the development of a new class of inorganic (geopolymer) membrane, with the same low cost clay-based presented earlier [29]. Also, specifically related to radioactive wastewater treatment, geopolymers behave similarly to zeolites, materials which are known for their abilities to adsorb toxic chemistry wastes. In the case of geopolymers, their three dimensional framework is responsible by locking the hazardous elements contained in the waste [3].

As the field of application for these materials varies widely, the final properties of the filter in a particular application are also diverse. Consequently, the search for the different routes to produce these foams such as, the replica technique, the sacrificial template method and the direct-foaming technique, each having its own set of properties, has attracted interest from the academic world [33].

2.4 Processing routes to macroporous ceramics

The processing routes presented here are classified into replica, sacrificial template and direct foaming methods, as schematically illustrated in Figure 2.4.

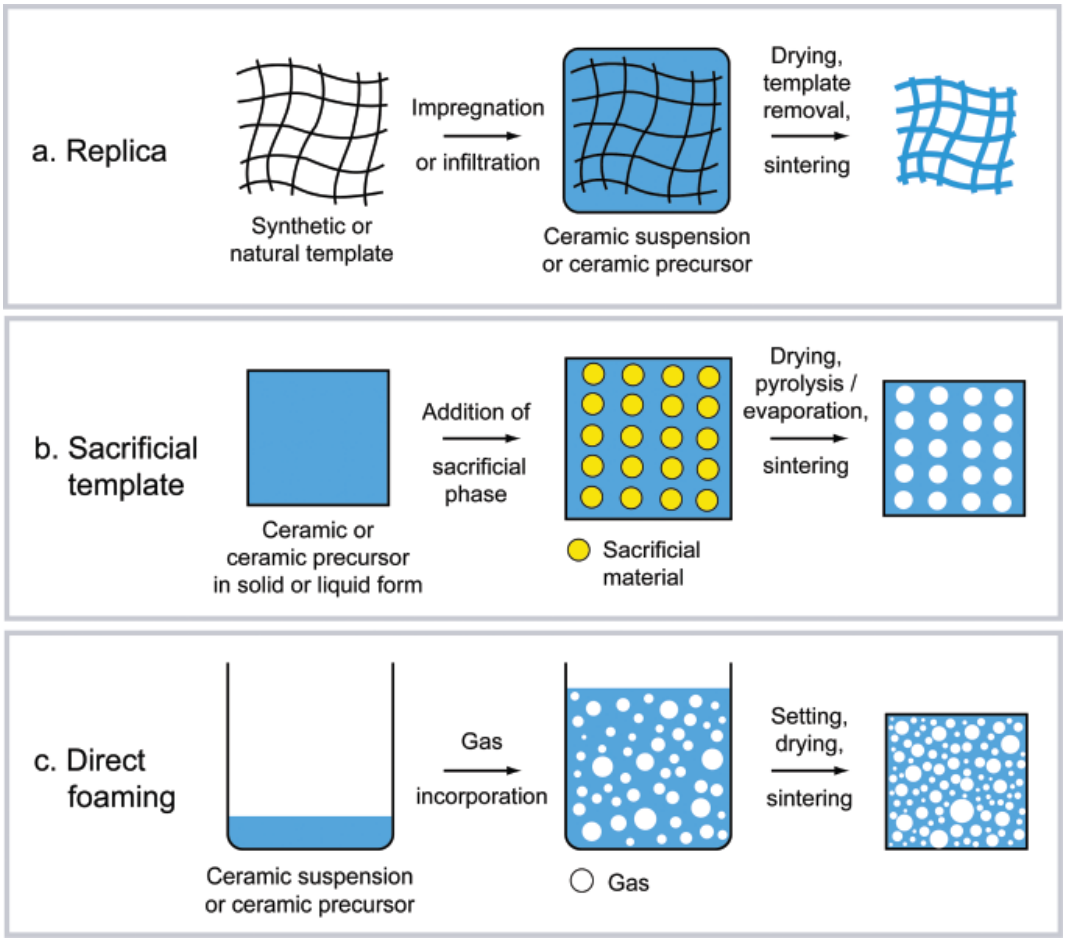

Figure 2.4 Scheme of possible processing routes used for the production of macroporous ceramics [33].

2.4.1 Replica technique

The replica method is based on the impregnation of a cellular structure with a ceramic suspension or precursor solution in order to produce a

macroporous ceramic exhibiting the same morphology as the original porous material. Many synthetic and natural cellular structures can be used as templates to fabricate macroporous ceramics through the replica technique.

2.4.2 Sacrificial template method

The sacrificial template technique usually consists of the preparation of a biphasic composite comprising a continuous matrix of ceramic particles or ceramic precursors and a dispersed sacrificial phase that is initially homogeneously distributed throughout the matrix and is ultimately extracted to generate pores within the microstructure. This method leads to porous materials displaying a negative replica of the original sacrificial template, as opposed to the positive morphology obtained from the replica technique described previously.

2.4.3 Direct foaming method

In direct foaming methods, porous materials are produced by incorporating air into a suspension or liquid media, which is subsequently set in order to keep the structure of air bubbles created. In most cases, the consolidated foams are afterwards sintered at high temperatures to obtain high-strength porous ceramics.

Belonging to the direct-foaming technique, the gelcasting process is used to obtain foams with porosity levels up to 90% from ceramic suspensions. This process consists in vigorously stirring a slurry containing water-soluble organic monomers and a surfactant [33]. The polymerization reaction occurring among the monomer molecules enables the rapid stabilization of the wet foam, followed by drying and sintering of the ceramic particles [33-35]. Wet foams are, in fact, thermodynamically unstable systems in which processes such as drainage of the liquid phase and gas bubble coarsening lead to uncontrolled

increase in cell size and ultimately foam collapse by rupture of the liquid film. Gas diffusion occurs between bubbles of different size and consequently different concentrations of gas, due to the difference in Laplace pressure between them (Ostwald ripening), leading to the degradation of the foam structure governed by the reduction of the Gibbs free energy of the system [33]. To avoid this, surfactants can be used as surface-active agents for the stabilization of wet foams, because they stabilize the liquid-gas interface decreasing the surface tension of the system. These long-chain amphiphilic molecules adsorb at the gas bubble surface with their hydrophilic tail in contact with the aqueous phase. The foaming ability of a surfactant is related to its effectiveness to lower the interfacial energy or the surface tension at the gas-liquid interface. Surfactants are classified, according to the nature of the hydrophilic group, as anionic, cationic, non-ionic, and amphoteric [36].

In the case of a slurry containing geopolymer precursors, which has several ions in solution (K^+, Al^{3+}, Fe^{3+}, SiO_4^{2-}), non-ionic surfactants have a more pronounced effect since they possess hydrophilic groups without electric charges. The type of surfactant can influence the cell size, size distribution and degree of interconnection among adjacent cells (open/closed cell ratio). The wet foam can be rapidly gelled simply by exploiting the geopolymerization reaction itself, with no need for organic monomers or other stabilization/gelling additives.

2.5 Saponification

As it is well known, the hydrolysis of fat or oil in alkaline medium produces glycerol and fatty acid salts (soap) for cleaning purpose, for example, and the reaction is called saponification [37].

An example of this reaction is showed in Figure 2.5.

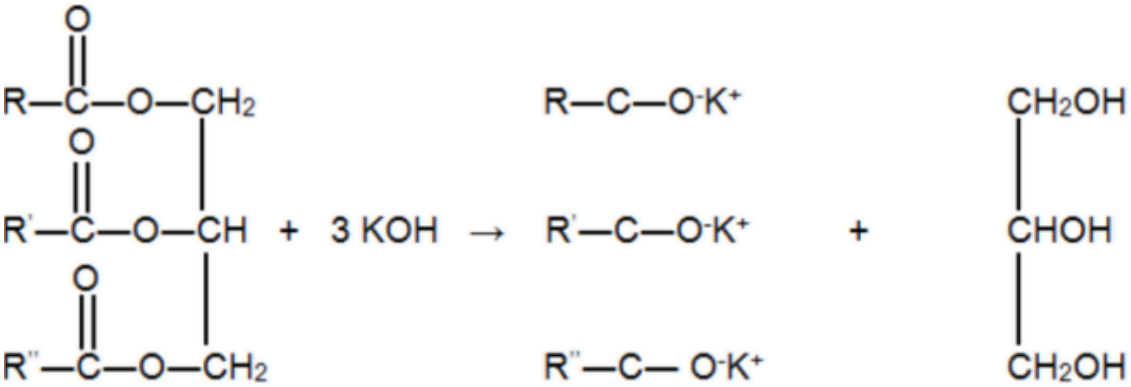

Figure 2.5 Saponification reaction of a triglyceride with KOH to form a mixture of potassium carboxylates (soap) and glycerol.

As suggested in the equation, soap is a salt composed of a mixture of carboxylate anions, due a variety of fatty acid residues in each triglyceride molecule, and a univalent cation provided by the alkaline medium.

Concerning the saponification reaction, one important analytical chemical parameter explored here, which should be quoted, is the saponification value (SV), that is linked to the average molecular weight of all fatty acids and represents the quantity in grams of potassium hydroxide required to saponify 1 g of oil [38].

Also, in the present work, this parameter (SV) was used to determine the amount of KOH which should be add with the oil to ensure the *in situ* formation of surfactant molecules by the saponification reaction.

2.6 Triglycerides sources

Vegetable oils and fats are mainly constituted of triglycerides that consist of one molecule of glycerol combined with three molecules of fatty acids. These latter contain a long chain of carbon atoms, linked by single bonds and combined with hydrogen, ending with carboxyl group. Fatty acids are almost entirely straight chain aliphatic carboxylic acids. The broadest definition includes all chain lengths, but most natural fatty acids are C_4 to C_{22}, with C_{18}

most common. Besides that, fatty acids can be divided into two classes: saturated and unsaturated. In the latter one or more couples of two adjacent carbon atoms are linked by a double bond. If there is more than one double bond, the fatty acid is polyunsaturated, as compared to monounsaturated when there is only one double bond [38].

Biodiesel is a mixture of fatty acid alkyl esters mostly produced from the transesterification of fats and oils. In this process, the triglycerides contained in the oil react with an alcohol, commonly methanol, and a catalyst, usually sodium hydroxide (NaOH), to yield fatty acid methyl esters [39].

Taking into account how the saponification reaction was applied here, there are some important attributes which represents a different aspect of the produced soap [40].

- ✓ Bubbly lather: refers to the soap's ability to lather up and get bubbly. Higher values will tend to produce fluffy foam rather than creamy foam with little or no bubbles, usually in the range from 14 to 46.
- ✓ Creamy lather: this value indicates the stability and creaminess of the lather. Usually, increasing bubbly will decrease creamy and vice versa. The higher creamy numbers will tend to produce a creamy lather with lesser amounts of bubbles or foams, usually in the range from 16 to 48.

3 MATERIALS AND METHODS

3.1 Materials

3.1.1 Gelcasting route (GCR)

Experiments were carried out using as geopolymer precursors metakaolin obtained from the calcination at 750°C for 6 hours in a muffle of kaolin (Minasolo - Minerals and Abrasives Grains (Brazil)), metakaolin HP Ultra (Metacaolim do Brasil (Brazil)), fly ash class F (#200 mesh; Tractebel Energia (Brazil)), and as alkaline activators commercial sodium hydroxide, potassium hydroxide KOH pellets (85% purity, Dinâmica Química Contemporânea Ltda (Brazil)), sodium silicate (Si/Na = 3.30, density = 1.39, viscosity = 420 cP, and potassium silicate (Si/K = 2.05, density = 1.38 g/l, viscosity = 430 cP; Una Prosil - Usina Nova América (Brazil)). Considering the high content of iron oxide (Fe_2O_3) present in the fly ash (10.2 wt%), a maximum addition of 30 wt% of fly ash with respect to metakaolin was used, because, as quoted by Lloyd et al. [5], during alkaline activation iron dissolves from iron-rich fly ash particles and forms either crystalline or colloidal hydrates.

In order to decrease the viscosity of the suspension, polyacrylic acid (Dolapix CE-64, Zschimmer & Schwarz) was used.

For the stabilization of the wet foams, two non-ionic surfactants were added in different amounts: Tween 80, a Polyoxyethylene 20 sorbitan monooleate - $C_{64}H_{124}O_{26}$ (VWR BDH Prolabo) and Triton X-100, a Polyethylene glycol tert-octylphenyl ether - $C_{14}H_{22}O(C_2H_4O)_n$,n = 9-10 (Sigma-Aldrich).

3.1.2 Gelcasting / Saponification / Peroxide Combined Route (GCSPCR)

For this route, samples were produced using the same raw materials described previously (GCR), up to the surfactant addition. Other components

were also used as sources of different triglycerides: sunflower oil, olive oil, babassu oil, coconut oil, castor oil, palm stearin, bovine lard, soybean biodiesel and hydrogen peroxide (10 vol.), to contribute to the macro-pore formation.

With the aim to show the efficiency of the proposed technique, sunflower oil foams were also produced with *i)* the addition of oil but no hydrogen peroxide (saponification reaction) and *ii)* with the addition of hydrogen peroxide but no oil (peroxide reaction). To make this comparative test, hydrogen peroxide and sunflower oil were added always in the same amounts specified previously.

Prior to the characterization, the glycerol generated by the saponification reaction was extracted by hot water exchanging it every 30 minutes until it remained clear, visually indicating complete extraction. This step of the extraction of glycerol can also be used to confirm the extent of the geopolymerization reaction, since non-fully condensed geopolymer materials are sensitive to water and undergo swelling or complete destruction [3]. Also, glycerol and others organic compounds could be extract by heat treatment.

3.2 Methods

Since the experimental development proposed here was done in three steps as follows:

- ✓ First step (Brazil): was done all initial characterization of raw materials and formulation of the geopolymer, presented in Appendix A;
- ✓ Second step (Italy): studied and applied the gelcasting route (GCR) in order to obtain open-cell geopolymer foams;
- ✓ Third step (Italy / Brazil): studied and applied the gelcasting / saponification / peroxide combined route (GCSPCR).

All methodology will be present and discussed according the two routes studied.

In the same way, always according the applied route, were evaluated some physical properties of the geopolymer foams, without any comparative intent, but to understand and set the process parameters and respective effect on the reached properties in each route.

3.2.1 Gelcasting route (GCR)

The first step in the preparation the geopolymer foams was the preparation of a 15 M KOH solution, which should be used after 24 hours [41]. Then, a solution of potassium-based activators and distilled water was prepared in a mixer (500 rpm, 30 minutes, Ika-Werke Ost Basic, Staufen, Germany), following the oxide molar ratios presented in Table A.7. To this solution, Dolapix CE-64 was added (0.32 wt% on the total weight). Then, MSMK and FA were added at room temperature to the activator solution, stirring at 1000 rpm for 30 minutes, producing suspensions with a solid content ranging from 61 to 71 wt%.

The geopolymer precursor suspension was placed in an oven at 80ºC for 20 minutes to initiate the geopolymerization reaction, which is the key to enabling the retention of porous morphology of the wet foam subsequently produced. Thereafter, the suspension was removed from the oven and stirred again while adding dropwise one of the surfactants.

Surfactant addition ranged from 2 to 4 wt% with respect to total weight, and the suspension was stirred at different mixing velocities (800, 1500 and 2000 rpm for 5 minutes) in order to generate wet foams by the entrapment and stabilization of air bubbles.

Finally, the geopolymer foam was cast in a polystyrene mold and placed for 1h at 80ºC into an oven after sealing it into a plastic bag. The sample was then removed from the plastic bag and left at 80°C for further 4 hours. It should be noted that the samples were characterized as prepared, and were not subjected to any heat treatment at high temperature. If necessary, the produced components could be heat treated up to 1200°C in air without melting. Figure

3.1 shows the flowchart of process used for fabricating geopolymer foams by gelcasting.

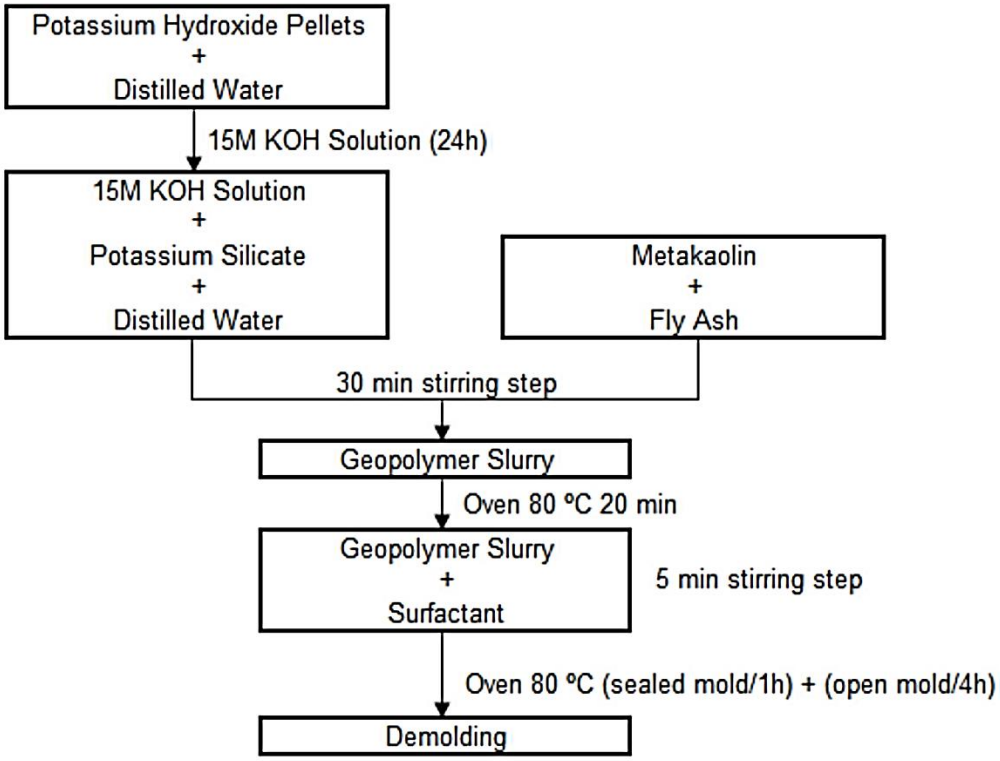

Figure 3.1 Schematic diagram for the production of geopolymer foams by gelcasting route [42].

Geopolymer foams were heat treated in a tube furnace (Carbolite CWF1200, Derbyshire, UK) at 700 and 1200°C in air with heating rate of 2 1°C/min, dwelling time of 2 h and cooling rate of 10°C/min, in order to assess how the physical properties of the geopolymer foams were affected by the thermal treatment.

3.2.1.1 Total and open porosity

The bulk density of the geopolymer foams was computed by dividing the mass of foam cut into a parallelepiped divided by its geometric volume measured, with a caliper. The total pore volume (X_p) was obtained based on the equation 2.1, where ρ_0 is the true (skeleton) density of the pore-free solid

material [43], measured with an helium pycnometer (Accupyc 1330, Micromeritics, Norcross, GA), and also, the open porosity was quantified by “Archimedes” Principle.

$$X_p = 100 \times \left(1 - \frac{\rho}{\rho_0}\right) \quad (3.1)$$

3.2.1.2 Mechanical strength

The compressive strength of as prepared samples was determined using a Universal Testing Machine (Instron 1121, Canton, Massachusetts, USA), with a constant crosshead displacement of 1 mm/min. At least 5 specimens per type were tested.

3.2.1.3 Permeability

The air-permeation behavior of porous geopolymers was investigated at room temperature using a laboratory-made air permeator at the Istituto Nazionale di Fisica Nucleare, Laboratori Nazionali di Legnaro (INFN-LNL), Italy, which is based on an action-response device, making a correlation between the pressure drop applied across a porous medium and the resulting flow rate or velocity of the fluid output [44]. Experiments were carried out on disk-shaped samples, which were tightly fixed with rubber rings inside the sample holder that provided a useful flow diameter of 1.99 mm with air flow, allowed to flow upward through the disk, at room temperature (20–24°C) and atmospheric pressure (1 atm). Pressure drop (ΔP) across the disk was measured by either one of two digital manometers (Greisinger Electronic GmbH, Regenstauf, DE, model GMH 3161-01 CE, range 0–25 mbar, resolution of 0.01 mbar and model GMH 3161-13 CE, range 0–2000 mbar, resolution of 1 mbar) and the resulting volumetric air flow rate across the disk was measured by a laboratory made soap-bubble

flow meter with useful volume of 50 mL and resolution of 0.1 mL. At least 20 sets of pressure drop and flow rate curves were acquired in steady-state conditions to ensure an accurate fitting analysis.

3.2.1.4 Morphological analysis

The morphology of the foams was investigated using an optical stereoscope (Wild Heerbrugg, Type 376788, coupled with a digital camera) and a Scanning Electron Microscopy (SEM, FEI Quanta 200, Hillsboro, Oregon, USA).

The pore size distribution was evaluated from the acquired images using the Axio Vision 4.8.2 LE image processing software (Carl Zeiss, Oberkochen, Germany).

Values obtained by image analysis were converted to 3D values using the stereological equation (3.2), in order to determine the effective cell-size [45].

$$D_{sphere} = \frac{D_{circle}}{0.785} \tag{3.2}$$

3.2.1.5 Specific surface area

The Brunauer-Emmett-Teller specific surface area (SSA) was determined by multipoint BET method using the adsorption data in the relative pressure (P/P_0) range 0.05–0.3 obtained by a Quantachrome Nova Station A (Quantachrome Instruments, Boynton Beach, USA).

All the samples were degassed at 300°C prior to nitrogen adsorption measurements.

3.2.1.6 Linear thermal shrinkage

A dilatometer (DIL 402 PC, Netzsch, Selb, DE) was used to measure the shrinkage of the geopolymer up to 1250°C in air with heating rate of 10°C/min.

3.2.1.7 TG/DTA analysis

TG/DTA analysis was performed by a Simultaneous Thermal Analyzer (STA 409, Netzsch, Selb, DE) up to 1400°C in air with heating rate of 10°C/min.

3.2.2 Gelcasting / saponification / peroxide combined route (GCSPCR)

When the vegetable oil is added to the highly alkaline geopolymer suspension (pH ~9.5), it generates *in situ* carboxylate surfactants (soap molecules) through the saponification reaction, which consists of the hydrolysis of the triglycerides found in oils or fats, plus glyceride, a water soluble molecule (glycerol) which can be extracted by water after the curing process [63]. While previous work exploited the formation and extraction of glycerol to create micro- and meso-pores increasing the specific surface area of the material, we used the surfactant molecules (produced *in situ*) to generate stable wet macrocellular foam with interconnected porosity, obtained by stirring (direct foaming, aided by the gas generated from the decomposition of the peroxide, followed by gelcasting to set the structure).

For this route, samples were produced using the same raw materials described previously (GCR), up to the surfactant addition. Thereafter, the suspension was removed from the oven and then 25 wt% of triglyceride source

(oil or fat) and respective amount of KOH solution, considering the SV, were added, mixing at 500 rpm for 5 minutes. Then, the combined suspension was placed in an oven at 80ºC for 30 minutes, being stirred again at 1500 rpm for 5 minutes, and then 6 wt% of hydrogen peroxide was added.

Finally, the geopolymer foam was cast in a polystyrene mold and placed for 1h at 80ºC into an oven after sealing it into a plastic bag, and then removed from the plastic bag and left at 80°C for further 4 hours.

The process is illustrated in Figure 3.2.

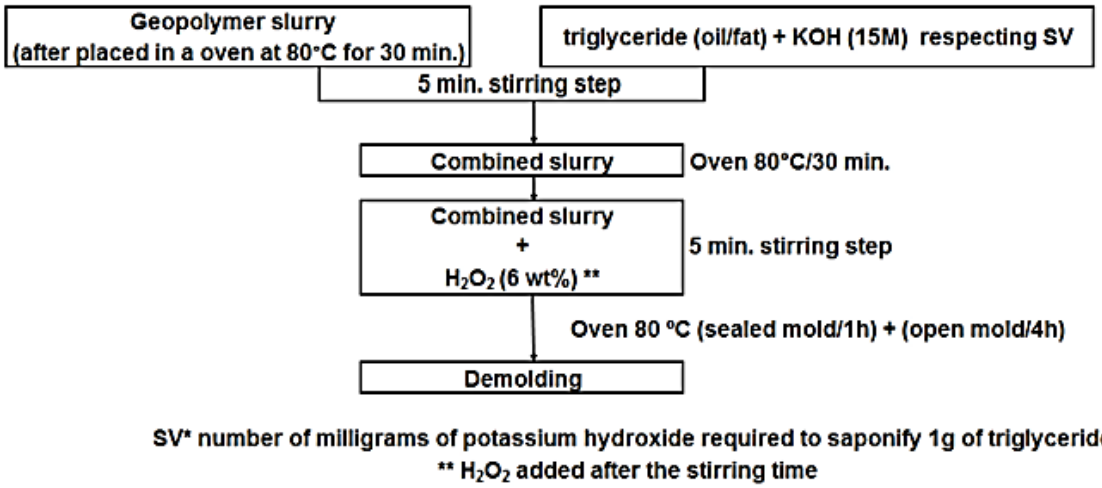

Figure 3.2 Schematic diagram for the production of geopolymer foams by gelcasting/saponification/peroxide combined route [46].

To this route, the same set of physical properties evaluated in gelcasting route was performed, only changing the equipments, since this study was completed in Brazil.

Geopolymer foams were heat treated in box furnace (Lindberg / Blue M BF511732C, Asheville, USA) at 300, 600, 900 and 1200°C in air with heating rate of 2°C/min, dwelling time of 2 h and cooling rate of 10°C/min, in order to assess how the physical properties were affected by the thermal treatment.

3.2.2.1 Total and open porosity

Both total and open porosity were evaluated similarly that to the GCR, even using a helium pycnometer of the same make and model to measure the true density.

3.2.2.2 Mechanical strength

The compressive strength of as prepared samples was determined using a Universal Testing Machine (Instron 5500R, Canton, Massachusetts, USA), with a constant crosshead displacement of 1 mm/min. At least 5 specimens per type were tested.

3.2.2.3 Permeability

Likewise to the GCR, the air-permeation behavior was investigated at room temperature using a laboratory-made air permeator at University of Ribeirão Preto / UNAERP (Brazil).

3.2.2.4 Morphological analysis

The morphology of the foams was investigated using an Olympus LEXT OLS4000 3D Laser Measuring Microscope, which was used also to evaluate the pore size distribution, and a Scanning Electron Microscopy (SEM, FEI Quanta 200, Hillsboro, Oregon, USA). As previously mentioned, values obtained by image analysis were converted to 3D values using the stereological equation (3.2), in order to determine the effective cell-size [45].

3.2.2.5 Specific surface area

The Brunauer-Emmett-Teller specific surface area (SSA) was determined by multipoint BET method using a Quantachrome Nova 1000e (Quantachrome Instruments, Boynton Beach, USA).

3.2.2.6 Linear thermal shrinkage and TG/DTA analysis

Considering that these characteristics are intrinsically related to the materials and not with the processing route, and were adopted the same geopolymer base composition, these measures were not repeated and were considered results previously obtained for the GCR.

4 RESULTS AND DISCUSSIOIN

Likewise presented in the Materials and Methods section, the achieved results will be also presented according the used route.

4.1 Gelcasting route (GCR)

4.1.1 Total and open porosity

With the aim of producing components possessing a high amount of total porosity, we first evaluated the influence of the solid content in the slurry on this feature, maintaining fixed all other parameters to a specific value, which was set according to preliminary optimization experiments (surfactant content = 2 wt%; mixing speed = 1500 rpm).

In Figure 4.1 are presented the data which indicate that, as expected, with increasing the solid content in the suspension a reduction in total porosity occurred for both types of surfactant, because of the increase in viscosity in the slurries. We can observe that Triton X-100 appeared to be more effective in incorporating and maintaining a large amount of gas into the liquid, which led to a larger amount of total porosity after gelling and drying. This behavior is certainly related to the difference in the chemical structure of the two surfactants, but further investigations are necessary to determine the accurate acting mechanism and others differences among them.

Early stability theories assumed that the foam stability was determined by the adsorbed surfactant which controlled the mechanical–dynamical properties of the surface layer (surface tension gradients) [47]. Also, important parameters to be taken into consideration are the surface viscosity, surface occupancy, gravity drainage and capillary suction.

Considering these aspects, Gibbs and Marangoni [47] proposed two theories of elasticity for surfactant solutions, both dealing with the surface

elasticity effect caused by different mechanisms. In this sense, surfactants with different chemical structure and foaming properties can notably influence the microstructure of porous scaffold prepared by the direct foaming method.

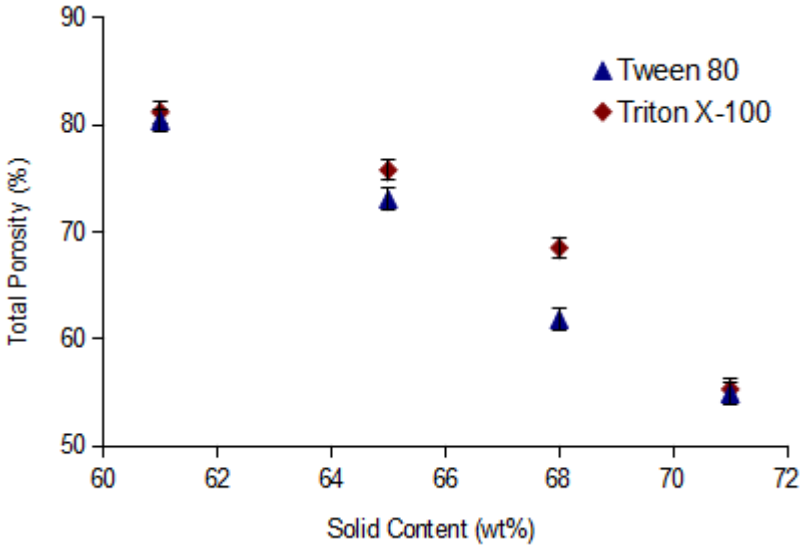

Figure 4.1 Effect of solid content in the slurry on total porosity. All samples were produced using 2 wt% of surfactant and mixing at 1500 rpm mixing speed.

The solid content of the slurry was set at 68 wt% to evaluate the effect of the mixing speed (800, 1500 and 2000 rpm) for two amounts of surfactant (2 and 4 wt%).The results are reported in Figure 4.2. which shows that, again, samples produced withTritonX-100 surfactant possessed a higher total porosity, in comparison to those produced using Tween 80. With increasing mixing speed, the total amount of porosity decreased, and no significant difference between the two types of surfactant used as well as their amount was observed. The overall change in porosity was about 8 vol% in all cases, when going from 800 to 2000 rpm and both for 2 or 4 wt% of surfactant, and the decrease in porosity was particularly limited (15 vol%) when increasing mixing speed from 800 to 1500 rpm. The reason for this could be ascribed to an increase of shear stress in the suspension at higher rotational speed, which resulted in a lower total volume of entrapped air into the suspensions [48-50].

As far as the amount of surfactant was concerned, the data indicate that, regardless of the mixing speed used, an average increase in total porosity

was achieved when passing from 2 to 4 wt% of surfactant addition, which was of 10% for samples produced using Tween 80 and of 15% for those made using Triton X-100. Increasing the surfactant concentration favors its adsorption at the gas/liquid interface and decreases the surface tension, thereby promoting foaming.

For a certain concentration $C_{max,}$ the surface tension is minimal and foaming is maximum. This concentration is close to the critical micelle concentration (CMC), which represents the minimal surfactant quantity to reach the minimal surface tension. For higher concentrations, the surface tension remains minimal, but the addition of more surfactant will generate an increase in the viscosity of the system, which inhibits the foaming effect [51].

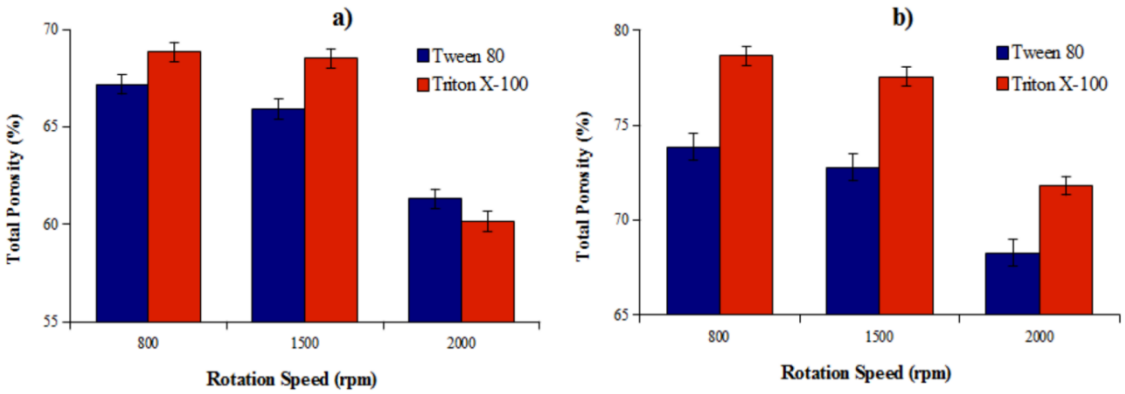

Figure 4.2 Effect of rotation speed and surfactant content in the slurry (solid content set at 68 wt%); a) 2 wt% surfactant; b) 4 wt% surfactant.

Figure 4.3 reports the total and open porosity values for the samples investigated in this study, showing that, for a surfactant content of 2 wt%, an open porosity in the range of 52 vol% for Tween 80 and of 46 vol% for Triton X-100 was generated. Similarly, for a surfactant addition of 4 wt%, the open porosity was in the range of 56 and 54 vol% for Tween 80 and Triton X-100, respectively. These results confirm that surfactants with different chemical structure and foaming ability can influence the microstructure of porous geopolymers fabricated by gelcasting.

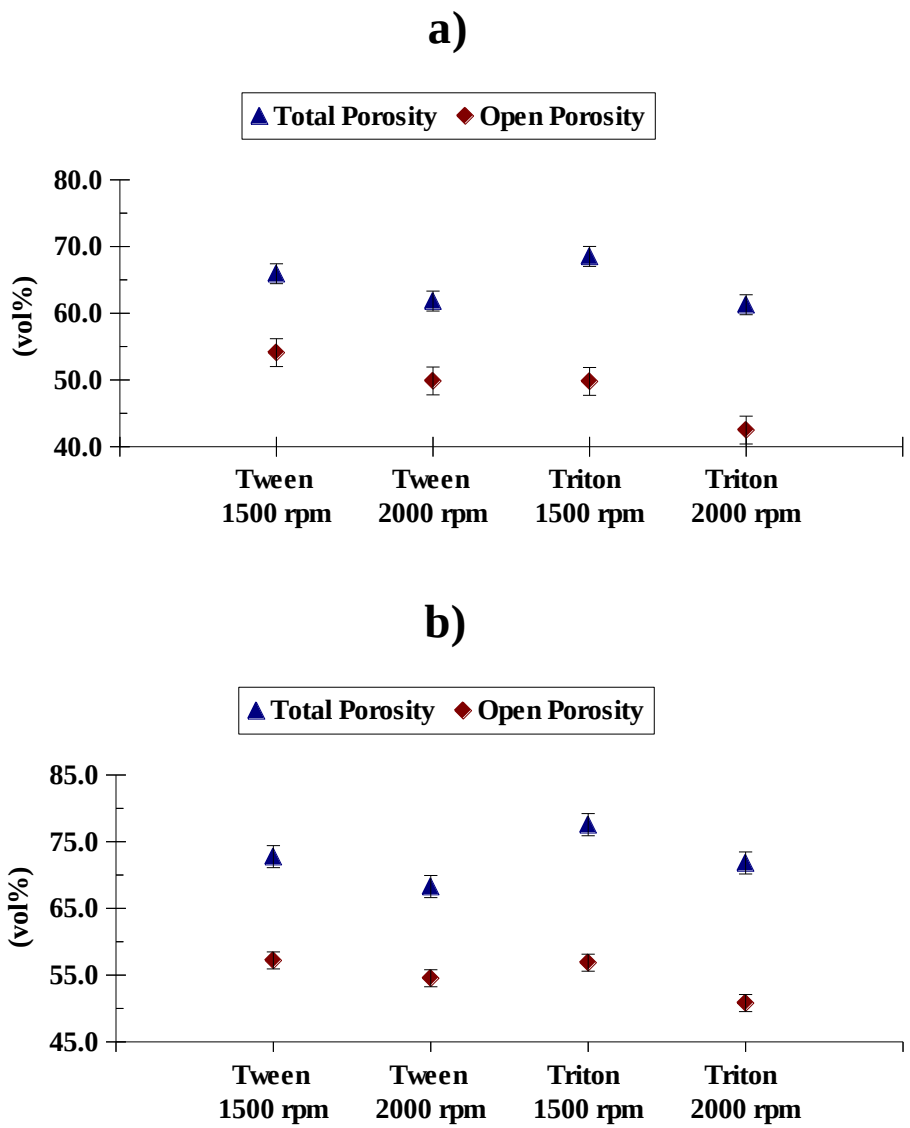

Figure 4.3 Relation between total porosity and open porosity estimated by the Archimedes Principle; surfactant content set at 2 wt% (a) and 4 wt% (b).

Additionally, the data indicate that the Tween 80 surfactant was a more effective surfactant, as in all cases its use led to smaller cell sizes indicating the more effective reduction in surface energy of the liquid/gas interfaces in the geopolymer foams, enabling to stabilize a larger amount of bubble surfaces.

It is also important to observe that the processing parameters (slip rheology, foam volume, type of surfactant, idle time prior to polymerization, and other features) affect also the ratio between open and closed cells in the foams [56, 57]. Moreover, foams with different characteristics (total porosity, average cell size and size distribution) possess a different average strut thickness, which results in different mechanical properties.

The heat treatment at 700°C had no pronounced effect on the amount of total porosity, as showed in Figure 4.4 for samples prepared using 2 wt% (a) and 4 wt% (b) of surfactant, respectively. However, increasing the heat treatment temperature up to 1200°C led to a ~6.0 to 20.0 vol% decreases in the total porosity, depending on the type and content of surfactant.

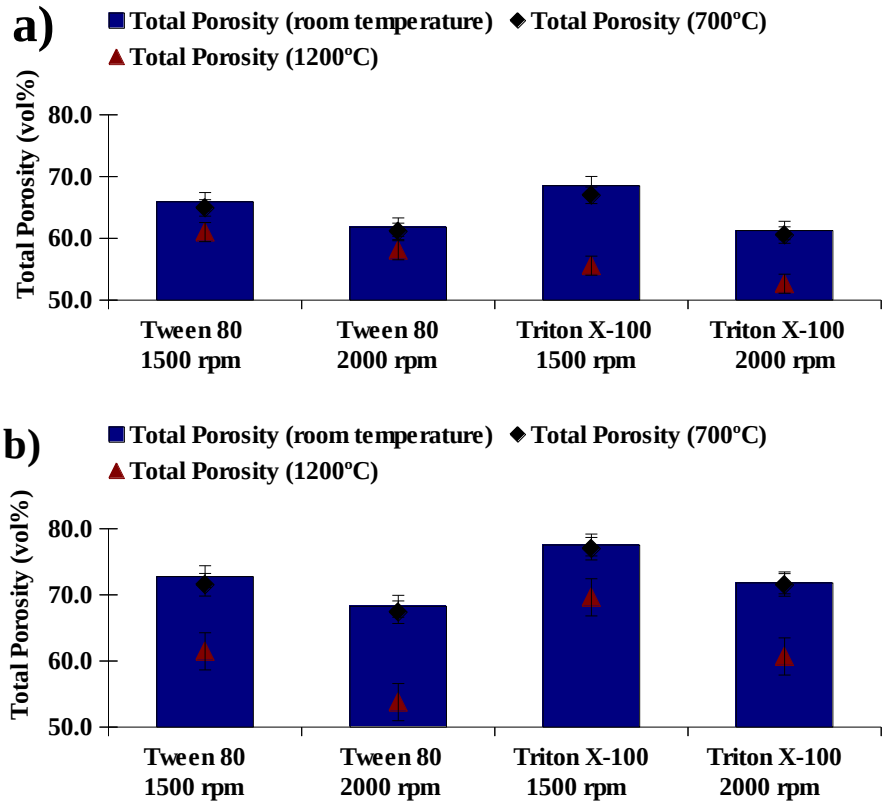

Figure 4.4 Total porosity as a function of the heat treatment of geopolymer foams: (a) 2 wt% of surfactant; (b) 4 wt% of surfactant.

4.1.2 Mechanical strength

The correlation between compressive strength, relative density and total porosity of the geopolymer foams is shown in Figure 4.5. For samples produced using 2 wt% of Tween 80 (Figure 4.5a), an increase of ~41% in the compressive strength (from 2.35 to 3.32 MPa) was observed when the total porosity decreased ~6% (from 66 to 62%). This decrease on the total porosity was accompanied by a ~18% increase of the relative density (from 0.75 to 0.85). Also, samples produced using 2 % of Triton X-100 as a surfactant had a similar behavior, with similar changes in property values: ~40% increase (from 1.94 to 2.72 MPa) for the compressive strength; ~10% decrease (from 69 to 61%) for the total porosity, and ~26% increase (from 0.69 to 0.87) for the relative density.

This trend was more pronounced for samples produced using 4 wt% of surfactant (see Figure 4.5b). For Tween 80, a ~84% increase (from 0.97 to 1.79 MPa) for the compressive strength was observed, when the total porosity decreased ~6% (from 72 to 68%), with an associate ~28% increase (from 0.47 to 0.60) in the relative density. For Triton X-100, a ~64% increase (from 0.45 to 0.74 MPa) of the compressive strength was observed when the total porosity decreased ~7% (from 77 to 72%), with an associate ~26% (from 0.49 to 0.62) increase in the relative density. Such behavior can be explained considering that the compressive strength of porous materials is depending on the amount of solid material present in each sample, represented by the relative density, and is also affected by the average pore size, with decreasing strength with increasing pore size [60]. The highest values of compressive strength for the Tween 80 surfactant could be explained by its different chemical composition and behavior, resulting in a higher densification of the struts (see later). We should also remember that the strength of porous ceramics increases with decreasing cell size, and therefore the effect of surfactant on cell size would also play a role in controlling the strength of the components. Tween 80 surfactant was shown to produce smaller cell sizes than Triton X-100, at least for some processing conditions [61]. Regarding this feature, investigations on

the strength of samples produced with 2 wt% of Tween 80 (2000 rpm) indicate an increase of ~14% in the compressive strength (from 3.32 ± 0.40 to 3.97 ± 0.40 MPa) and ~184% (from 3.32 ± 0.40 to 9.44 ± 0.30 MPa) after heat treatment at 700 and 1200°C respectively.

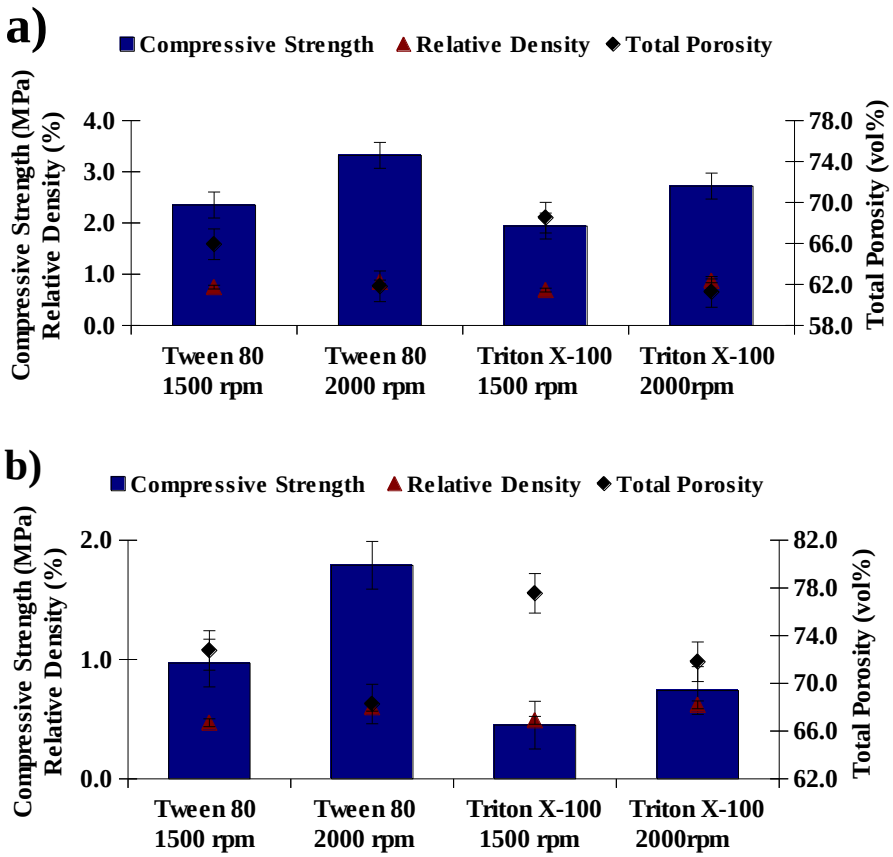

Figure 4.5 Correlation among compressive strength, relative density and total porosity of geopolymer foams. (a) 2 wt% of surfactant; (b) 4 wt% of surfactant.

4.1.3 Permeability

The permeability measurement results were treated according to Forchheimer's equation (4.1), which describes the flow resistance through

porous media for a wide range of fluid velocities [58], and the permeability coefficients k_1 (Darcian) and k_2 (non-Darcian) were evaluated according to Darcy's law which sets a linear dependence between ΔP and v_s [44, 59]:

$$\frac{\Delta P}{L} = \frac{\mu}{k_1} v_s + \frac{\rho}{k_2} v_s^2 \quad (4.1)$$

where L is the medium thickness along flow direction, v_s is the superficial velocity, μ is the absolute viscosity, ρ is the fluid density, k_1 (Darcian) and k_2 (non-Darcian) the permeability coefficients.

According to the equation 4.1 the term $\mu v_s/k_1$ represents the viscous effects of the fluid-solid interaction, whereas the term $\rho v_s^2/k_2$ represents the kinetic effects [59]. Fluid loses energy through viscous effects according to two ways: 1) by friction between the molecules of the fluid during draining; in this case, the higher the viscosity of the fluid (μ), the greater the friction will be and consequently the conversion of pressure energy into heat. 2) by friction between the fluid and the porous wall. Here, the contact area between them, represented by k_1, quantifies this loss of energy of the fluid. Higher the contact area, greater the resistance to fluid flow. Usually, the increase in area is associated with the reduction of particle size for granular structures or of pore size for cellular structures [59]. Besides that, any change in the processing parameters, which leads to an increase of the interconnected porosity and pore size, or the decrease of pore tortuosity and roughness, will lead to higher values of k_1 and k_2 [44].

Derived from the Kozeny–Carman or Ergun relationships [44], notwithstanding the limited validity for specific porous medium properties, the typical proportionalities between porosity P and the coefficients k_1 and k_2 may be described by the following relations (4.2 and 4.3):

$$k_1 \propto \frac{P^3}{(1-P)^2} \quad (4.2)$$

$$k_2 \propto \frac{P^3}{(1-P)} \quad (4.3)$$

Knowing the porosity of the material and applying these proportionalities (relations 4.2 and 4.3), it is possible to evaluate the permeability behavior of porous geopolymers and also to assess whether the coefficients measured are consistent with the underlying theory.

The permeability constants of geopolymer foams produced with different surfactants (type and content) and different mixing speed are compared in Figure 4.6, as a function of open porosity. An inversely proportional behavior can be observed, in accordance with the previous comments. This suggests that the amount of open and closed porosity was slightly different in the various samples. In Figure 4.6(a), for samples produced using a surfactant addition of 2 wt%, we can observe that an 8% increase in the open porosity (from 50 to 54%) led to a 2 and 3 orders of magnitude increase in k_1 and k_2 values, respectively, when using Tween 80. Likewise, when using Triton X-100 as a surfactant, a ~16% increase (from 43 to 50%) in the open porosity also led to an increase of 2 and 3 orders of magnitude in k_1 and k_2 values. Considering a surfactant addition of 4 wt%, Figure 4.6(b), an increase of ~6% in the open porosity (from 54 to 57%) led to an increase of 1 and 2 orders of magnitude in k_1 and k_2 values, respectively, when using Tween 80. Similarly, an increase of ~12% in the open porosity (from 51 to 57%) led to an increase of 1 order of magnitude for both, k_1 and k_2 values, when using Triton X-100 as a surfactant. This increase in the k_1 and k_2 values can be attributed due to the increase of the interconnected porosity (open porosity), as previously mentioned [44].

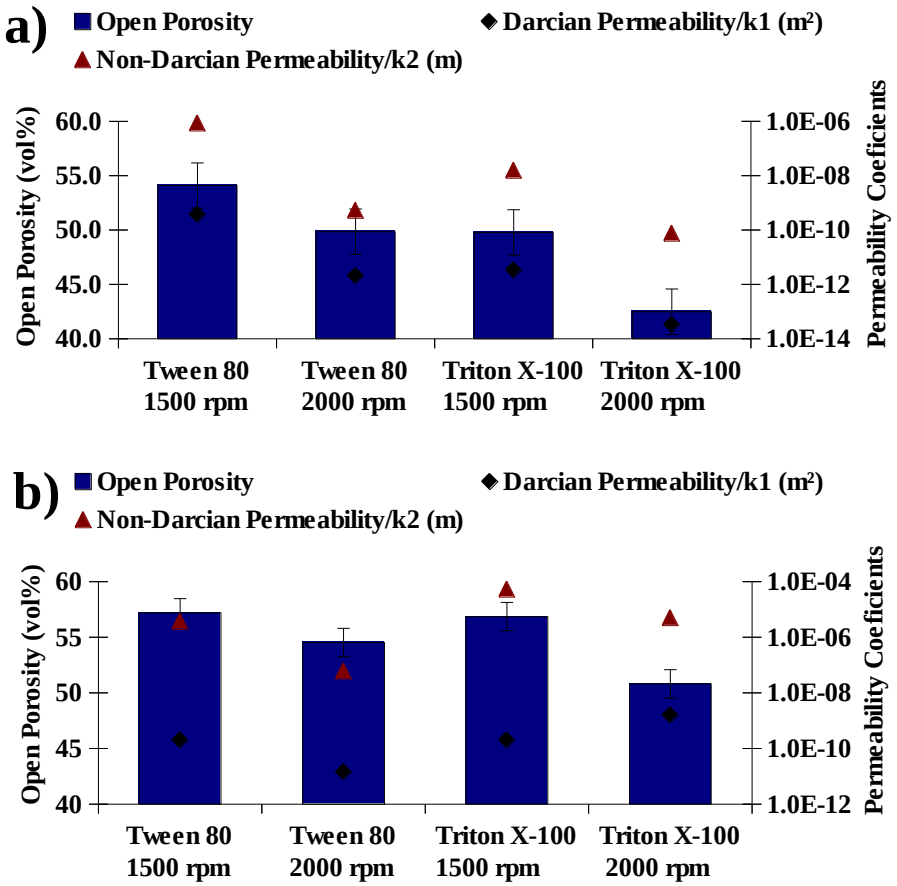

Figure 4.6 Permeability constants (k_1, k_2) of geopolymer foams produced with different surfactants (type and content) and different mixing speeds, as a function of open porosity estimated by the Archimedes Principle. (a) 2 wt% of surfactant; (b) 4 wt% of surfactant.

As shows Figure 4.7, this geopolymer foams presents similar behavior to those ceramic foams obtained by gelcasting, being suitable to replace ceramic components for use in filtration or adsorption applications.

The dispersion of the values shown in Figure 4.7 is the result of variations in process parameters (type and surfactant content, and mixing speed).

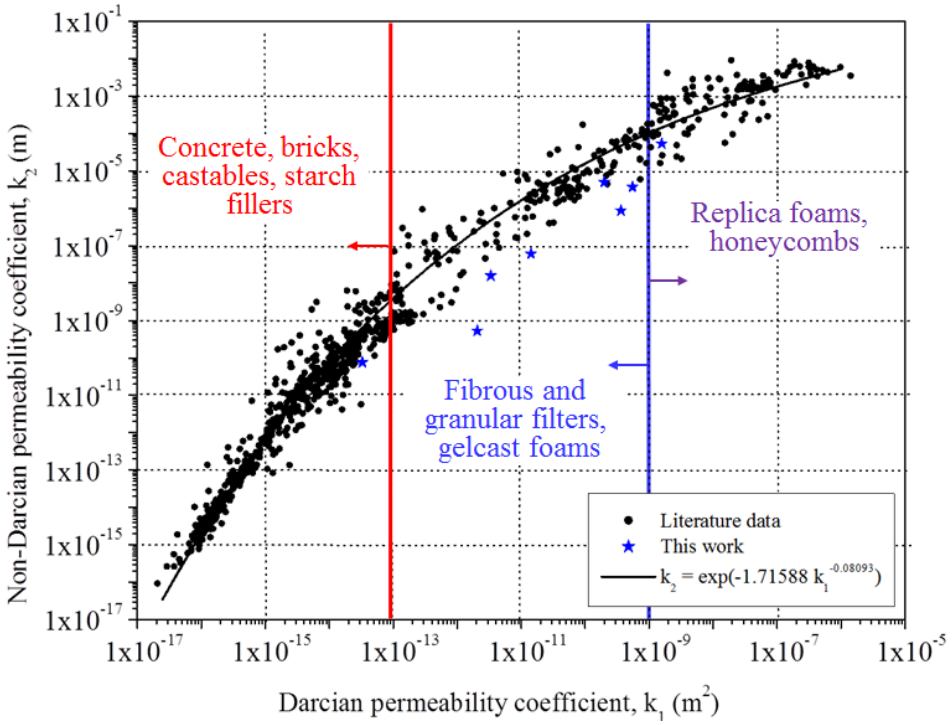

Figure 4.7 Location of k_1 and k_2 data for geopolymer foams obtained by gelcasting in a comprehensive permeability map [44].

4.1.4 Morphological analysis

When considering the effect of processing parameters (mixing speed, surfactant type and amount) on the morphology of the geopolymer foams, we observed that the samples possessed a different average cell size and size distribution depending on how they were obtained. Figures 4.8 and 4.9 show the optical images, taken at low magnification, illustrating the general morphology of the samples and report the cell size distribution computed by image analysis for each sample. Firstly, we can observe (see Figure 4.8) that when increasing the mixing speed from 1500 to 2000 rpm, the average cell size D_{50} decreased by 20% (from 345 ± 34 to 272 ± 36 µm) for samples produced using 2 wt% of Tween 80, and by 26% (from 463 ± 80 to 338 ± 53 µm) for samples produced using 2 wt% of Triton X-100.

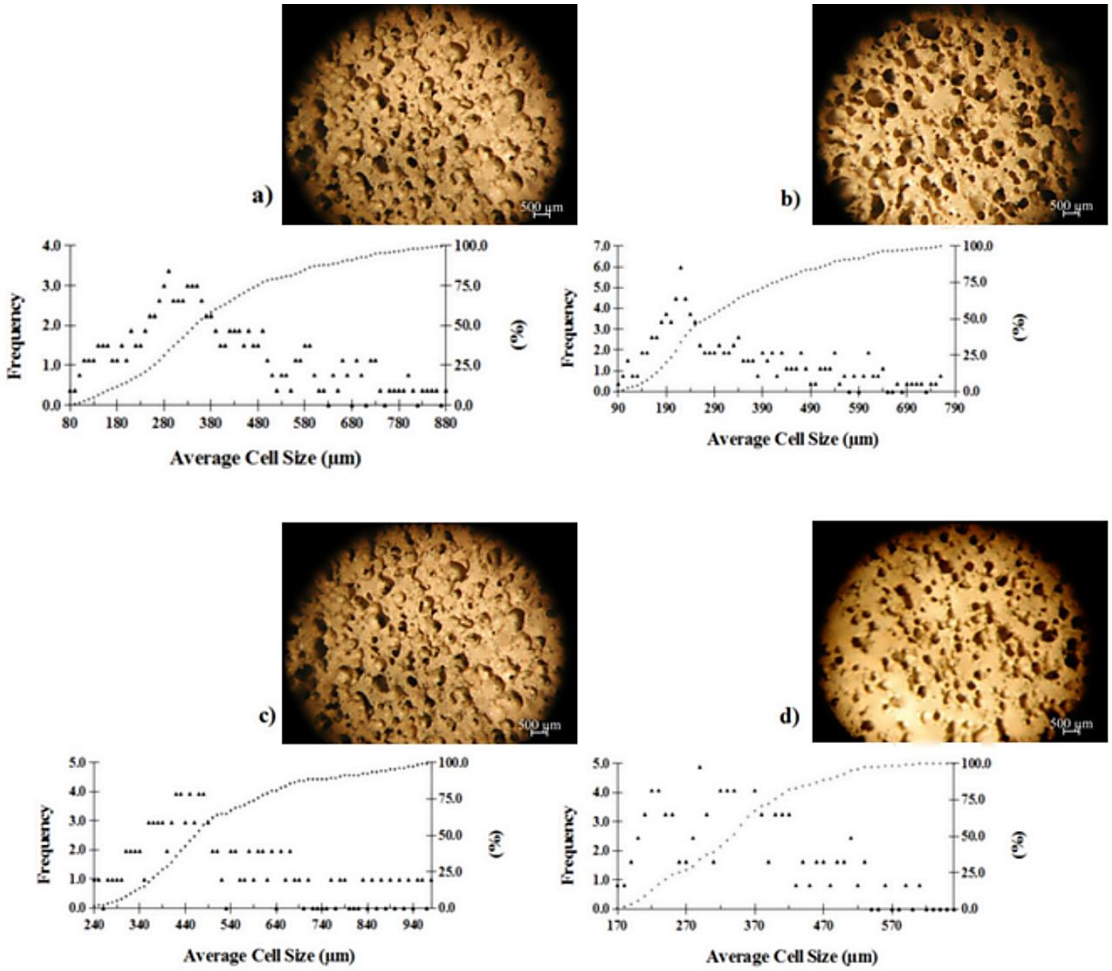

Figure 4.8 Effect of mixing speed on the average cell size and cell size distribution of samples produced using 2 wt% of surfactant (solid content set at 68 wt%). a) Tween 80, 1500 rpm; b) Tween 80, 2000 rpm; c) Triton X-100, 1500 rpm; d) Triton X-100, 2000 rpm. In the insets are shown the pore size distribution for each sample.

A similar decrease in D_{50} value (~25%, from 555 ± 90 to 453 ± 86 µm for samples made using Tween 80 and ~ 13%, from 530 ± 113 to 459 ± 90 µm for samples made using Triton X-100) occurred also for samples produced using a surfactant amount of 4 wt% (see Figure 4.9). This effect was also observed when producing liquid foams, and considering the stresses applied to the slurry by the mechanical shearing processes the Taylor model can be used to explain the rheological behavior and respective cell size obtained [52-54].

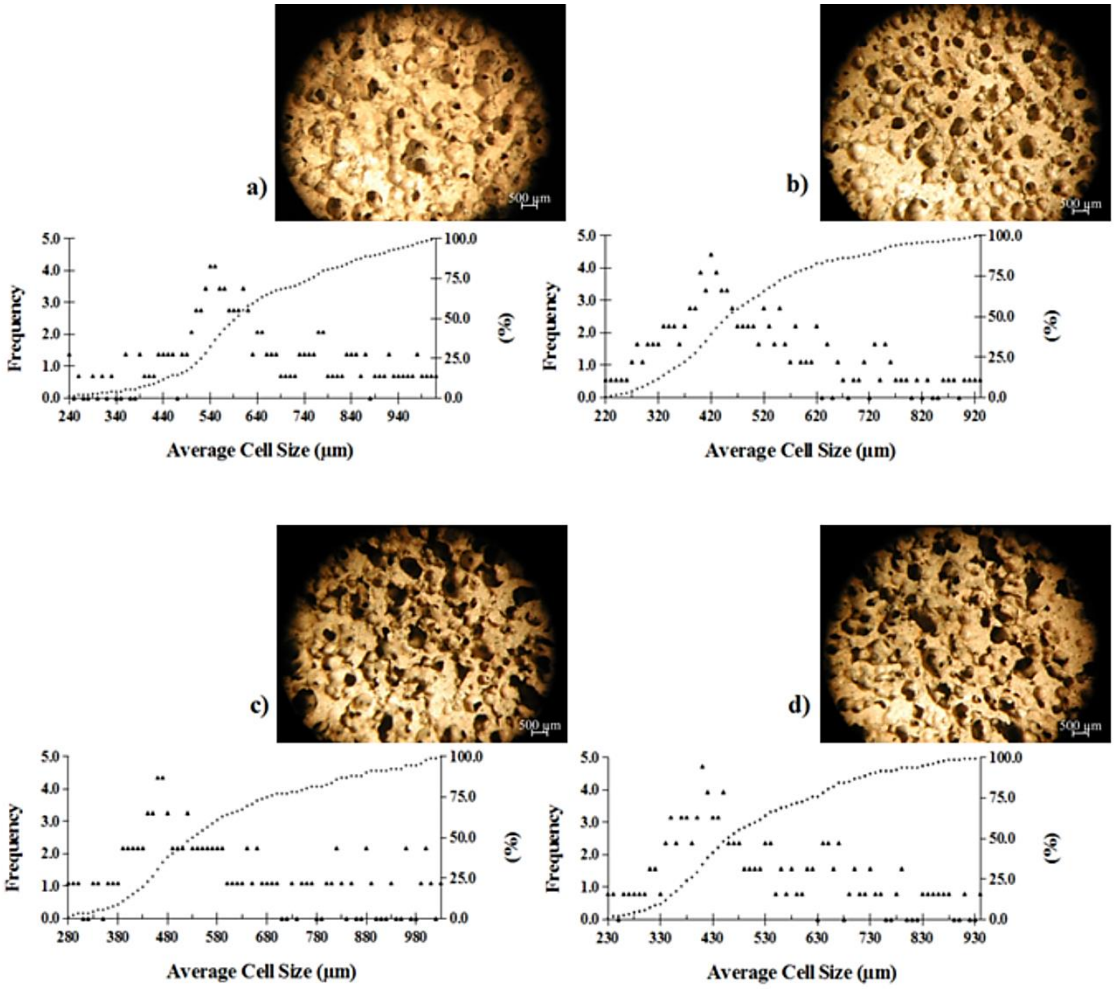

Figure 4.9 Effect of mixing speed on the average cell size and cell size distribution of samples produced using 4 wt% of surfactant (solid content set at 68 wt%). a) Tween 80, 1500 rpm; b) Tween 80, 2000 rpm; c) Triton X-100, 1500 rpm; d) Triton X-100, 2000 rpm. In the insets are shown the pore size distribution for each sample.

This model illustrates that, when an isolated, spherical droplet of radius R_0 with a relatively low viscosity η_d is dispersed in a fluid of higher viscosity η_c, the droplets will deform into an ellipsoid or elongated cylinder. Ordinarily, the rupture of these elongated cylinders in smaller droplets is achieved when reaching the so-called Rayleigh instability, which reduces the high interfacial energy possessed by the elongated droplets. Deformation of the dispersed phase only takes place when the shear stress $\eta_c\gamma$ exceeds the interfacial stress σ/R_0, where γ is the shear rate and σ is the interfacial tension.

The ratio between these two stresses is defined by the capillary number (Ca). When the capillary number overcomes a critical value Ca_{crit}, the elongated droplet will rupture into smaller droplets of average radius *R* according to equation (4.4). In this sense, Ca_{crit} depends on the viscosity ratio between the dispersed and continuous phase (η_d/η_c) and the type of flow [54, 55].

$$R \propto Ca_{crit}\frac{\sigma}{\eta_c \gamma} \tag{4.4}$$

This model has also been applied for the prediction of bubble size as a function of suspension composition for both, particle-stabilized emulsions and surfactant stabilized emulsions [55].

Secondly, it is possible to observe an inverse relation between the average cell size and the relative density, as shown by Figure 4.10 for a definite set of processing conditions. Specifically, at the same mixing speed of 1500 rpm, increasing the surfactant amount from 2 to 4 wt% increased the D_{50} nearly by 61% for samples produced using Tween 80, and about by 15% for samples produced using Triton X-100, while at the same time the relative density decreased by 20% and 28%, respectively. Also, the number of macropores increased further and the mean pore diameter also increased, causing the majority of pores to share pore edges and the interconnectivity to increase. This behavior is related to the increased foam volume obtained after stirring a slurry with 4 wt% of surfactant with respect to a slurry with 2 wt% of surfactant, processed at the same mixing speed. In this work, an increase in the volume of the wet foam on the order of 2 and 3 times with respectively 2 wt% and 4 wt% surfactant content was observed for both surfactants, regardless of the mixing speed. The volume of the wet foam is the first indication that the greater the volume obtained in the foam is, the greater the average pore size becomes [54].

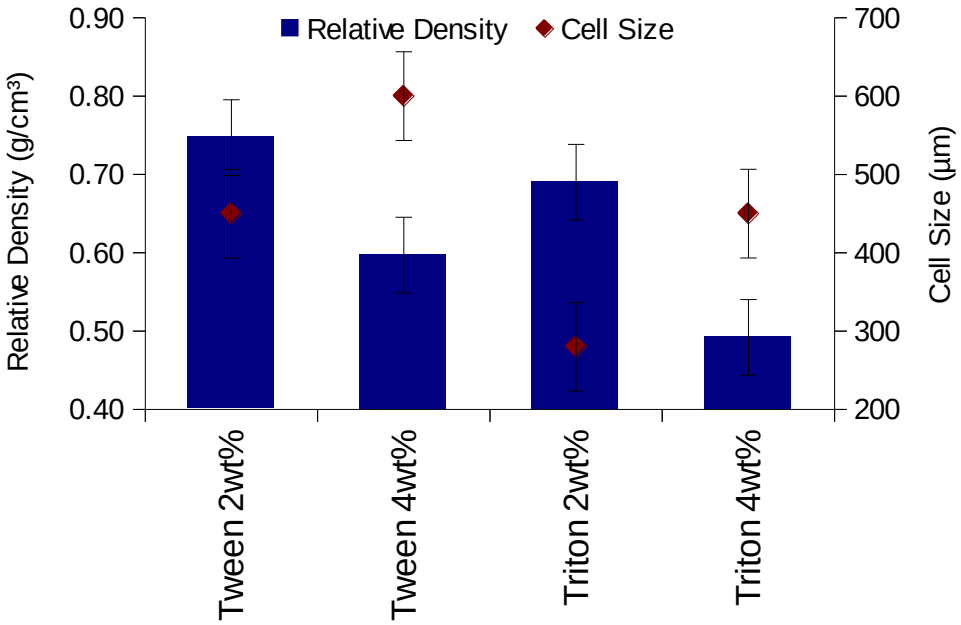

Figure 4.10 Effect of surfactant content on the average cell size and its relation with the relative density of samples (solid content set at 68 wt% and mixing speed at 1500 rpm).

Figure 4.11 shows SEM images of the microstructure of geopolymer foam obtained from a slurry with 68 wt% solids, 2 wt% Tween 80 surfactant and stirred at 2000 rpm, where it is possible to observe the presence of spherical and interconnected cells and dense struts.

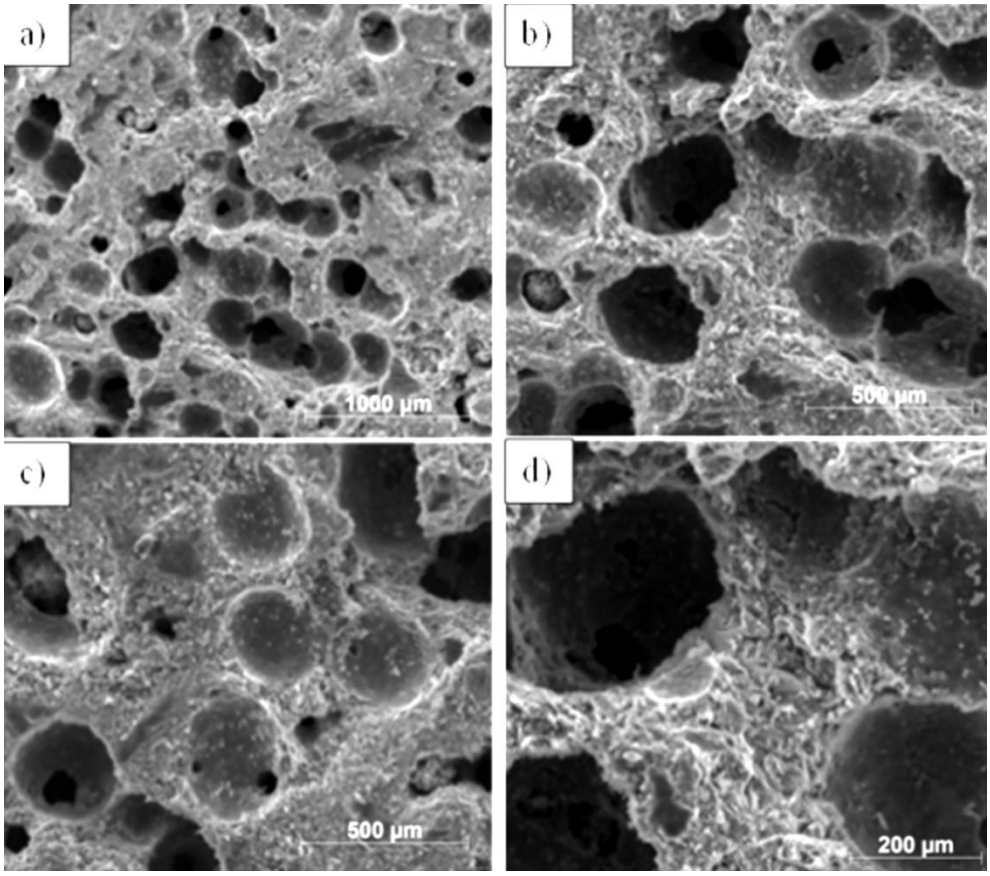

Figure 4.11 Morphology of geopolymer foam obtained from slurry with 68 wt% solids, 2 wt% surfactant Tween and stirred at 2000 rpm. (a) lowest magnification; (b) and (c) intermediate magnification in different regions; and (d) highest magnification.

4.1.5 Specific surface area

The specific surface area of the geopolymer foams decreased with increasing the heat treatment temperature. Samples made with 2 wt% of Tween 80, stirred at 1500 rpm and cured at 80°C, had a specific surface area of 56.89 m^2/g, which decreased to 44.20 m^2/g after heat treatment at 700°C and to 1.27 m^2/g after heat treatment at 1200°C, with a 98% decrease in SSA value. The decrease in specific surface area with an increase in calcination temperature was due to the loss of micro- and meso-pores present in the amorphous structure after geopolymerization, due to the transformation to a

crystalline phase with increasing temperature. Moreover, upon heating to 1200°C, the (partial) formation of a liquid phase occurred, when the geopolymer transformed into leucite (crystalline phase) embedded in fusible low-molecular poly(sialate) arising from the presence of non-stoichiometric contaminants [3].

4.1.6 Linear thermal shrinkage

Figure 4.12 shows the linear shrinkage, which could be divided into four characteristic regions as function of the thermal treatment

When temperature was lower than 100°C (region I), the geopolymer foam kept approximately dimensionally stable as only free water from large pores and surfaces was lost in this stage. Shrinkage in region II (100–300°C), region III (300–900°C) and stage IV (900–1150°C) were caused by capillary strain/dehydration, physical contraction during dehydroxilation/polymerization of Si–OH/Al-OH groups, and viscous sintering/crystallization, respectively. On heating to 1150°C the shrinkage was fully completed and the overall linear shrinkage value was about 10.5%.

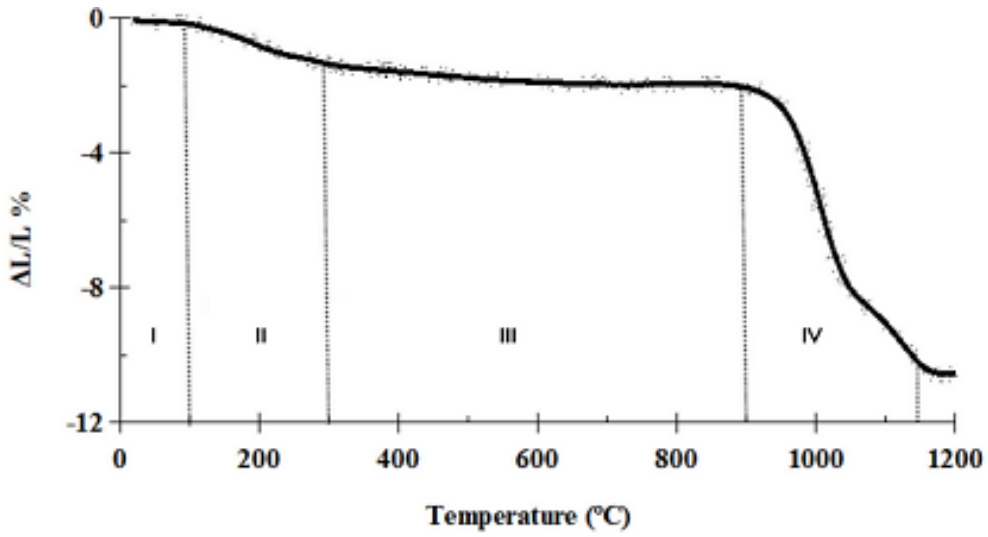

Figure 4.12 Linear shrinkage of geopolymer foam as a function of temperature.

The effect of the thermal treatment on the open porosity of the geopolymer foams is shown also in Figure 4.13. We can observe that the open porosity decreased more significantly (maximum loss of ~24 vol% for samples produced using 4 wt% of surfactant) than the total porosity values, especially after heating at high temperature. The reduction in open porosity is related to the formation of a liquid phase which closes the spaces between the particles constituting the microstructure of the materials, as already mentioned.

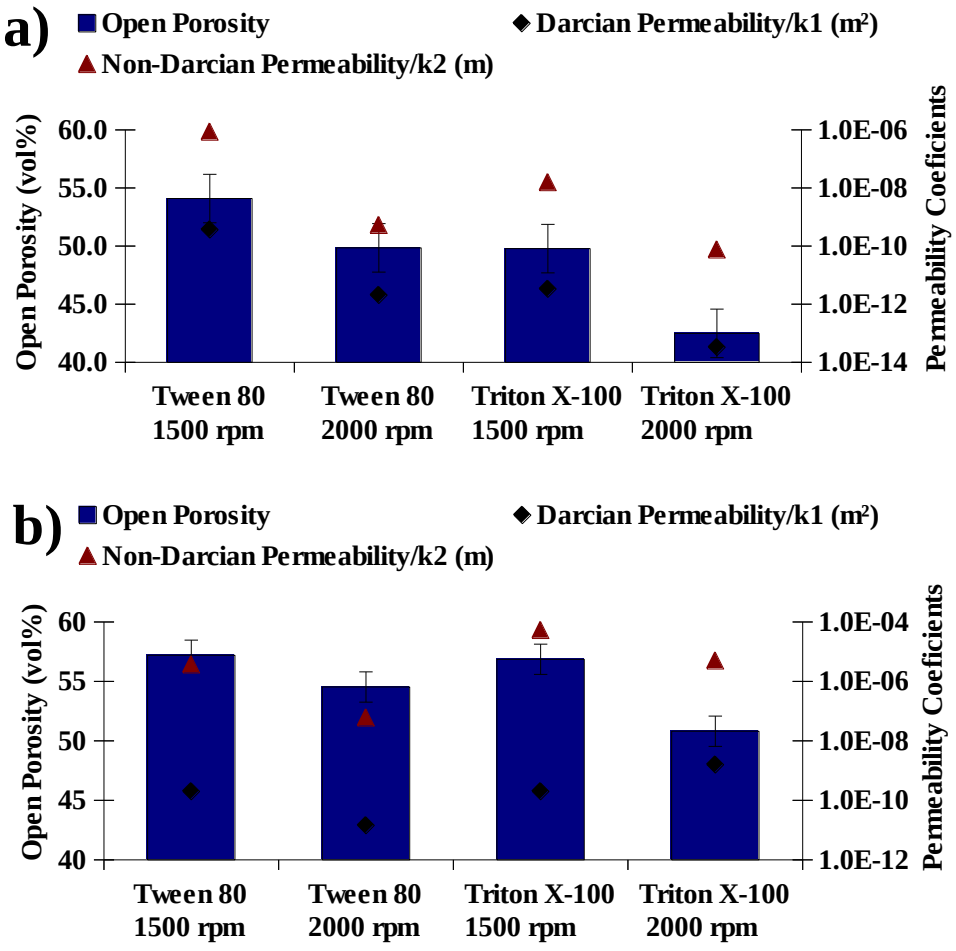

Figure 4.13 Open porosity as a function of the heat treatment of geopolymer foams with (a) 2 wt% of surfactant; (b) 4 wt% of surfactant.

4.1.7 TG/DTA analysis

The TG/DTA analysis curve of the geopolymer (see Figure 4.14) shows that in the 25-300°C range a weight loss associated with the loss of free water/dehydration [61, 62] occurred, while dehydroxilation/condensation of Si-OH/Al-OH [61, 62] with a concurrent weight loss took place between 300 and 500°C. Also from Figure 4.14, it could be noted that in the 700-1000°C range the phase change from amorphous to a metastable structure accompanied by densification occurred, and then finally, around 1180°C, the stable crystalline phase formed, as suggested by the exothermic peak corresponding to the crystallization of leucite (predicted phase according Figure A.4)

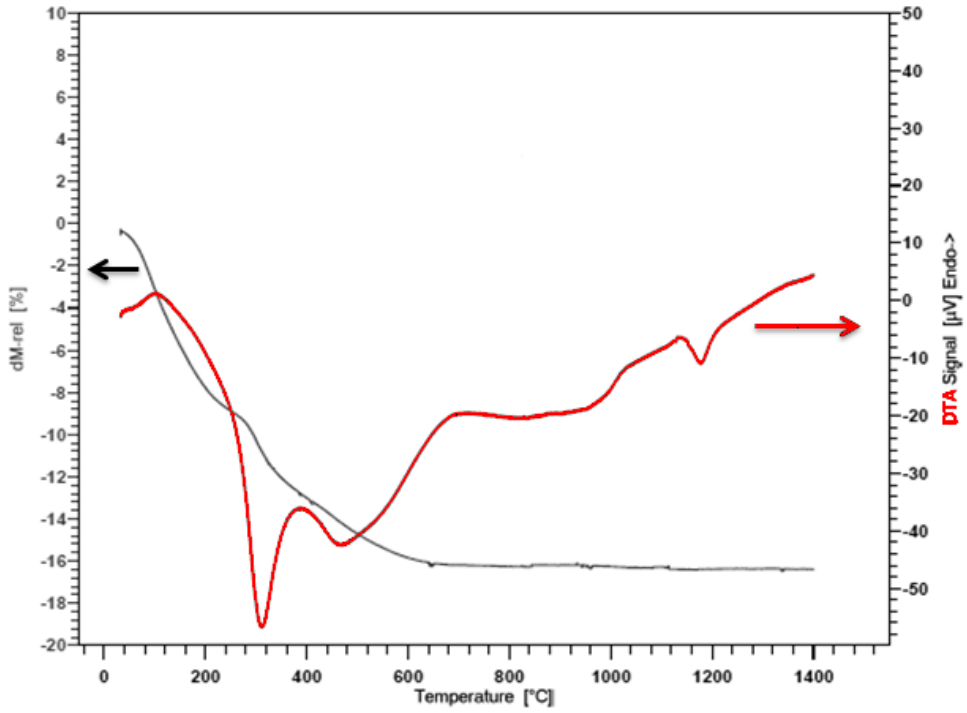

Figure 4.14 TG/DTA curve for a sample produced using surfactant Tween 80 (2 wt % – 1500 rpm).

In Figure 4.15 are shown the SEM micrographs of samples producing using Tween 80 (2 wt% - 1500 rpm) where it could be seen the effect of the temperature predicted and reported by the shrinkage and TG/DTA

analysis, and consistent with the experimental results shown in Figures 4.12 and 4.14.

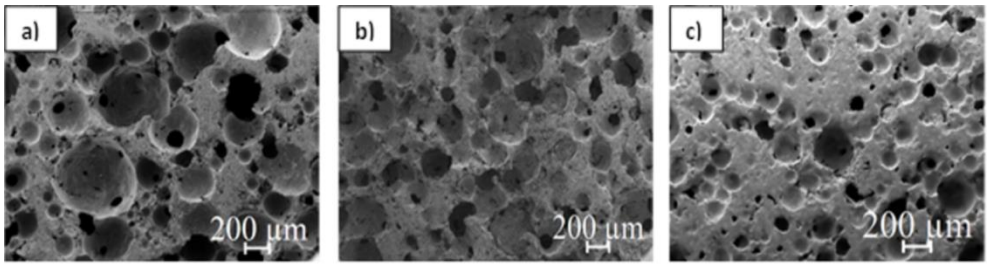

Figure 4.15 Effect of heat treatment on the surface morphology for a sample produced using Tween 80 as surfactant (2 wt% – 1500 rpm): (a) room temperature; (b) 700°C; (c) 1200°C.

Furthermore, another factor also evaluated by SEM (Figure 4.16) is regarding of the different surfactants and their effects on densification of struts, also responsible for the differences in the mechanical strength between the materials obtained.

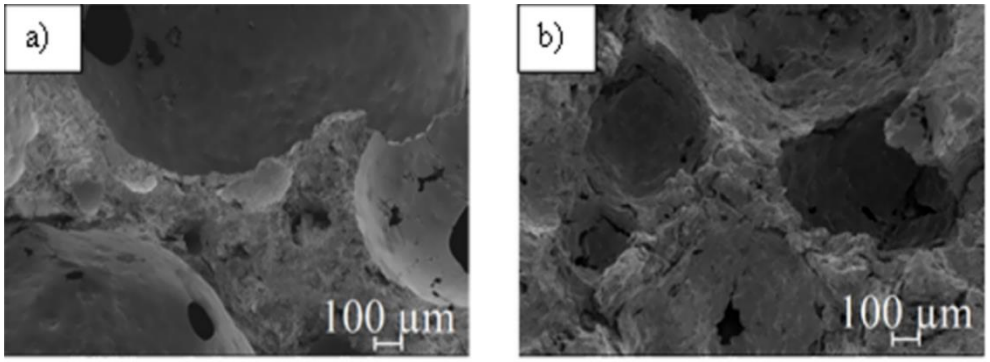

Figure 4.16 SEM image highlighting the struts of samples produced with different surfactants: (a) Tween 80; (b) Triton X-100, as prepared and dried.

4.2 Gelcasting/saponification/peroxide combine route (GCSPCR)

First of all, Figure 4.17 shows a comparison of the morphology of foams produced by: a) the saponification/peroxide/gelcasting combined route;

b) the saponification route (stirring, only oil, no H_2O_2 addition), and c) the peroxide route (stirring, only H_2O_2, no oil addition).

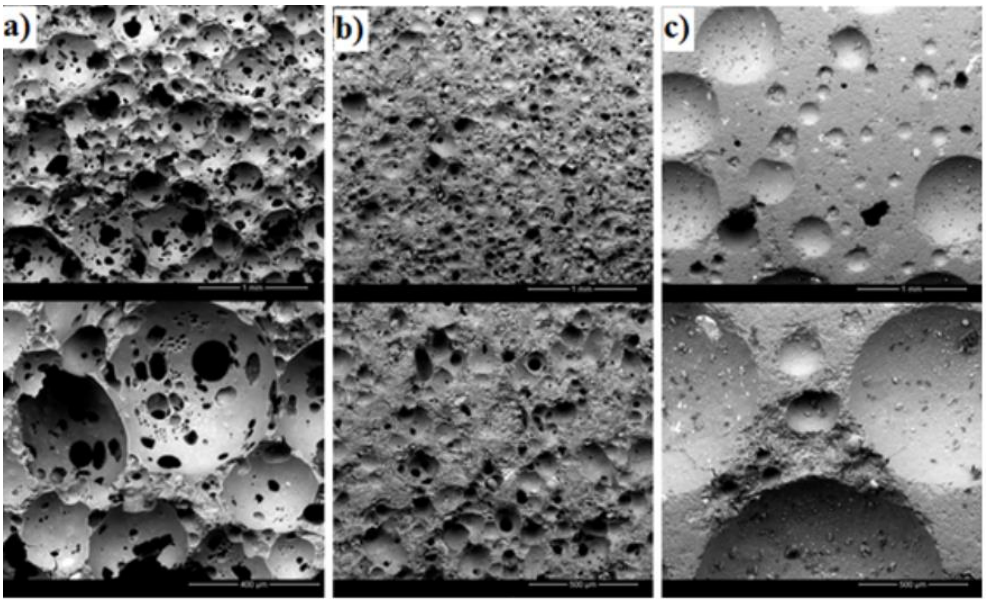

Figure 4.17 SEM micrographs of geopolymer foams, as-prepared and dried, produced using different processing approaches: (a) saponification/peroxide/gelcasting combined route; (b) saponification route; (c) peroxide route.

We can observe that the combined route (a) enabled the fabrication of foams with highly interconnected porosity and regular morphology (spherical cells), the saponification route (b) led to the formation of smaller cells, some with openings, while when using the peroxide route (c) larger but mainly closed cells were formed. Evidently, the *in situ* generation of a surfactant promoted the creation of cell windows (i.e. interconnections among cells), while the gas generated by the decomposition of the hydrogen peroxide allowed to increase the cell size. We should note that the cell size produced by a direct foaming process depends also on the viscosity of the slurry, which is affected by its composition. In particular, the introduction of oil and/or peroxide led to a decrease of viscosity with respect to the slurry in which only water was present.

Even within this context, and since this route is based on the *in situ* generation of a surfactant due the saponification reaction, the results presented here could be explained by the same mechanisms described when it was

evaluated the gelcasting route. Likewise that was pointed out that different surfactants provides different properties to the geopolymer foams, due their chemical structures, different sources of triglycerides also produce different surfactants, which implies in different geopolymer foams by this route.

4.2.1 Total and open porosity

Figure 4.18 shows a similar range of starting total porosity but with a tiny change depending on type of oil, impacting on the porosity at the meso-scale (a) and the effect of the heat treatment in (b).

This behavior could be explained by the effect of the temperature predicted and reported by the shrinkage and TG/DTA analysis, as presented and discussed in Figures 4.12 and 4.14. Besides that, Figure 4.18 (b) shows that even present a similar range of starting total porosity the effect of heat treatment is different among the triglyceride source, represented by the distinct gap between each temperature.

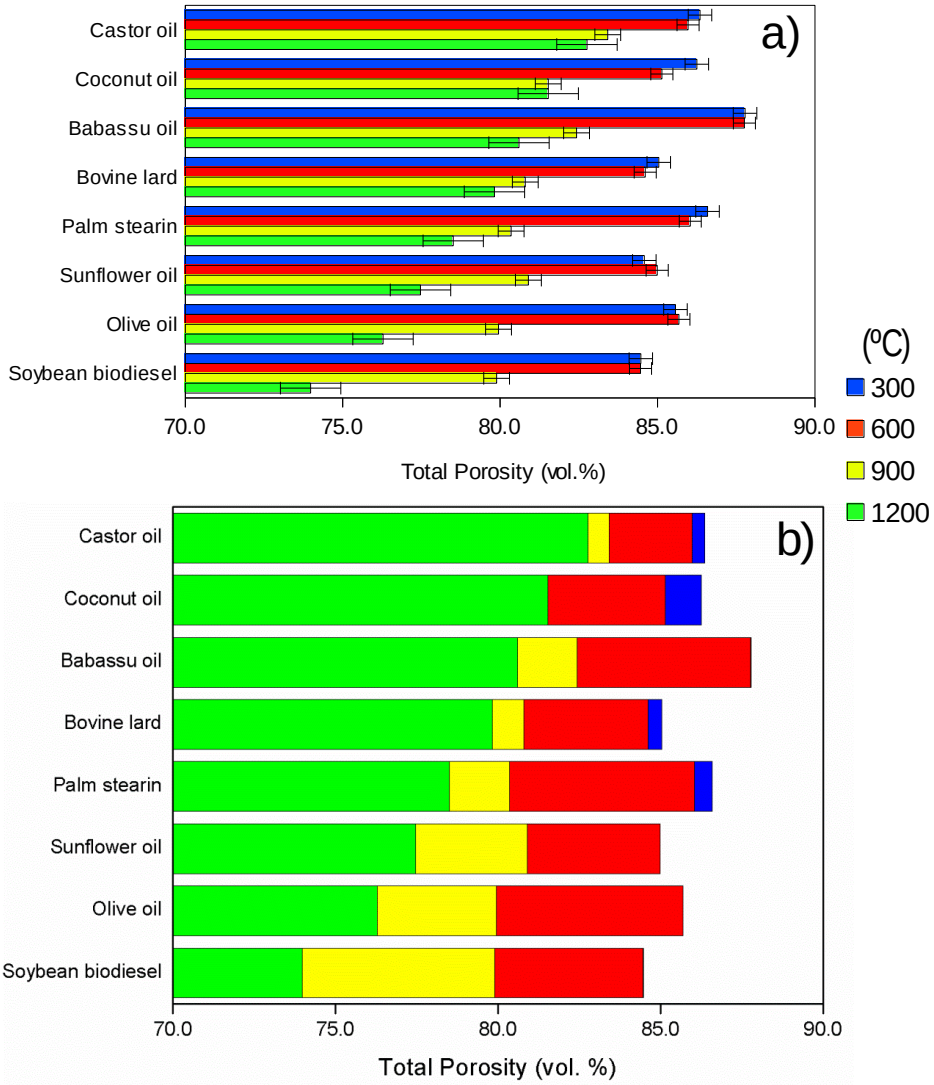

Figure 4.18 Effect of the type of triglyceride and temperature on the total porosity of the geopolymer foams. a) real values of the total porosity according the heat treatment of 300, 600, 900 and 1200°C and b) decrement values of the open porosity of each triglyceride source due the heat treatment in the same temperatures.

Already Figure 4.19 shows the effect of the triglyceride source and the temperature on the open porosity.

Here, it is important to note that the open porosity values at 600°C are higher than at 300°C, which means that 300°C is a too low temperature to remove all organic compounds produced by this route.

Afresh, Figure 4.19 (b) shows the effect of the heat treatment on the open porosity where, as well on the total porosity, displays a different performance mainly at 900 and 1200°C.

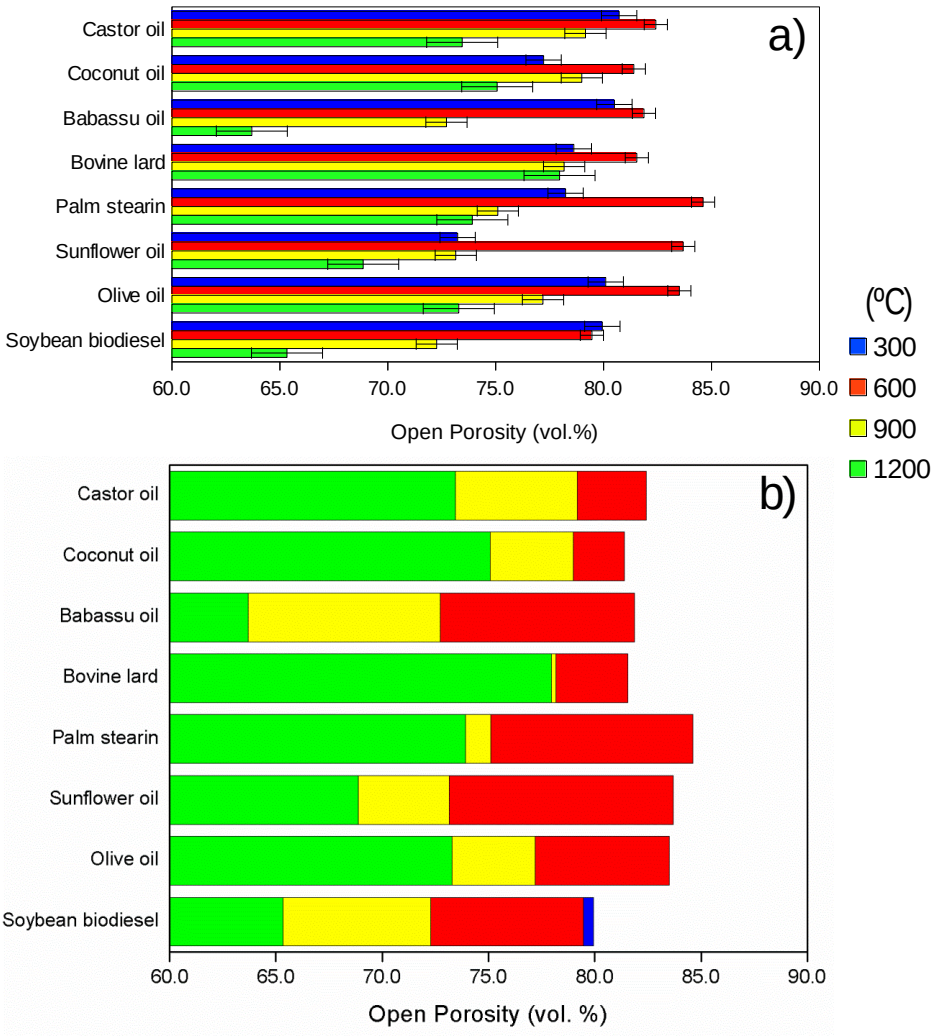

Figure 4.19 Effect of the type of triglyceride and temperature on the open porosity of the geopolymer foams. a) real values of the open porosity according the heat treatment of 300, 600, 900 and 1200°C and b) decrement values of the open porosity of each triglyceride source due the heat treatment in the same temperatures.

4.2.2 Mechanical strength

Regarding this feature, as shows Figure 4.20, could not be observed a major effect of the different chemical nature of surfactants, specifically at 300 and 600°C, which could be explained directly by the high value of total and open porosity of all samples, that has a more pronounced and significant effect than the type of triglyceride source itself (the type affect indirectly because it generates different porosities as seen in Figure 4.17)). The effect of the porosity on the strength is more evident at 1200°C, where the sintering (densification), with consequent decrease of the total and open porosity, becomes responsible by the rise of this property.

For instance it could be noted that, for a heat treatment from 300 to 1200°C, an increase in ~ 80% for the sunflower oil (lowest) and ~ 900% for the palm stearin (highest).

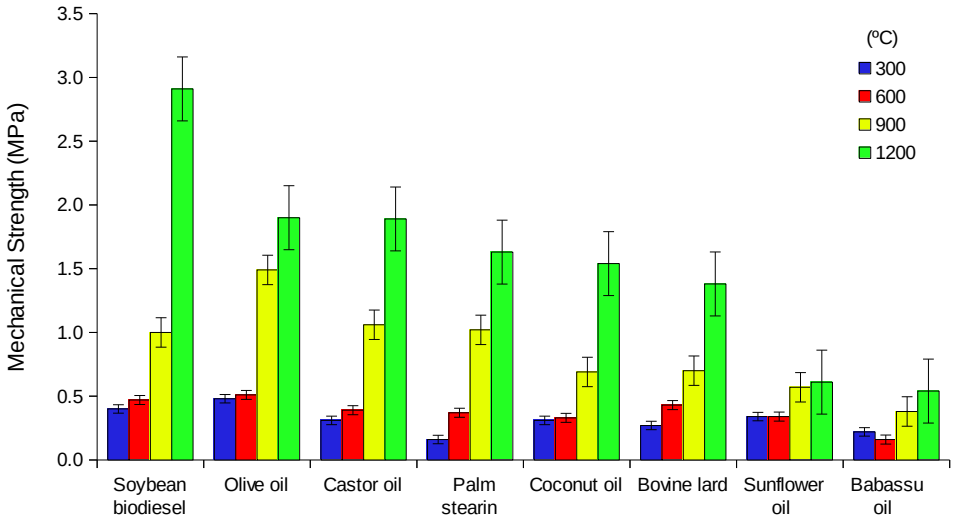

Figure 4.20 Effect of the type of triglyceride and heat treatment on the mechanical strength of the geopolymer foams.

4.2.3 Permeability

Concerning the air permeation behavior, the values of the permeability coefficients k_1 (Darcian) and k_2 (non-Darcian), in Forchheimer's

equation [35], fit well in a comprehensive permeability map, provided by Innocentini et al. [35], describing the behavior of porous components for filtration or adsorption applications (Figure 4.21). Foams from the peroxide route were the least permeable, behaving similarly to refractory bricks or porous ceramics produced using sacrificial fillers; foams from the saponification and the combined route had permeation typical for fibrous or granular filters and foams from gelcasting, with foams from the combined route almost as permeable as foams produced from the replica technique.

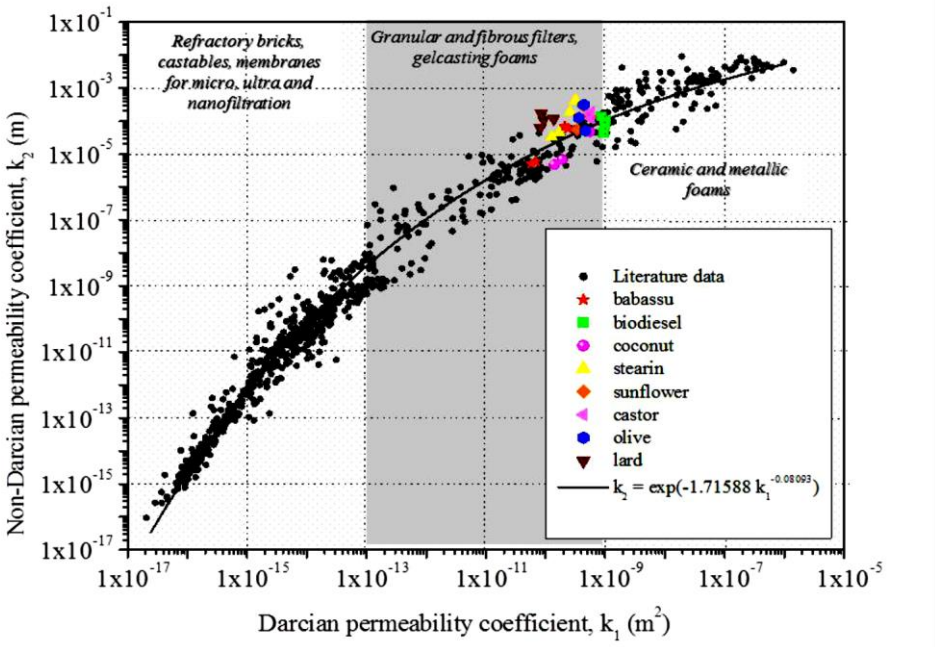

Figure 4.21 Location of k_1 and k_2 data for geopolymer foams obtained by gelcasting in a comprehensive permeability map [44].

Moreover, it is worth noting that the saponification reaction reduced the pH of the geopolymer foam in contact with water. To obtain pH values of samples, geopolymers were ground and dispersed in distilled water (30 mg of grounded material into 150 ml of distilled water). In fact, pH measurements after extraction of glycerol in contact with distilled water for 12h resulted in a value of ~8.0, which is much lower than the one obtained for a conventional geopolymer foam sample ~ 11.5), suggesting that, the repeated immersion in hot water to

remove the glycol might have preferentially removed relatively water-soluble material when compared to the effect seen in a conventional geopolymer not submitted at this procedure. This indicates that these geopolymer foams with hierarchical porosity could be employed in water filtration applications for human consumption.

4.2.4 Morphological analysis

As predicted by the literature [40], and considering the type of lather formed (creamy, bubbly) and viscosity, this feature shows a strong influence of the triglyceride source.

Regarding this, Figure 4.22 shows pictures obtained by the different triglyceride sources and heat treated at 300°C, where could be seen the effect of this parameter for bovine lard and palm stearin, those with the highest "creamy value" between the used sources (respectively 50 and 65), which implies in small cells and a narrow average cell size (Figure 4.23). Moreover, these two types of fat are solid at room temperature, which even firstly to add to the geopolymer slurry had melted in hot water (around 40°C) to become liquid, begin to solidify again during mixing, which reduces the effect of hydrogen peroxide.

On the other hand, sources with the highest “bubbly value”, as coconut and castor oil, with values of 67 and 90 respectively, and even soybean biodiesel due its low viscosity, provides a large average cell size. It is noteworthy that for soybean biodiesel, a larger average cell size is favored by its low viscosity, which has as a consequence a more effectiveness of hydrogen peroxide in promote this increase in the cells size.

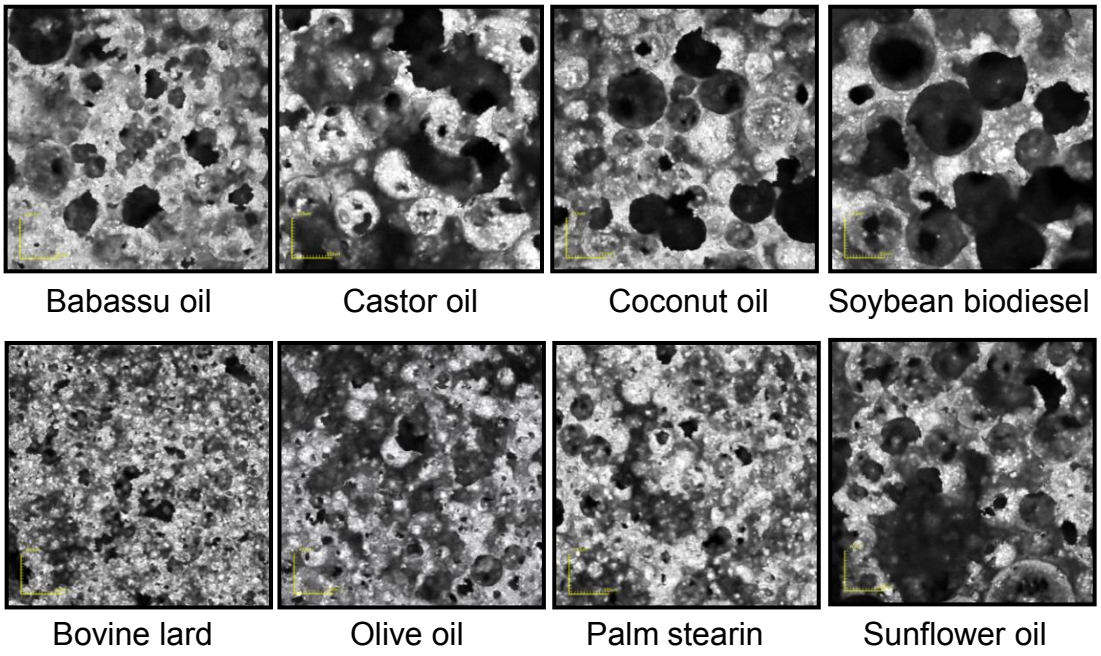

Figure 4.22 Effect of the type of triglyceride on the morphology (macro-pore architecture) of the geopolymer foams heat treated at 300°C.

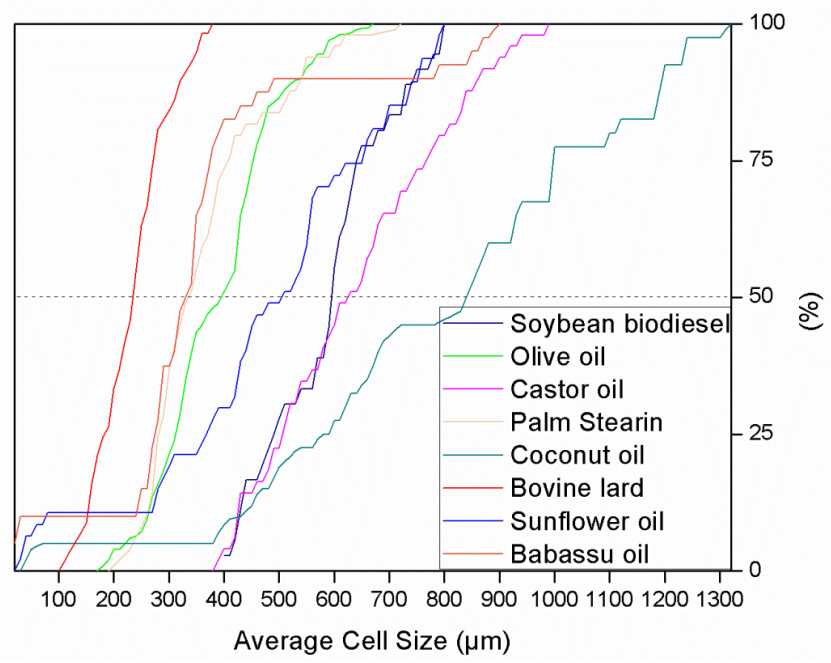

Figure 4.23 Average cell size of geopolymer foams according triglyceride source after heat treatment at 300°C.

Similarly, these data are respectively showed in Figure 4.24 and Figure 4.25 for the geopolymer foams after heat treatment at 600°C.

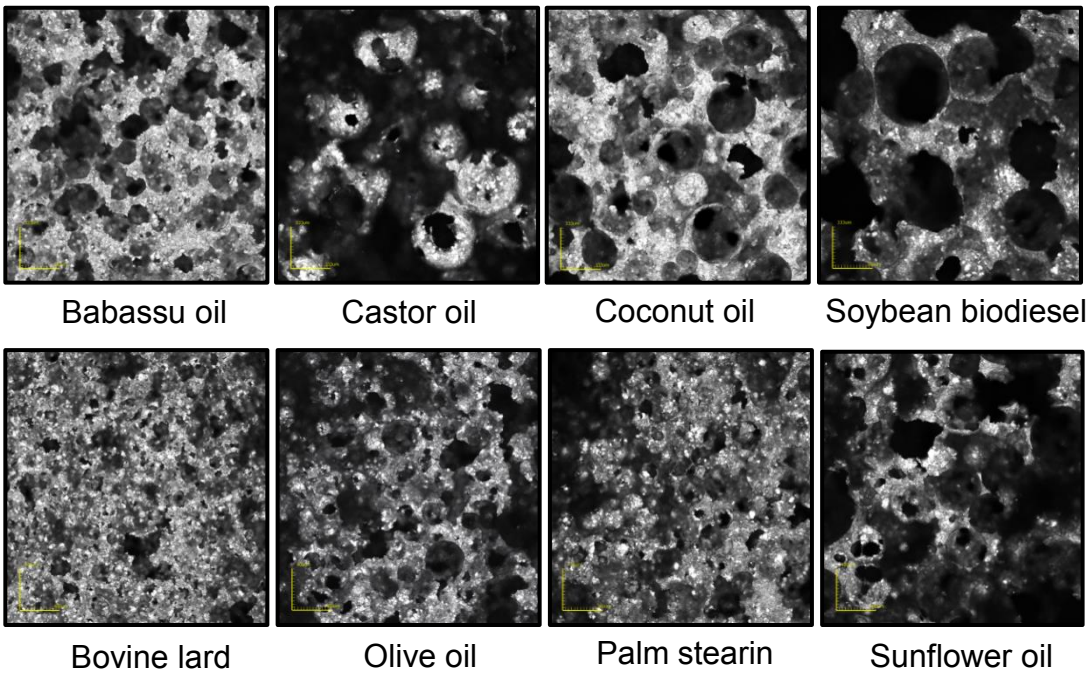

Figure 4.24 Effect of the type of triglyceride on the morphology (macro-pore architecture) of the geopolymer foams heat treated at 600°C.

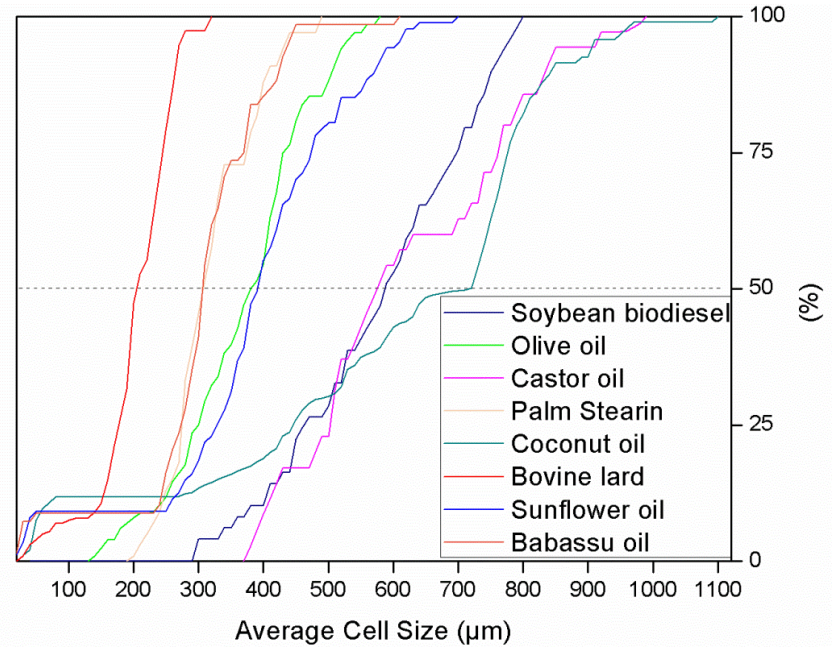

Figure 4.25 Average cell size of geopolymer foams according triglyceride source after heat treatment at 600°C.

Once again, these data are respectively showed in Figure 4.26 and Figure 4.27 for the heat treatment at 900°C. At this temperature it could be noted that all cell size distribution become narrower, due the shrinkage effect.

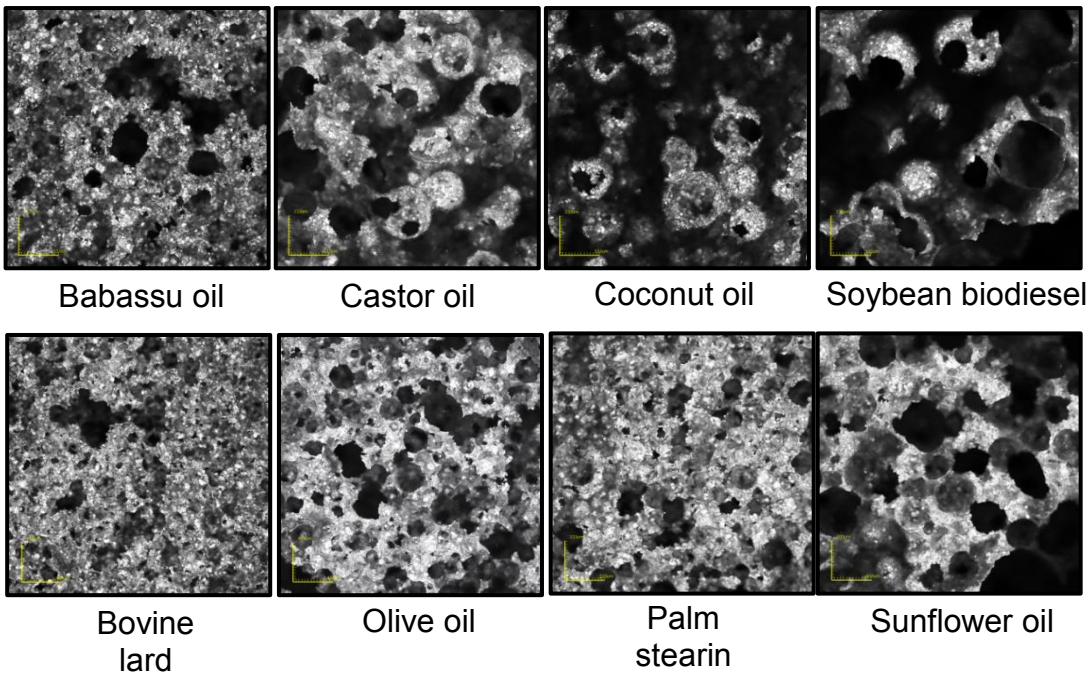

Figure 4.26 Effect of the type of triglyceride on the morphology (macro-pore architecture) of the geopolymer foams heat treated at 900°C.

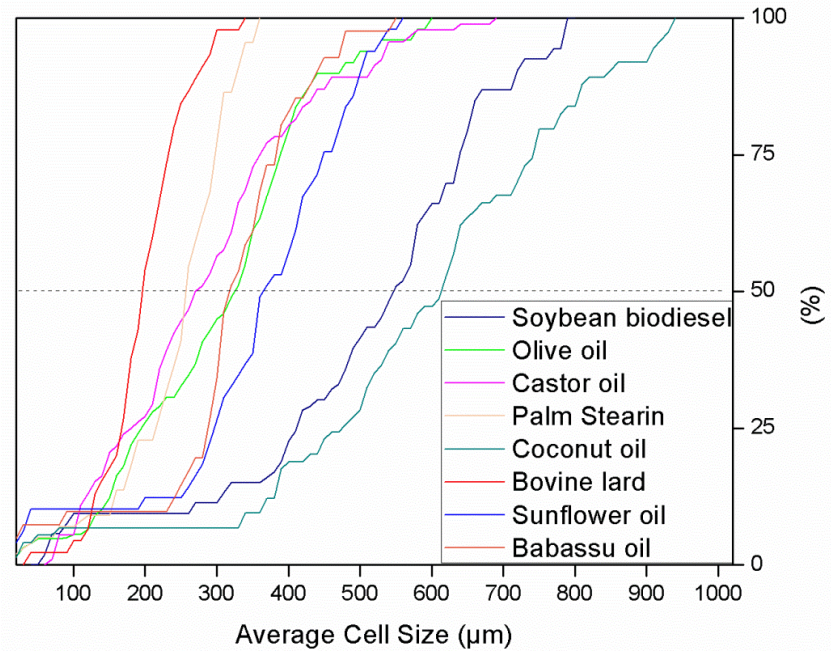

Figure 4.27 Average cell size of geopolymer foams according triglyceride source after heat treatment at 900°C.

Figures 4.28 and 4.29 show the morphological aspect of samples heat treated at 1200°C.

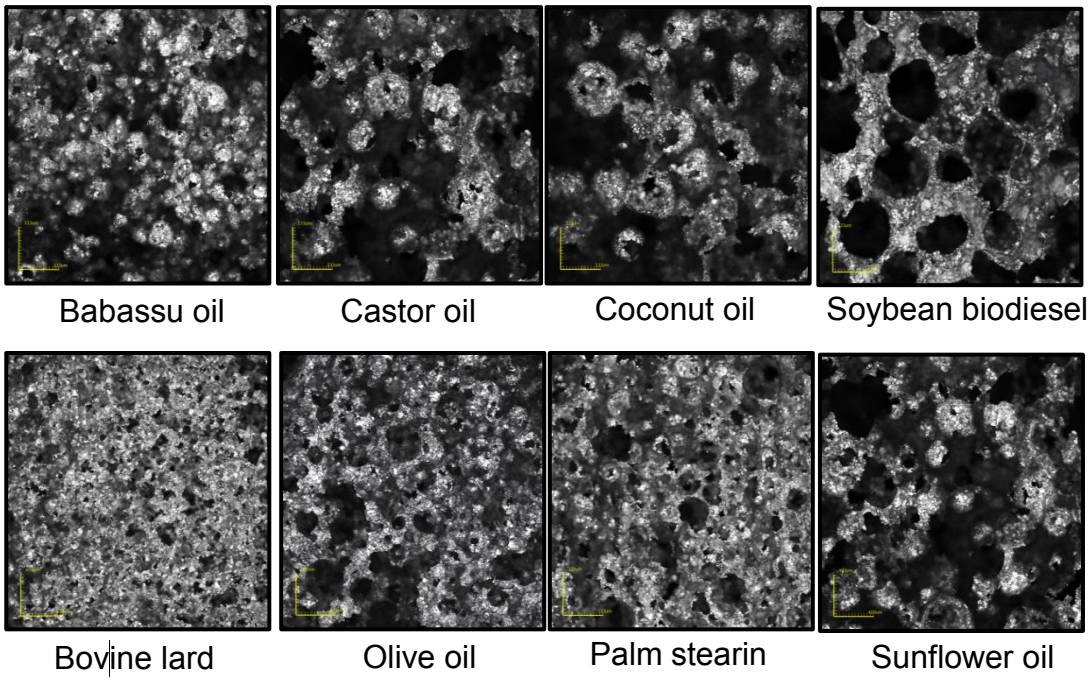

Figure 4.28 Effect of the type of triglyceride on the morphology (macro-pore architecture) of the geopolymer foams heat treated at 1200°C.

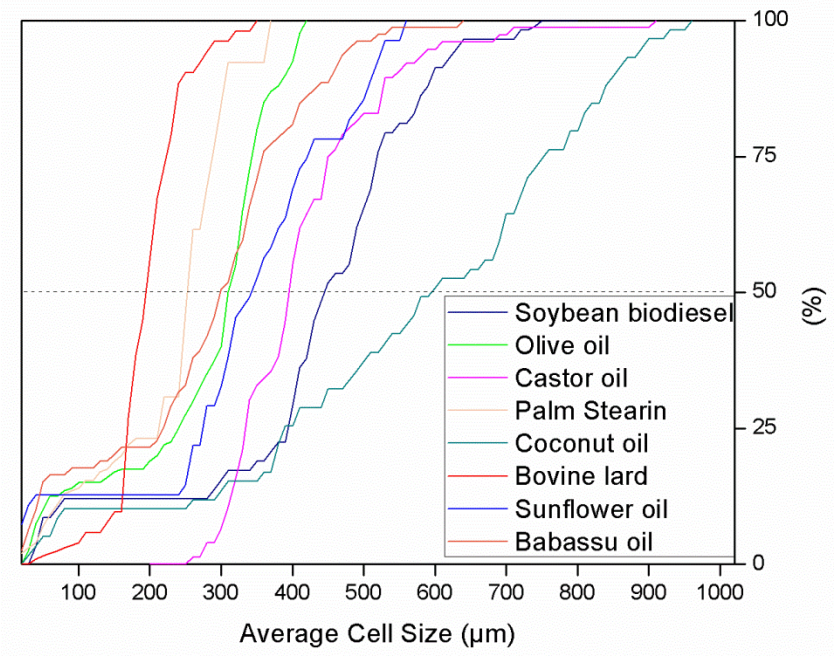

Figure 4.29 Average cell size of geopolymer foams according triglyceride source after heat treatment at 1200°C.

4.2.5 Specific surface area

Concerning the specific surface area, a comparative behavior between the triglycerides sources and also the effect of the temperature are shown in Figure 4.30.

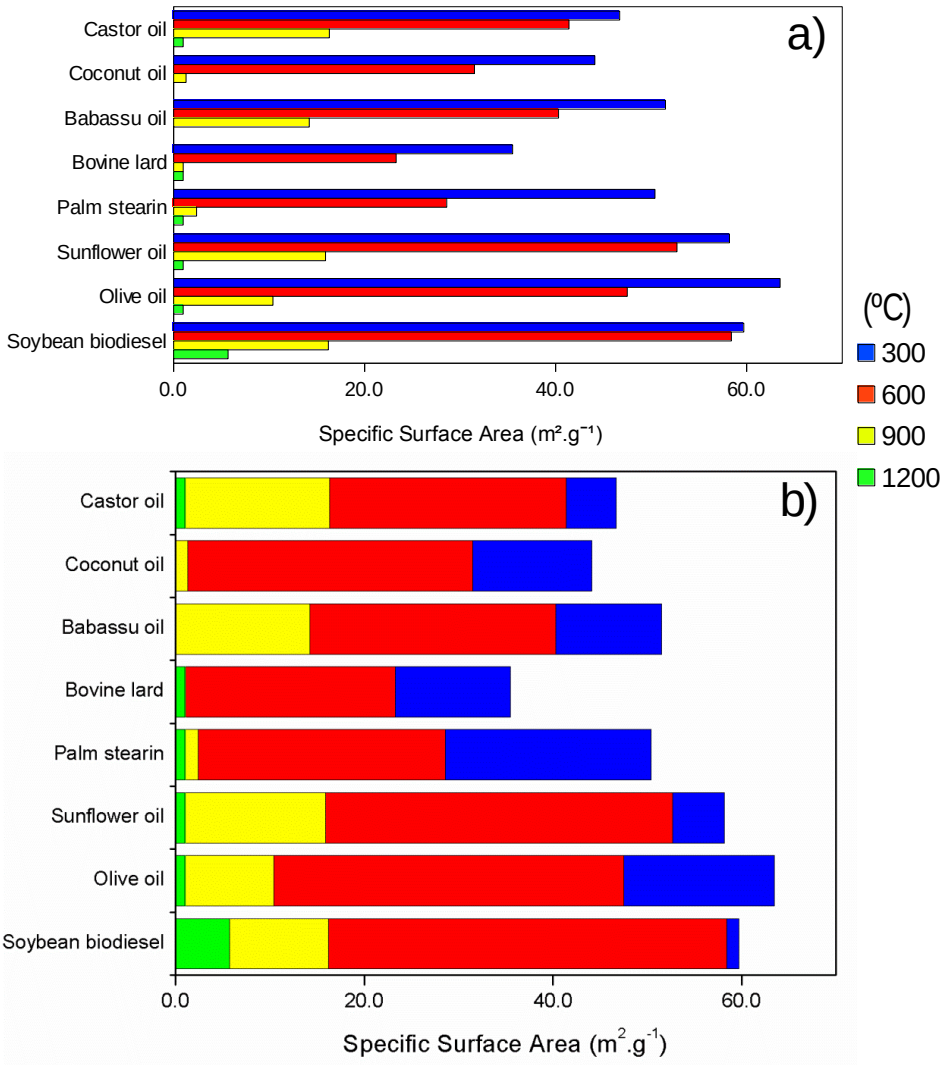

Figure 4.30 Effect of the type of triglyceride and temperature on the specific surface area of the geopolymer foams. a) real values of the specific surface area according the heat treatment of 300, 600, 900 and 1200°C and b) decrement values of the specific surface area of each triglyceride source due the heat treatment in the same temperatures.

Analyzing Figure 4.30(a) it could be seen a different range of starting specific surface area, with an increase of ~ 44.0% when comparing bovine lard (35.5 $m^2.g^{-1}$) and olive oil (63.5 $m^2.g^{-1}$). It's important to mention that specifically regarding this property, neither the features "bubbly" nor "cream" have a direct effect on the reached values for each triglyceride source. At this point it is worth noting that a possible explanation for this difference could be related to the amount of glycerol generated for each triglyceride source during the saponification reaction, which was subsequently extracted, leaving voids. However, one contrary point to this hypothesis is the soybean biodiesel, which during saponification does not generate glycerol, meanwhile appears as one of the sources which generated a porous geopolymer which presents the second highest initial specific surface area (59.7 $m^2.g^{-1}$).

Besides that, seeing Figure 4.30(b), is possible to see that up to 900°C, castor oil, sunflower oil and soybean biodiesel are be able to retains the specific surface area in ~16 m2.g-1, the highest values at this temperature, but there was not found a chemical characteristic in these triglyceride sources to explain this behavior. Also, taking account the chemical character of each oil, properties of "bubbly" and "cream" seem to not interfere directly on the develop of the specific surface area.

Already at 1200°C the effect of sintering is preponderant in reducing the specific surface area, and practically there is no more adsorption, which is confirmed by the results.

4.2.6 Linear thermal shrinkage and TG/DTA analysis

As previously mentioned, for this processing route were considered the results obtained for gelcasting route.

5 CONCLUSIONS

Considering firstly the GCR was established that is possible to produce geopolymer using the geopolymerization reaction to stabilize the gas bubbles introduced in the liquid slurry by rotational mixing. Also, it was shown that the processing parameters affect the characteristics of the foams. In particular, with increasing mixing speed the average cell size and relative density decreased, while with increasing the amount of surfactant the average cell size and total porosity increased. The type of non-ionic surfactant affected the overall morphology of the foams (e.g.: total porosity and open porosity, and average cell size) reflecting directly in some physical properties such as mechanical strength and permeability.

The relation between some physical properties of geopolymer foams produced by gelcasting and their dependence of the processing parameters were confirmed. Concerning the permeation behavior, an increase of 1 to 3 orders of magnitude of Darcian (k_1) and non-Darcian (k_2) coefficients as a result of the increase of open porosity with increasing amount of surfactant was observed. The compressive strength was inversely proportional to the total porosity. The addition of a higher amount of surfactant decreased the relative density of the foams and their strength. No statistically significant difference was observed for the addition of the two different surfactants for the permeability or the mechanical strength values.

By using this approach, it was possible to produce foams with a total pore volume as high as ~80 vol.%, with an amount of open porosity as high as ~60 vol.%.

Furthermore, a novel approach (GCSPCR) for the production of highly porous, open cell geopolymer foams with relatively high specific surface area (~ 65 $m^2.g^{-1}$) was developed. Due the saponification reaction, the in situ formation of surfactant molecule is able to create more cell windows, increasing the permeability in comparison to a simple and commonly peroxide route. By this route it was possible to produce foams with a total pore volume as high as ~88 vol.%, with an amount of open porosity as high as ~80 vol.%.

The variation of the source of triglycerides (type of oil) has a direct influence on some physical properties of porous geopolymers, expanding the potential application in several new fields, including filtration and adsorption applications. However, it was not possible to observe any influence of this variation on the permeation behavior.

For both routes, the heat treatment decreased the total porosity and the specific surface area, especially at the highest temperature (~1200°C), because of the shrinkage, crystallization and (partial) viscous flow occurring in the geopolymer material.

These results, as well as the advantage of using a sustainable and low cost manufacturing process, encourages additional efforts to optimize the use of gelcasting and the gelcasting/saponification/peroxide combined route to produce open cell geopolymer foams.

6 SUGGESTIONS FOR FUTURE WORKS

To the gelcasting route evaluate the influence of different surfactants, and also the effect of curing process (time and temperature) and heat treatment on the physical properties of geopolymer foams.

To the gelcasting/saponification/peroxide combined route, explore different additions and different triglycerides sources; evaluate the effect of heat treatment and the possible addition of a third component, such as a pore forming agent and fibers, to increase the mechanical strength.

Preliminary study of pore forming agent addition showed an increase of 35% of the specific surface area, in some cases for values of 85 $m^2.g^{-1}$.

7 REFERENCES

[1] DAVIDOVITS, J. Geopolymers - Inorganic polymeric new materials. **Journal of Thermal Analysis**, v. 37, p. 1633–1656, doi:10.1007/BF01912193, 1991.

[2] PRUD'HOMME, E. et al. In situ inorganic foams prepared from various clays at low temperature. **Applied Clay Science**, v. 51, p. 15–22, doi:10.1016/j.clay.2010.10.016, 2011.

[3] DAVIDOVITS, J. **Geopolymer Chemistry and Applications**. [S.l.]: Institut Géopolymère, 2011. p. 632

[4] PRUD'HOMME, E. et al. Silica fume as porogent agent in geo-materials at low temperature. **Journal of the European Ceramic Society**, v. 30, p. 1641–1648, doi:10.1016/j.jeurceramsoc.2010.01.014, 2010.

[5] ABDULLAH, M. M. A. B. et al. Fly Ash Porous Material using Geopolymerization Process for High Temperature Exposure. **International Journal of Molecular Sciences**, v. 13, p. 4388–4395, doi:10.3390/ijms13044388, 2012.

[6] WEERDT KLAARTJE. **Geopolymers - State of the art COIN Project Report 37 - 2011**. . Oslo: [s.n.]. Disponível em: <http://www.sintef.com/home/Publications/EmployeePublications/?orgunit=1433&year=2011&coarsecategory=Rapport>. Acesso em: 13 ago. 2014, 2011.

[7] DUXSON, P. et al. Geopolymer technology: The current state of the art. **Journal of Materials Science**, v. 42, p. 2917–2933, doi:10.1007/s10853-006-0637-z, 2007.

[8] RAHIER, H. et al. Low-temperature synthesized aluminosilicate glasses .1. Low-temperature reaction stoichiometry and structure of a model compound. **Journal of Materials Science**, v. 31, p. 71–79, 1996.

[9] PALOMO, A.; LÓPEZ DELA FUENTE, J. I. Alkali-activated cementitous materials: Alternative matrices for the immobilisation of hazardous wastes.

Cement and Concrete Research, v. 33, n. 2, p. 281–288, doi:10.1016/S0008-8846(02)00963-8, 2003.

[10] SHI, C.; KRIVENKO, P. V.; ROY, D. M. Alkali-Activated Cements and Concretes. In: MATERIALS RESEARCH. **Anais**... [S.l: s.n.]. Disponível em: <http://books.google.com.co/books?id=h8oO7R98z_kC>, 2006.

[11] MALLICOAT, S.; SARIN, P.; KRIVEN, W. M. NOVEL, ALKALI-BONDED, CERAMIC FILTRATION MEMBRANES. **Developments in Advanced Ceramics and Composites**, v. 26, p. 37–44, 2005.

[12] SOFI, M. et al. Engineering properties of inorganic polymer concretes (IPCs). **Cement and Concrete Research**, v. 37, n. 2, p. 251–257, doi:10.1016/j.cemconres.2006.10.008, 2007.

[13] BAO, Y.; GRUTZECK, M. W.; JANTZEN, C. M. Preparation and Properties of Hydroceramic Waste Forms Made with Simulated Hanford Low-Activity Waste. **Journal of the American Ceramic Society**, v. 88, n. 12, p. 3287–3302, doi:10.1111/j.1551-2916.2005.00775.x, 2005.

[14] DUXSON, P. et al. Understanding the relationship between geopolymer composition, microstructure and mechanical properties. **Colloids and Surfaces A-Physicochemical and Engineering Aspects**, v. 269, p. 47–58, doi:10.1016/j.colsurfa.2005.06.060, 2005.

[15] DUXSON, P. et al. The effect of alkali and Si/Al ratio on the development of mechanical properties of metakaolin-based geopolymers. **Colloids and Surfaces A: Physicochemical and Engineering Aspects**, v. 292, p. 8–20, doi:10.1016/j.colsurfa.2006.05.044, 2007.

[16] ROWLES, M.; O'CONNOR, B. Chemical optimisation of the compressive strength of aluminosilicate geopolymers synthesised by sodium silicate activation of metakaolinite. **Journal of Materials Chemistry**, v. 13, n. 5, p. 1161–1165, doi:10.1039/b212629j, 2003.

[17] SWADDLE, T. W. Silicate complexes of aluminum(III) in aqueous systems. **Coordination Chemistry Reviews**, v. 219-221, p. 665–686, doi:10.1016/S0010-8545(01)00362-9, 2001.

[18] SWADDLE, T. W.; SALERNO, J.; TREGLOAN, P. A. Aqueous aluminates, silicates, and aluminosilicates. **Chemical Society Reviews**, v. 23, n. 5, p. 319–325, doi:10.1039/cs9942300319, 1994.

[19] CASEY, W. H. Why small? The use of small inorganic clusters to understand mineral surface and dissolution reactions in geochemistry. **Reviews of Geophysics**, v. 41, n. 2, p. 1008–1028, doi:10.1029/2002RG000118, 2003.

[20] LASAGA, A. Role of surface speciation in the low-temperature dissolution of minerals. **Nature**, v. 331, n. 6155, p. 431–433, doi:10.1038/331431a0, 1988.

[21] BARBOSA, V. F. F.; MACKENZIE, J. D. Synthesis and thermal behaviour of potassium sialate geopolymers. **Materials Letters**, v. 57, p. 1477–1482, doi:10.1016/S0167-577X(02)01009-1, 2003.

[22] PERERA, D. S.; TRAUTMAN, R. L. Geopolymers with the Potential for Use as Refractory Castables. **Advances in Technology of Materials and Materials Processing**, v. 7, n. 4, p. 187–190, doi:10.2240/azojomo0173, 2006.

[23] LEE, S.-J. et al. Comparative analysis of fouling characteristics of ceramic and polymeric microfiltration membranes using filtration models. **Journal of Membrane Science**, v. 432, p. 97–105, doi:10.1016/j.memsci.2013.01.013, 2013.

[24] GORGOJO, P.; LA IGLESIA, Ó. DE; CORONAS, J. **Inorganic Membranes: Synthesis, Characterization and Applications**. [S.l.]: Elsevier, 2008. v. 13p. 135–175

[25] OHJI, T. et al. Macro-porous ceramics: processing and properties, **International Materials Review 57** (2012) 115-131

[26] KIM, H. et al. Control of pore size in ceramic foams: Influence of surfactant concentration. **Materials Chemistry and Physics**, v. 113, p. 441–444, doi:10.1016/j.matchemphys.2008.07.099, 2009.

[27] VASANTH, D.; PUGAZHENTHI, G.; UPPALURI, R. Fabrication and properties of low cost ceramic microfiltration membranes for separation of

oil and bacteria from its solution. **Journal of Membrane Science**, v. 379, n. 1-2, p. 154–163, doi:10.1016/j.memsci.2011.05.050, 2011.

[28] IVANETS, A. I. et al. Preparation and properties of microfiltration membranes based on natural crystalline SiO_2. **Ceramics International**, v. 40, n. 8, p. 12343–12351, doi:10.1016/j.ceramint.2014.04.080, 2014.

[29] NANDI, B. K.; UPPALURI, R.; PURKAIT, M. K. Preparation and characterization of low cost ceramic membranes for micro-filtration applications. **Applied Clay Science**, v. 42, n. 1-2, p. 102–110, doi:10.1016/j.clay.2007.12.001, 2008.

[30] ZHOU, J. et al. Separation of stable oil–water emulsion by the hydrophilic nano-sized ZrO_2 modified Al_2O_3 microfiltration membrane. **Separation and Purification Technology**, v. 75, n. 3, p. 243–248, doi:10.1016/j.seppur.2010.08.008, 2010.

[31] LIANGXIONG, L.; WHITWORTH, T. M.; LEE, R. Separation of inorganic solutes from oil-field produced water using a compacted bentonite membrane. **Journal of Membrane Science**, v. 217, n. 1-2, p. 215–225, doi:10.1016/S0376-7388(03)00138-8, 2003.

[32] WANG, Z. et al. Membrane cleaning in membrane bioreactors: A review. **Journal of Membrane Science**, v. 468, p. 276–307, doi:10.1016/j.memsci.2014.05.060, 2014.

[33] STUDART, A. R. et al. Processing routes to macroporous ceramics: A review. **Journal of the American Ceramic Society**, v. 89, p. 1771–1789, doi:10.1111/j.1551-2916.2006.01044.x, 2006.

[34] ORTEGA, F. S. et al. Alternative gelling agents for the gelcasting of ceramic foams. **Journal of the European Ceramic Society**, v. 23, p. 75–80, doi:10.1016/S0955-2219(02)00075-4, 2003.

[35] SCHEFFLER, M.; COLOMBO, P. **Cellular Ceramics: Structure, Manufacturing, Properties and Applications**. [S.l: s.n.], 645 p, 2005.

[36] GONZENBACH, U. T. et al. Macroporous Ceramics from Particle-Stabilized Wet Foams. **Journal of the American Ceramic Society**, v. 90, n. 1, p. 16–22, doi:10.1111/j.1551-2916.2006.01328.x, 2007.

[37] BURSALI, N.; ERTUNC, S.; AKAY, B. Process improvement approach to the saponification reaction by using statistical experimental design. **Chemical Engineering and Processing: Process Intensification**, v. 45, n. 11, p. 980–989, doi:10.1016/j.cep.2006.02.010, 2006.

[38] TOSCANO, G. et al. Vegetable oil and fat viscosity forecast models based on iodine number and saponification number. **Biomass and Bioenergy**, v. 46, p. 511–516, doi:10.1016/j.biombioe.2012.07.009, 2012.

[39] GARCÍA-MORENO, P. J. et al. Optimization of biodiesel production from waste fish oil. **Renewable Energy**, v. 68, p. 618–624, doi:10.1016/j.renene.2014.03.014, 2014.

[40] TREW, S. W.; GOULD, Z. B., **The Complete Idiot's Guide to Making Natural Soaps**, Aubrey Durkin, 2010. p. 11-24.

[41] RICKARD, W. D. A. et al. Assessing the suitability of three Australian fly ashes as an aluminosilicate source for geopolymers in high temperature applications. **Materials Science and Engineering A**, v. 528, p. 3390–3397, doi:10.1016/j.msea.2011.01.005, 2011.

[42] CILLA, M. S.; MORELLI, M. R.; COLOMBO, P. Geopolymer foams by gelcasting. **Ceramics International**, v. 40, n. 4, p. 5723–5730, doi:10.1016/j.ceramint.2013.11.011, 2014.

[43] HENON, J. et al. Potassium geopolymer foams made with silica fume pore forming agent for thermal insulation. **Journal of Porous Materials**, v. 20, p. 37–46, doi:10.1007/s10934-012-9572-3, 2013.

[44] BIASETTO, L. et al. Gas permeability of lanthanum oxycarbide targets for the SPES project. **Journal of Nuclear Materials**, v. 440, n. 1-3, p. 70–80, doi:10.1016/j.jnucmat.2013.04.038, 2013.

[45] **ASTM D3576 - 04(2010) Standard Test Method for Cell Size of Rigid Cellular Plastics**. Disponível em: <http://enterprise.astm.org/SUBSCRIPTION/filtrexx40.cgi?REDLINE_PAGES/D3576.htm>. Acesso em: 14 ago. 2014.

[46] CILLA, M. S.; MORELLI, M. R.; COLOMBO, P. Open cell geopolymer foams by a novel saponification/peroxide/gelcasting combined route.

Journal of the European Ceramic Society, v. 34, p. 3133–3137, doi:10.1016/j.jeurceramsoc.2014.04.001, 2014.

[47] WANG, X.; RUAN, J.-M.; CHEN, Q.-Y. Effects of surfactants on the microstructure of porous ceramic scaffolds fabricated by foaming for bone tissue engineering. **Materials Research Bulletin**, v. 44, n. 6, p. 1275–1279, doi:10.1016/j.materresbull.2009.01.004, 2009.

[48] ENGELSEN, C. et al. AUTEX. **Autex Research Journal**, v. 2, n. 1, p. 14–27, 2002.

[49] HIRT, D. E. et al. Dynamic surface tension of hydrocarbon and fluorocarbon surfactant solutions using the maximum bubble pressure method. **Colloids and Surfaces**, v. 44, p. 101–117, doi:10.1016/0166-6622(90)80191-6, 1990.

[50] ORTEGA, F. S. et al. Effect of aeration technique on the macrostructure and permeability of gelcast ceramic foams. **Cerâmica**, v. 48, n. 306, p. 79–85, doi:10.1590/S0366-69132002000200006, 2002.

[51] RUL, S. et al. Carbon nanotubes prepared in situ in a cellular ceramic by the gelcasting-foam method. **Journal of the European Ceramic Society**, v. 23, n. 8, p. 1233–1241, doi:10.1016/S0955-2219(02)00286-8, 2003.

[52] BARG, S. et al. New cellular ceramics from high alkane phase emulsified suspensions (HAPES). **Journal of the European Ceramic Society**, v. 29, p. 2439–2446, doi:10.1016/j.jeurceramsoc.2009.02.003, 2009.

[53] JONES, J. R.; HENCH, L. L. Effect of surfactant concentration and composition on the structure and properties of sol-gel-derived bioactive glass foam scaffolds for tissue engineering. **Journal of Materials Science**, v. 38, p. 3783–3790, doi:10.1023/A:1025988301542, 2003.

[54] BARG, S.; KOCH, D.; GRATHWOHL, G. Processing and properties of graded ceramic filters. **Journal of the American Ceramic Society**, v. 92, p. 2854–2860, doi:10.1111/j.1551-2916.2009.03301.x, 2009.

[55] GONZENBACH, U. T. et al. Tailoring the microstructure of particle-stabilized wet foams. **Langmuir**, v. 23, p. 1025–1032, doi:10.1021/la0624844, 2007.

[56] SEPULVEDA, P. et al. Production of porous hydroxyapatite by the gel-casting of foams and cytotoxic evaluation. **Journal of Biomedical Materials Research**, v. 50, p. 27–34, doi:10.1002/(SICI)1097-4636(200004)50:1<27::AID-JBM5>3.0.CO;2-6, 2000.

[57] GANESH, I. et al. An aqueous gelcasting process for sintered silicon carbide ceramics. **Journal of the American Ceramic Society**, v. 89, p. 3056–3064, doi:10.1111/j.1551-2916.2006.01198.x, 2006.

[58] DEY, A. et al. Investigations on Material and Mechanical Properties, Air-Permeation Behavior and Filtration Performance of Mullite-Bonded Porous SiC Ceramics. **International Journal of Applied Ceramic Technology**, v. 11, n. 5, p. 804-816, doi: 10.1111/ijac.12090, 2014.

[59] INNOCENTINI, M. D. M.; PANDOLFELLI, V. C. Issues concerning the evaluation of permeability in refractory concretes with Darcy and Forchheimer equations. **Cerâmica**, v. 45, n. 292-293, p. 61–67, doi:10.1590/S0366-69131999000200003, 1999.

[60] HUEC, J. C. LE et al. Influence of porosity on the mechanical resistance of hydroxyapatite ceramics under compressive stress. **Biomaterials**, v. 16, p. 113–118, doi:10.1016/0142-9612(95)98272-G, 1995.

[61] KAMSEU, E. et al. Enhanced thermal stability in K_2O-metakaolin-based geopolymer concretes by Al_2O_3 and SiO_2 fillers addition. **Journal of Materials Science**, v. 45, n. 7, p. 1715–1724, doi:10.1007/s10853-009-4108-1, 2010.

[62] HE, P. et al. Thermal evolution and crystallization kinetics of potassium-based geopolymer. **Ceramics International**, v. 37, p. 59–63, doi:10.1016/j.ceramint.2010.08.008, 2011.

[63] MEDPELLI, D.; SEO, J.-M.; SEO, D.-K. Geopolymer with Hierarchically Meso-/Macroporous Structures from Reactive Emulsion Templating. **Journal of the American Ceramic Society**, v. 97, n. 1, p. 70–73, doi:10.1111/jace.12724, 2014.

[64] HENON, J. et al. Porosity control of cold consolidated geomaterial foam: Temperature effect. **Ceramics International**, v. 38, p. 77–84, doi:10.1016/j.ceramint.2011.06.040, 2012.

[65] LLOYD, R. R. et al. Spatial distribution of pores in fly ash-based inorganic polymer gels visualised by Wood's metal intrusion. **Microporous and Mesoporous Materials**, v. 126, p. 32–39, doi:10.1016/j.micromeso.2009.05.016, 2009.

[66] CILLA, M. S.; MORELLI, M. R.; COLOMBO, P. Effect of process parameters on the physical properties of porous geopolymers obtained by gelcasting. **Ceramics International**, v. 40, n. 8, p. 13585–13590, doi:10.1016/j.ceramint.2014.05.074, 2014.

APENDIX A

Firstly, all raw materials were characterized, as shown below, in order to know its behavior when applied to the geopolimerization reaction.

- ✓ X-ray fluorescence (XRF);
- ✓ X-ray difratometry (XRD);
- ✓ Real density (helium picnometer);
- ✓ Specific surface area (BET).

X-ray fluorescence (XRF)

The chemical analysis of the precursors was made by XRF, using a spectrometer PW 2404 (Philips, Netherland) at Saint-Gobain laboratory in Vinhedo (Brazil).

Tabel A.1 Chemical analysis of precursors -* supplier - ** XRF

Raw materials (%)	**SiO_2**	**Al_2O_3**	**Fe_2O_3**	**Na_2O**	**K_2O**	**TiO_2**	**CaO**	**MgO**	**LOI**
HPMK*	56.2	34.8	2.2	0.0	1.9	1.3	0.0	0.2	2.6
MSMK**	49.7	35.0	0.5	0.1	1.5	0.0	0.1	0.2	3.0
FA **	55.3	19.8	10.2	0.0	2.3	1.0	1.3	0.7	2.8

X-ray difratometry (XRD)

At this point of the work, this technique was used mainly to evaluate the amorphous character of precursors, since this property is relevant to geopolymerization reaction. For this test was used a Diffractometer D5000 (Siemens, DE) with 40 kV and 40 mA in a sealed Cu source.

Phases were identified by DIFFRACplus – EVA software (JCPDS database) and are showed as follows.

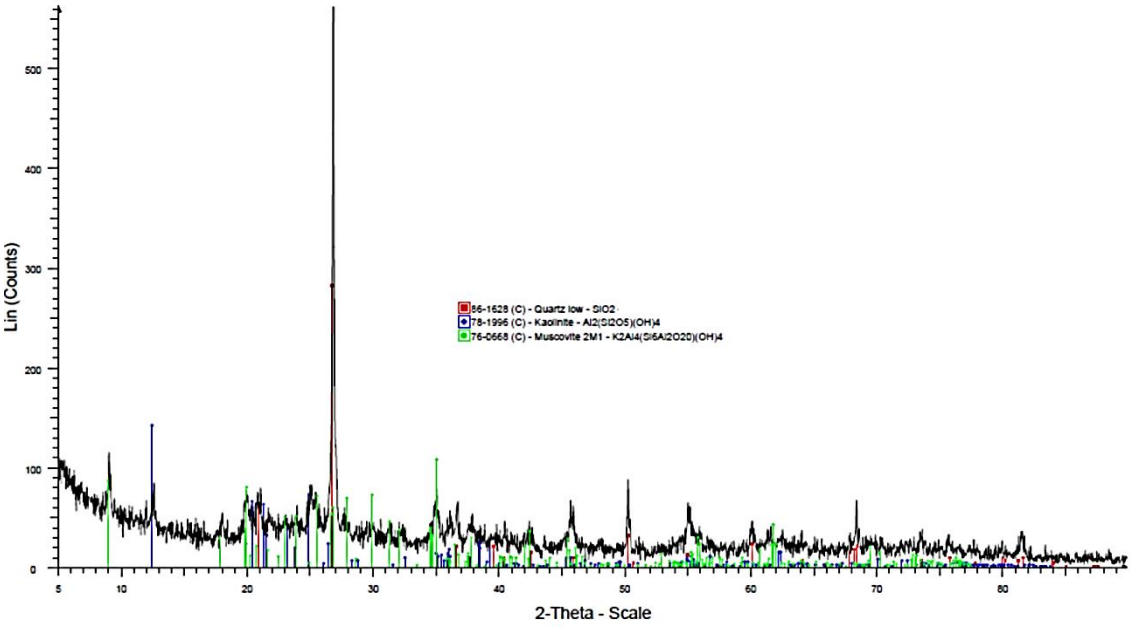

Figure A.1 XRD pattern of HP metakaolin (HPMK).

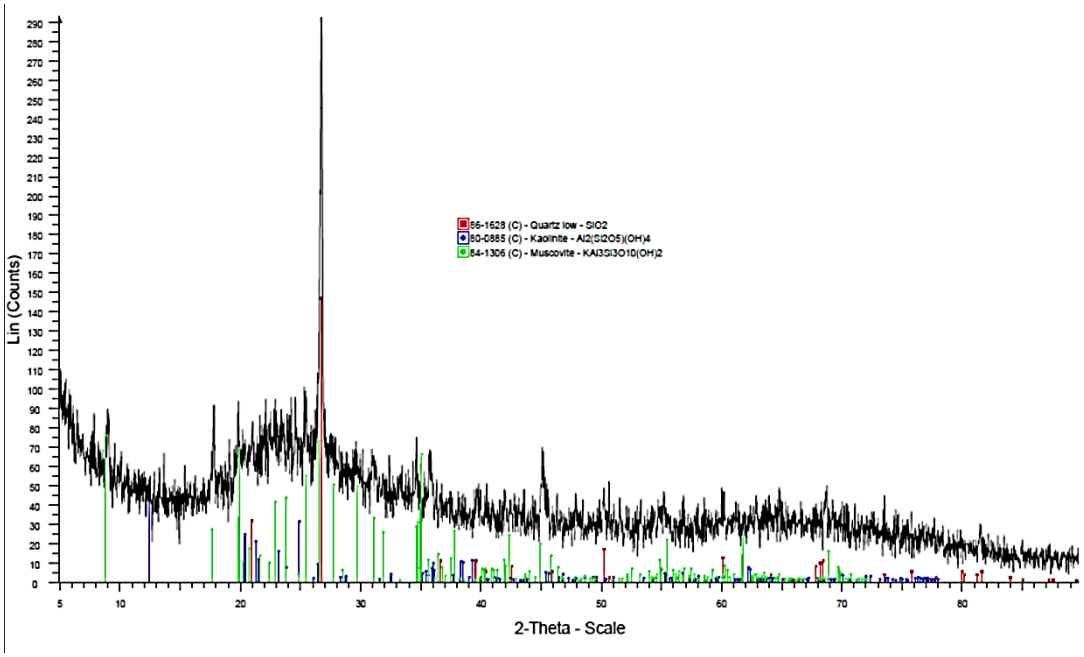

Figure A.2 XRD pattern of Minasolo metakaolin (MSMK).

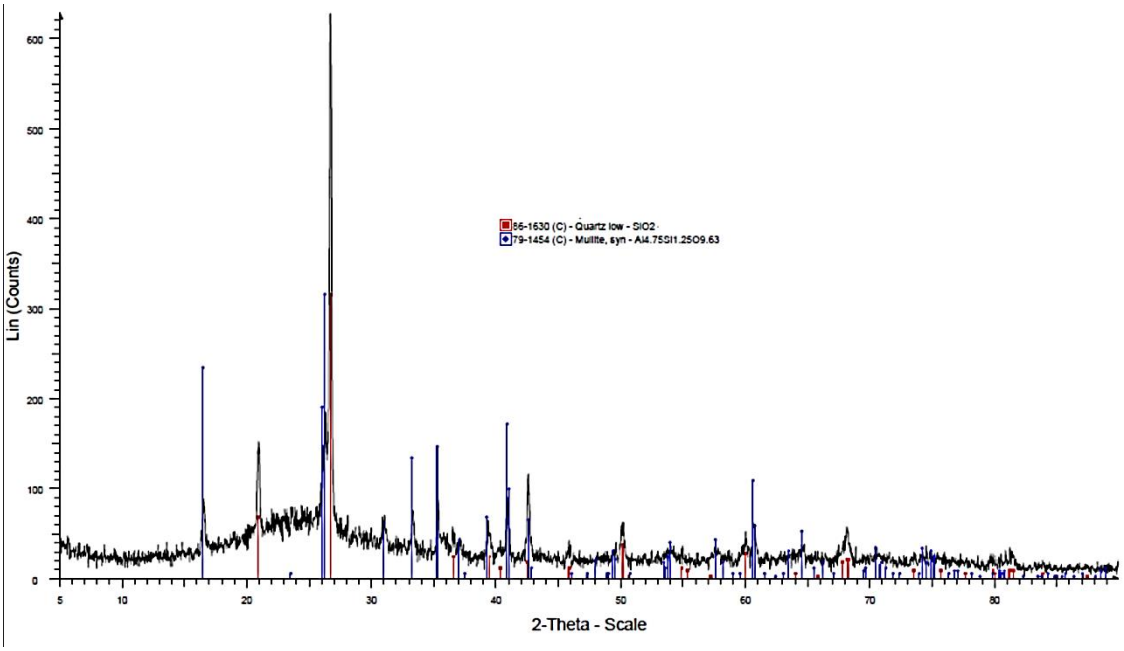

Figure A.3 XRD pattern of fly-ash (FA).

Real density (helium picnometer)

This property was measured with a helium pycnometer (Accupyc 1330, Micromeritics, Norcross, GA).

Tabel A.2 Real density of precursors

Precursors	**Bulk density (g/cm^3)**
HPMK	2.54
MSMK	2.60
FA	2.59

Specific surface area (BET)

The Brunauer-Emmett-Teller specific surface area (SSA) was determined by multipoint BET method using the adsorption data in the relative pressure (P/P0) using a Gemini 2370 (Micromeritics, Norcross, GA).

Tabel A.3 Specific surface area of precursors

Precursors	Specific surface area(m^2/g)
HPMK	26.0
MSMK	25.0
FA	3.0

Based on the results, and respecting the molar ratios previously cited, were prepared different compositions changing the type and amount of precursors and activators.

One example of this composition with the stoichiometry calculation is shown as follows.

Stoichiometry calculation

Considering the formulation below, and using the data previously reported to the precursors and activators we considered the stoichiometric calculation:

52.50 g MSMK (70 wt%)
22.50 g FA (30 wt%) } Precursors

70.00 g potassium silicate
20.00 g potassium hydroxide (15 M) } Activators

To prepare a KOH 15M solution:

MM (KOH): 56

710 g H_2O + 840 g KOH (A.1)

1550 g solution → 840 g KOH (A.2)

20.00 g solution → x = 10.84 g KOH (A.3)

20.00 g solution → x = 9.16 g H_2O (A.4)

To express the amount of K_2O into KOH:

KOH	→	K_2O+H_2O	(A.5)
2*56	→	x+18	(A.6)
		x = 47	(A.7)

56.00 g KOH	→	47.00 g K_2O	(A.8)
10.84 g KOH	→	x = **9.10 g K_2O**	(A.9)

For the potassium silicate, according the technical data sheet:

100.00 g silicate	→	26.48 g SiO_2	(A.10)
70.00 g silicate	→	x = **18.54 g SiO_2**	(A.11)

100.00 g silicate	→	12.75 g K_2O	(A.12)
70.00 g silicate	→	x = **8.93 g K_2O**	(A.13)

100.00 g silicate	→	60.60 g H_2O	(A.14)
70.00 g silicate	→	x = **42.42 g H_2O**	(A.15)

So, for the suggested composition, Table A.6 shows the amount of each oxide and also the amount of water.

Table A.4 Amount of the oxide presented in the geopolymer composition

Raw material	SiO_2 (g)	Al_2O_3(g)	K_2O (g)	H_2O (g)
MSMK	25.84	18.20	0.78	
FA	13.83	4.95	0.58	
Potassium hydroxide (15 M)			9.10	9.16
Potassium silicate	18.54		8.93	42.42
Total	58.21	23.15	19.39	51.58

Using this information, it’s possible to calculate the oxide molar ratios:

$$\frac{SiO_2}{Al_2O_3} = \left(\frac{\frac{58.21}{60}}{\frac{23.15}{102}}\right) = 4.27 \qquad (3.80 — 4.50) \qquad (A.16)$$

$$\frac{K_2O}{Al_2O_3} = \left(\frac{\frac{19.39}{94}}{\frac{23.15}{102}}\right) = 0.91 \qquad (0.80 — 1.60) \qquad (A.17)$$

$$\frac{K_2O}{SiO_2} = \left(\frac{\frac{19.39}{94}}{\frac{58.21}{60}}\right) = 0.21 \qquad (0.20 — 0.48) \qquad (A.18)$$

$$\frac{H_2O}{K_2O} = \left(\frac{\frac{51.58}{18}}{\frac{19.39}{94}}\right) = 13.89 \qquad (10.00 — 25.00) \qquad \text{…..……(A.19)}$$

Furthermore, based on the amount and respective percentage of oxides in the geopolymer composition, as reported in Table A.5, and using the phase equilibrium diagram (Figure A.4) of the these majoritarian oxides (SiO_2, Al_2O_3 and K_2O) is possible to predict the phase which should be formed due geopolymerization reaction.

Table A.5 Amount of majoritarian oxides in the geopolymer composition.

Oxide	SiO_2	Al_2O_3	K_2O
Amount (g)	58.21	23.15	19.39
wt. %	57.78	22.98	19.24

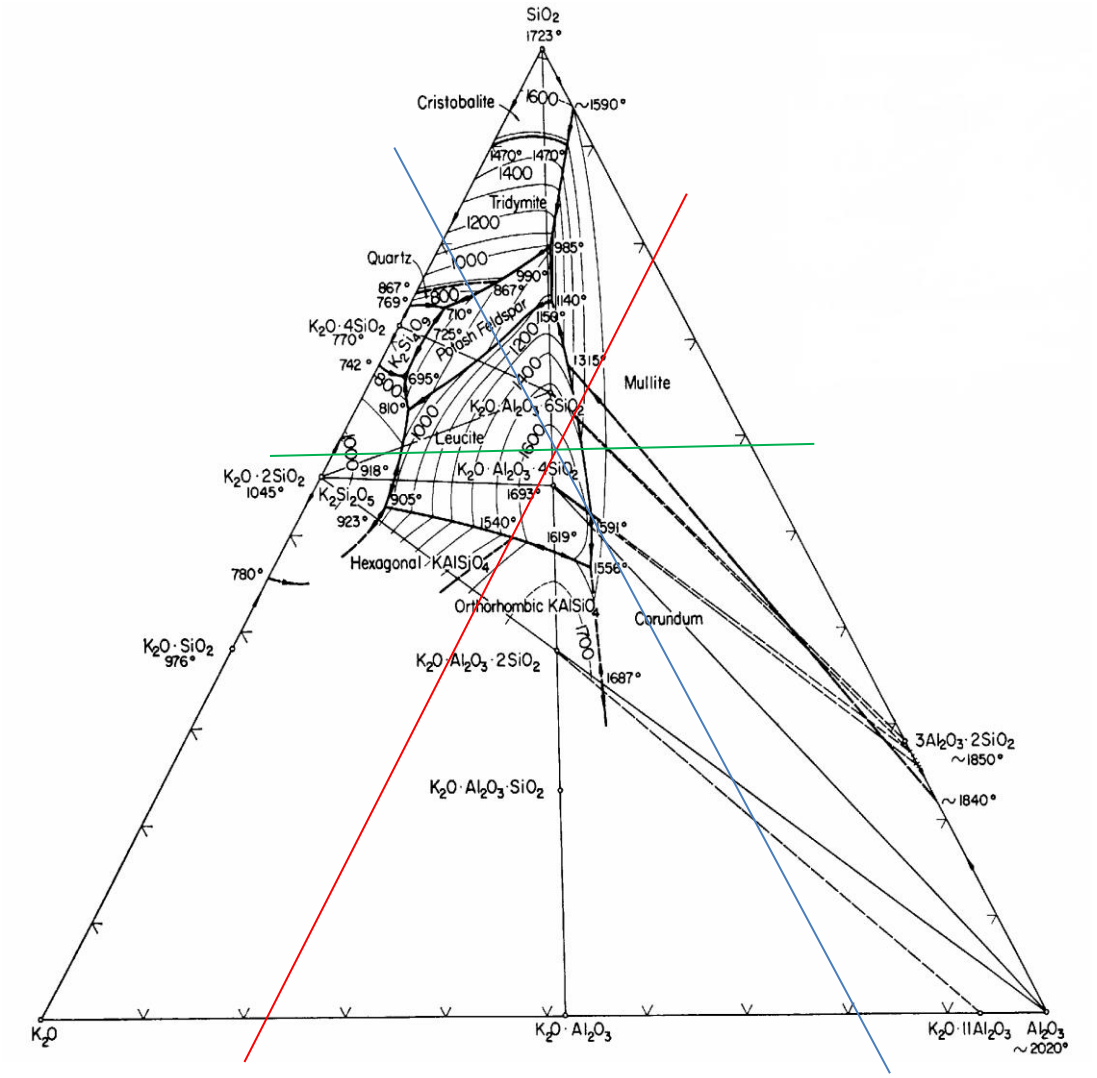

Figure A 4 Phase equilibrium diagram of the three majority oxide in the geopolymer composition where the green line represents the SiO_2, red line represents the Al_2O_3 and blue line represents the K_2O and their intersection sets the composition according Table A.5

Beyond that, this composition was evaluated by XRD (Figure A.5) to confirm the statement proposed about phase formation by the geopolymerization reaction.

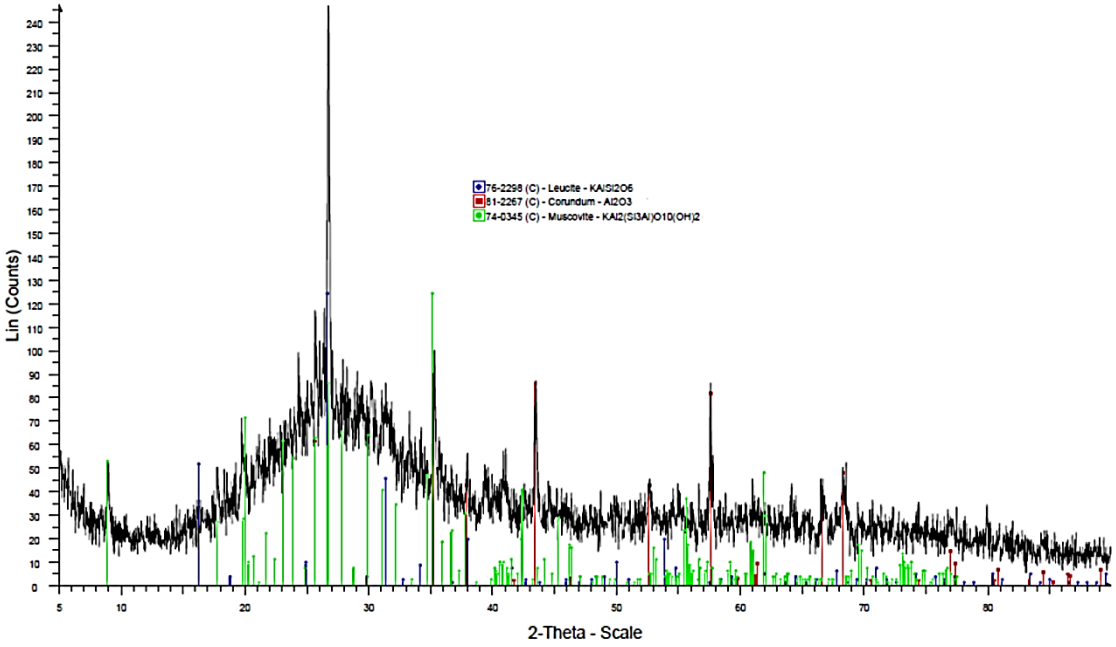

Figure A.5 XRD pattern of the geopolymer composition.

This composition was taken as an example of the stoichiometry involved in the process due to present the best results concerning the mechanical strength and thermal stability, one of the goals of this work and that will be presented in the follow.

Moreover, for the other compositions were also adopted the same concept of stoichiometric calculation.

Methodology of previously investigations

In order to evaluate the influence of raw materials on the mechanical and thermal properties of the geopolymer, always applying the same oxide molar ratios, were prepared different compositions, listed in Table A.6.

Table A.6 Different geopolymer compositions with variations in the precursors (metakaolin: type and amount) and activators (type of based alkaline solution).

	Precursors			Activators	
Composition	MSMK (wt %)	HPMK (wt %)	FA (wt %)	Na	K
1	100		0	X	
2	90		10	X	
3	70		30	X	
4		100	0	X	
5		90	10	X	
6		70	30	X	
7	100		0		X
8	90		10		X
9	70		30		X
10		100	0		X
11		90	10		X
12		70	30		X

Basically, the first step adopted to make the geopolymer, following the oxide molar ratio calculation, was the preparation of a 15 M NaOH and KOH, which should be used after 24 hours [32]. Then, a solution of the activators, comprising the hydroxide solution and respective silicate (NAOH/sodium silicate; KOH/potassium silicate) were prepared in a mechanical stirrer (500 rpm, 30 minutes). Then, metakaolin and fly ash were then added respectively in this sequence at room temperature to the activator solution, stirring at 1000 rpm for 30 minutes after each addition.

Thereafter, the geopolymer was cast in polystyrene to form the samples to the mechanical strength test and in a cone-shaped paper mold to form the samples to the thermal stability test. Then, all molds were placed in an oven for 60 minutes at 80ºC after sealing it into a plastic bag. The samples were then removed from the plastic bag and left at 80°C for further 4 hours, being placed at room temperature for 96 hours, up to perform the tests.

Mechanical Strength

The compressive strength of the as prepared samples was determined using a universal testing machine Hounsfield (8746, England). At least 5 specimens per composition were tested.

Results are reported in Figure A.6, where it could be noticed, as quoted by Davidovits [1, 3], the amorphous character of the precursors has a significant role in this feature, increasing their tendency to combine chemically in the presence of an alkaline solution, thereby conferring better results to MSMK compositions when compared with those made with HPMK.

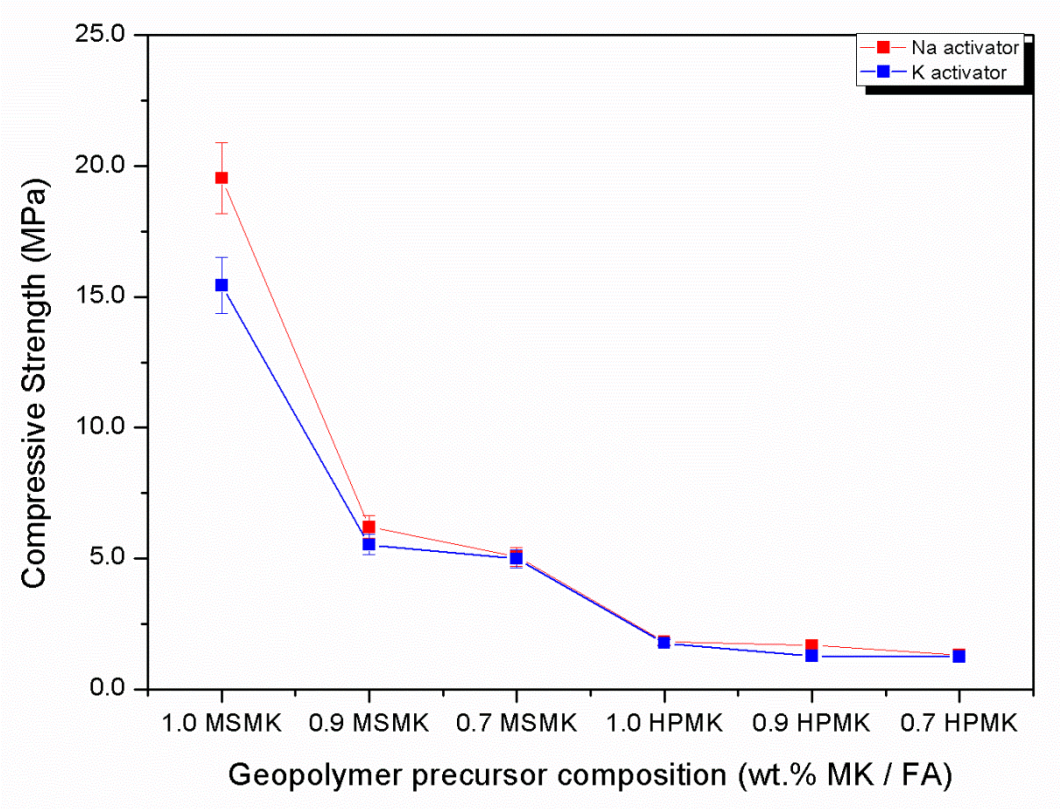

Figure A.6 Effect of the type and amount of metakaolin (MSMK and HPMK) and type of alkali based solution.

This information could be confirmed when compared the amorphous character of HPMK (Figure A.1) and MSMK (Figure A.2) by the diffractograms analysis.

Thermal stability

Samples (cones) were heat treated in a *Lindberg Blue CF56724C* furnace, whereas similar firing curves: heating rate of 5°C/min., landing time of 5 min. and cooling rate of 10°C/min. for an empirical evaluation of the thermal stability and how this property could be affected by different precursors and activators.

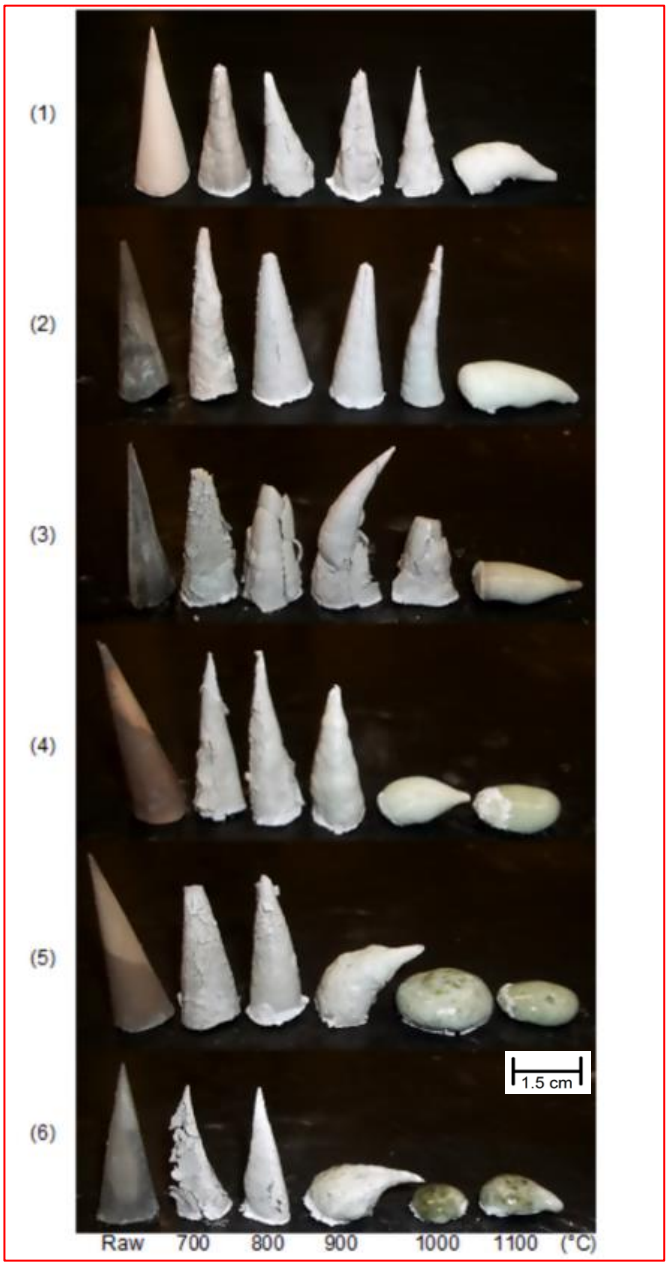

Figure A.7 Effect of temperature in different geopolymer composition activated with Na based solution.

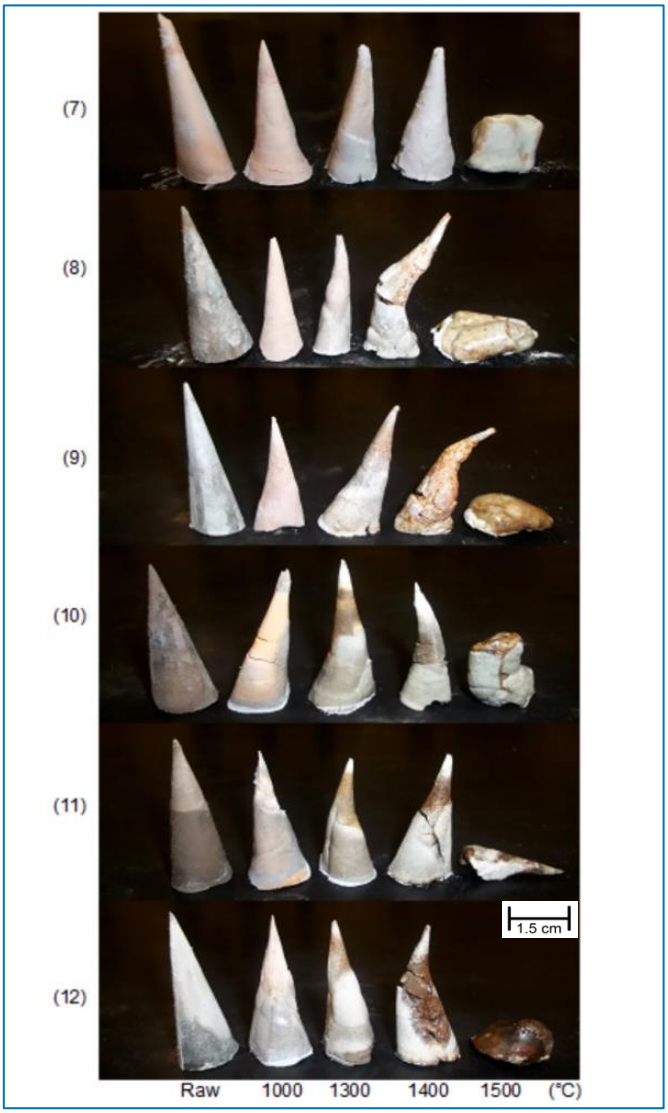

Figure A.8 Effect of temperature in different geopolymer composition activated with K based solution.